PASSIVE AND ACTIVE CONTROL
OF
BOUNDARY LAYER TRANSITION

Thesis by

Daniel Mark Nosenchuck

In Partial Fulfillment of the Requirements

for the Degree of

Doctor of Philosophy

California Institute of Technology

Pasadena, California

1982

(Submitted April 26, 1982)

Acknowledgements

I give deep thanks to Professor Hans W. Liepmann, whose foresight, guidance, encouragement, and support are greatly appreciated. I have profited from the valuable guidance given by Dr. Steven Barker and Dr. Garry Brown during the early phases of the research. I also thank Professor Toshi Kubota for his help, and for many valued discussions throughout the years.

Steve Taylor and Harry Robey have contributed much to all phases of the research; my sincerest thanks goes to both of them. I give special thanks to Dan Lang, who was always willing to help out with his vast knowledge of electronics and computer systems.

I also wish to thank Jack Kingan for the expert craftsmanship of many critical hardware components, and Harry Hamaguchi for his careful and rapid photographic work. The many diverse services provided by Jackie Beard are appreciated.

The help of the faculty, graduate students, the Aero and Central Shops, and Aero services personnel is gladly acknowledged.

The support of the Graduate Aeronautical Laboratories of the California Institute of Technology (GALCIT) and the

Office of Naval Research (ONR) is appreciated. The research described in this thesis was supported by ONR Contract N00014-81-K-0551.

ABSTRACT

It is well known that laminar-turbulent boundary layer transition is initiated by the formation of Tollmien-Schlichting laminar instability waves. The amplification rates of these waves are strongly dependent on the shape of the boundary layer velocity profile. Consequently, the transition process can be controlled by modifying the velocity profile. This can be accomplished by controlling the pressure gradient (dp/dx), using boundary layer suction, installing surface roughness elements, or by surface heating or cooling. Methods used to modify the transition process through changes in the mean velocity profile are called "passive" in this paper. There exists a large set of experiments and theory on the application of passive methods for boundary layer control. In the present work only surface heating will be addressed.

Transition measurements were made on a heated flat plate in water. Results are presented for several plate wall temperature distributions. An increase by a factor of 2.5 in transition Reynolds number was observed for a 5°C isothermal wall overheat. Buoyancy effects on transition were minimal due to the small Richardson and Grashof numbers encountered in the experiments.

The amplification of laminar instability waves is a comparatively slow process, taking place over many boundary layer thicknesses. After the slow amplification of the laminar instability waves, transition occurs by a strong three-dimensional dynamic instability. It appears possible to attenuate (or reinforce) the instability waves by introducing amplitude- and phase-controlled perturbations into the laminar boundary layer using a feedback control system. This method is called "active" control and forms the larger part of the research reported in this thesis.

A combination of sensors, activators and feedback control electronics is required for active control. The sensors used in the experiments are flush-mounted hot film wall shear probes. A new type of activator was developed using thin, flush-mounted surface heating elements to excite instability waves in the laminar boundary layer by periodic (active) heating.

Experimental evidence is presented illustrating the effects of periodically heated flush mounted strips in perturbing a flat plate boundary layer in water. The results of superposition of forced laminar instability waves are also given. Finally, an active feedback-control system using a single hot film probe and strip heater was developed to control natural laminar instability waves in real time. It is shown that when the natural waves were attenuated, the

transition length was increased by 25%, requiring only 10 watts of strip heater power. To accomplish the same transition delay using passive heating, the internal heating pads had to supply 1900 watts of power.

TABLE OF CONTENTS

LIST OF FIGURES

LIST OF SYMBOLS

ENGLISH SYMBOLS

A_0	initial natural T-S wave amplitude
b	spanwise length of strip heater
c	complex T-S wave propagation speed, $c_r + ic_i$
c_i	temporal growth rate of T-S waves
C_p	pressure coefficient, $(p - P_\infty)/\frac{1}{2}\rho U_\infty^2$
c_p	specific heat at constant pressure
c_r	instability T-S wave phase speed
F	nondimensional T-S wave frequency, $\frac{2\pi f\nu}{U_\infty^2}$
f	T-S wave frequency (Hz)
g	gravitational acceleration
Gr_x	local Grashof number, $\frac{g \Lambda \Delta T x^3}{\nu^2}$
k	thermal conductivity
L	distance between heater, H0, and probe, P0
L_{tr}	transition length, measured from leading edge
P_∞	freestream reference pressure, measured upstream of flat plate
p	pressure
Pr	Prandtl number, $\frac{\nu}{k}$

q	heat flux per unit area
Q	total heat flux
Re	Reynolds number
Re_x	local Reynolds number, $\frac{Ux}{\nu}$
$Re_{x;cr}$	critical Reynolds number
$Re_{x;tr}$	transition Reynolds number
Re^*	boundary layer displacement thickness Reynolds number, $\frac{U\delta^*}{\nu}$
Ri	Richardson number, $\frac{-g\left(\frac{\partial \rho}{\partial y}\right)}{\rho\left(\frac{\partial u}{\partial y}\right)^2_w}$
St	Stanton number, $\frac{Q}{\rho U_\infty C_p T b \Delta}$
T	ambient temperature
t	time
T_a	ambient temperature
T_w	plate wall temperature
u	streamwise velocity component
u_θ	velocity at thermal boundary layer thickness height
U_∞	freestream velocity
v	normal velocity component
w	spanwise velocity component
x	streamwise coordinate, measured from plate leading edge

y	normal coordinate, measured from plate surface
z	general spanwise coordinate

GREEK SYMBOLS

α	wavenumber
β	Falkner-Skan wedge flow parameter
δ	boundary layer 99% velocity thickness
δ^*	boundary layer displacement thickness
δ_f	flap angle
Δ	strip heater width
Δx	distance between H0 and P0
ΔT	local wall overheat, $T_w - T_a$
Θ	thermal boundary layer thickness
κ	thermal diffusivity, $\frac{k}{\rho C_p}$
λ	wavelength
Λ	coefficient of thermal expansion
μ	absolute viscosity
ν	kinematic viscosity, $\frac{\mu}{\rho}$
π	3.14159...
ρ	density
τ	shear stress
τ_A	apparent shear stress, $-\rho\overline{u'v'}$
τ_L	laminar shear stress, $\mu\left(\frac{\partial u}{\partial y}\right)$
ϕ	phase shift

Φ	total phase shift between heater and probe
ω	dimensionless frequency
Ω	impedance, ohms

SUBSCRIPTS

a	ambient
w	wall
x	at location x
∞	far field

SUPERSCRIPTS

$\overline{\quad}$	time mean
'	differentiation; fluctuation
*	complex conjugate, displacement thickness

1 Introduction

1.1 Background

The control of laminar-turbulent transition in boundary layer flow is still a major problem in applied fluid mechanics. Blasius (1908) (zero pressure gradient) flow on a flat plate is often taken to be the classic boundary layer case. A known mechanism that affects the transition process is the development and growth of Tollmien-Schlichting (T-S)* waves. The T-S waves are two-dimensional perturbations which grow in the laminar boundary layer and are precursors to the development of fully turbulent boundary layer flow. The T-S waves are governed by the Orr-Sommerfeld equation, which assumes quasi-parallel flow,

$$(U - c)(v'' - \alpha^2 v) - U''v + \frac{i\nu}{\alpha}(v'''' - 2\alpha^2 v'' + \alpha^4 v) = 0 \qquad (1)$$

where α and c are the complex wave number and propagation speed, respectively, of the disturbances, U_∞ is the mean velocity in the boundary layer, v is the normal disturbance velocity component in the boundary layer, and ν is the kinematic viscosity. Equation (1) was independently derived by

* Laminar instability waves will be referred to in this report as such, and also as Tollmien-Schlichting, or T-S waves, the specific name given to laminar instability waves in the boundary layer.

Orr (1907) and Sommerfeld (1908). The eigensolutions of Equation (1) show that there is a finite range of frequencies at low Reynolds numbers where infinitesimal disturbances are unstable. This region is bounded by the neutral, or so-called "thumb curve", on a frequency vs Reynolds number plot. Outside the thumb-shaped region, all disturbances are damped. An example of a neutral curve for Blasius boundary layer flow is shown in Figure 1. Lord Rayleigh (1880) had previously shown, for the case of zero viscosity (or infinite Reynolds number), that the following relation holds:

$$v'' - \left(\frac{U''}{U-c} + \alpha^2\right) v = 0 \ , \tag{2}$$

which is the inviscid form of the Orr-Sommerfeld equation. The complex conjugate of Equation (2) is

$$v^{*''} - \left(\frac{U''}{U-c^*} + \alpha^2\right) v^* = 0 \ . \tag{2a}$$

By multiplying Equation (2) by v^* (the complex conjugate of v), Equation (2a) by v, subtracting the latter from the former, and integrating the difference, one finds

$$c_i \int \frac{U''|v|^2}{|U-c|^2}\, dy = \frac{1}{2i}\left[v^*v' - vv^{*'}\right] \tag{3}$$

Rayleigh then applied the boundary conditions that the disturbance vanish at the plate wall and at infinity, thus

$$c_i \int_0^\infty \frac{U''|v|^2}{|U-c|^2}\, dy = 0 , \qquad (3a)$$

where c_i is the temporal growth rate for instability waves. Rayleigh noted that this relation implied that a necessary condition for boundary layer instability (i.e. $c_i \neq 0$) was that the velocity profile have a point of inflection. That this was also a sufficient condition for instability was shown by Tollmien (1929). Prandtl (1921) found that, even at very high Reynolds numbers, the effect of viscosity has to be included in the viscous sublayer near the wall. Therefore the right hand side of Equation (3), which applies for the region outside the viscous sublayer, is not necessarily zero. Hence, Prandtl found that the effect of viscosity is destabilizing for certain ranges of Reynolds numbers and perturbation frequencies. Tollmien (1929), in extending the computational analysis of Heisenberg (1924), computed the instability diagram for the Blasius profile. Additional numerical work was carried out by Schlichting (1932), and further theoretical work by Lin (1945).

The existence of T-S waves was well founded in theory; however, it took the landmark experiments of Schubauer

and Skramstad (1947) to prove the physical existence of the waves. It is curious that although the theory had been in existence for quite some time, T-S waves were not experimentally verified until 1941 (the experiments quoted above, in addition to the experiments of Liepmann (1943), discussed in the following pages, were classified during WWII and not openly published until 1947). Early experimental attempts (Burgers (1924) and Dryden (1934)) were made in search of the waves, but it took a combination of the sensitive hot wire anemometer, and the low turbulence level (0.02%) wind tunnel at the National Bureau of Standards, to unequivocally verify the presence of T-S waves in an unstable laminar boundary layer. This chain of events helped to point out that other mechanisms, in addition to T-S waves, were at work during transition. Klebanoff, Tidstrom, and Sargent (1962) experimentally demonstrated that any weak three-dimensionality present in the boundary layer is strongly amplified. The initial T-S wave instability has very small amplification rates, thus it grows quite slowly over a relatively large distance along the plate. However, once the waves show a lack of spanwise phase coherence, the subsequent growth of the initial instability is explosive, with the ensuing rapid development of turbulent flow. The early experimental facilities had rather high background turbulence levels which induced the early formation of three-

dimensionality in the boundary layer. The region of linear growth was almost entirely bypassed, making it understandably difficult to detect any T-S waves that were present.

Two clear paths toward the control of transition emerge from the groundwork laid in the past 100 years. The first involves the modification of the mean velocity profile, while the second method concerns itself with the cancellation of developing perturbations within the boundary layer.

1.2 Passive Heating

The stability of laminar boundary layer flow depends strongly on the curvature of the velocity profile near the wall. The x-momentum equation is quite helpful in pointing out various methods which may be employed to postpone (or accelerate) the occurrence of an inflectional velocity profile, effectively shifting the origin of the transition process. The x-momentum equation,

$$\rho\left(u \frac{\partial u}{\partial x} + v \frac{\partial u}{\partial y}\right) = - \frac{dp}{dx} + \frac{\partial}{\partial y}\left(\mu \frac{\partial u}{\partial y}\right) , \qquad (4)$$

may be written with variable viscosity and the no-slip condition imposed. At the wall of the plate,

$$\frac{dp}{dx} - \left(\frac{\partial \mu}{\partial y}\right)_w \left(\frac{\partial u}{\partial y}\right)_w + \rho v_w \left(\frac{\partial u}{\partial y}\right)_w = \mu \left(\frac{\partial^2 u}{\partial y^2}\right)_w \quad . \tag{5}$$

The condition for boundary layer stability at infinite Reynolds number is the lack of an inflection point throughout the boundary layer, i.e.

$$\frac{\partial^2 u}{\partial y^2} < 0 \; ; \quad 0 \leq y \leq \delta \; . \tag{6}$$

A popular method used to delay transition is to impose a favorable pressure gradient ($dp/dx < 0$) on the body by changing the body shape or modifying the mean flow. In many cases it is difficult to manipulate the external flow or the overall geometry in order to alter the imposed pressure gradient. It is therefore often desirable to control the flow at the wall itself. The terms in Equation (5) suggest that suction ($v_w < 0$) would tend to stabilize the boundary layer (for nonseparating flows), which is indeed the case as shown by Pretsch (1942). Pretsch demonstrated that suction velocity profiles exhibit a far greater degree of stability than those for Blasius flow. Finally, the case $(\partial \mu / \partial y > 0)_w$ also stabilizes the boundary layer. To look at this case in more detail, one may note that, in general, $\mu = \mu(T)$. Therefore, Equation (5) becomes (for Blasius flow with no suction):

$$- \frac{d\mu}{dT} \left(\frac{\partial T}{\partial y}\right)_w \left(\frac{\partial u}{\partial y}\right)_w = \mu \left(\frac{\partial^2 u}{\partial y^2}\right)_w \quad . \tag{7}$$

In water (and most common liquids) $d\mu/dT < 0$. Thus, steady wall heating in water leads to increased stability. The opposite effect occurs for a gas in which heating is destabilizing. Liepmann and Fila (1947) noted that the term $- \frac{d\mu}{dT} \left(\frac{\partial T}{\partial y}\right)_w \left(\frac{\partial u}{\partial y}\right)_w$ can be thought of as an effective dp/dx to demonstrate the relation between surface heating and stability. The use of steady heating to modify the mean boundary layer velocity profile is referred to in this paper as "passive" heating, or "passive" control.

The effects which promote stability are summarized below.

(i) $(dp/dx) < 0$,

(ii) $v_w < 0$,

(iii) (a) $\left(\frac{\partial T}{\partial y}\right)_w < 0$, for $\frac{d\mu}{dT} < 0$ (liquid),

(b) $\left(\frac{\partial T}{\partial y}\right)_w > 0$, for $\frac{d\mu}{dT} > 0$ (gas).

Thus, there is a qualitative (not necessarily quantitative) equivalence among pressure gradient, suction, and wall heating.

Wazzan, Okamura, and Smith (1968) studied the modified Orr-Sommerfeld equation in which the effects of variable viscosity are accounted for. They found that on a flat plate in water at a 45°C constant overheat at room temperature, Re_{crit} was increased by a factor of 22. Transition was predicted to occur when the most amplified boundary layer disturbance grew by a factor of e^9 times its initial amplitude, an empirical criterion suggested by A.M.O. Smith (1957). The growth rates used in the "e to the ninth" calculation were those predicted by linear stability theory.

The general effect of passive heating is to shift farther downstream the region along the plate where the T-S waves amplify. This is shown qualitatively in Figure 1 by the shift in the neutral curve (and critical Reynolds number) to the right with heating. Perturbations, which would otherwise begin to amplify at a relatively low Reynolds number, are damped when the plate is heated. They begin to amplify at lower rates farther down the plate, thus delaying the transition process. Wazzan et al. (1970) and Lowell (1974) predicted the detailed behavior of the neutral stability curves and the disturbance growth rates for parallel heated boundary layer flow.

Strazisar, Reshotko, and Prahl (1977) studied the growth rates of artificially excited instability waves in the boundary layer of a heated flat plate in water. They

found reasonable agreement with the theory, although the maximum overheat used was less than 4.5°C. They were not concerned with the possible effects of buoyancy on stability, thus their plate was tested in only one configuration (instrumented side facing down).

Barker (1977) conducted an experiment in a heated "flow tube" to check the predictions of Wazzan et al. at relatively high overheats (>5°C). The flow tube had a thin boundary layer relative to the tube radius to approximate the boundary layer over a flat plate. Barker found good agreement of the measured transition Reynolds number with the theory up to a 5.5°C overheat. Beyond that point, the theory predicted significantly higher transition Reynolds numbers than what was measured, which led Barker to speculate that buoyancy effects, neglected by the theory, were possibly an important aspect of the heated boundary layer transition process. The discrepancy between theory and experiment was one of the prime motivations to conduct the present passive heating experiments.

In the present experiments, the stability of a flat plate boundary layer in water was studied under varying wall overheats and temperature distributions. The effects of buoyancy on transition were examined by testing the plate in several orientations (instrumented side up, down, and vertical). The experimental results were compared to those pre-

dicted to see to what extent the theory remains valid without accounting for the density stratification in the boundary layer fluid. It was found that for moderate isothermal plate overheats (up to 5°C) the experiments agreed well with the theory; no significant buoyancy-induced effects on transition Reynolds numbers were observed.

1.3 Active Heating

Time-dependant periodic surface heating may be used to introduce perturbations into the boundary layer. This technique is called "active" heating in this paper. Active control is defined, in this paper, as the use of active heating to produce controlled time-and space-dependant perturbations within the boundary layer to modify perturbations already present in the boundary layer.

The linearity of the governing Orr-Sommerfeld equation allows the solutions to be superposed. If two waves of equal amplitude and frequency are present, but 180° out of phase, they would cancel each other with no effect on boundary layer stability. Active control therefore involves the real-time detection of naturally-occurring laminar instability waves, and the synthesis of a second set of waves of the same character but 180° out of phase with those naturally occurring. The net result is to delay the occurrence of transition by reducing the amplitude of the disturbance at a given point in the boundary layer.

The principle of active control was first alluded to in a paper by Liepmann (1943), studying the effect of the initial level of the perturbations in the boundary layer on transition. Liepmann calculated the "apparent" shear stress, τ_A, produced by the boundary layer oscillations, where

$$\tau_A = - \rho \overline{u'v'} . \tag{8}$$

The maximum "apparent" shear stress in the boundary layer, normalized by the laminar shear stress, τ_L, where

$$\tau_L = \mu \left(\frac{\partial u}{\partial y} \right) \tag{9}$$

is plotted vs Reynolds number in Figure 2 for different levels of the initial neutrally stable boundary layer disturbance. Liepmann used the criterion that, at transition, the apparent shear was of the same order of magnitude as the laminar shear. Liepmann's analysis provides part of the physical reasoning for the e^9 empirical criterion of Smith (1957).

As an example of the effects of controlling disturbances within the boundary layer, an initial velocity perturbation level of 0.2% was chosen. As shown in Figure 2, this initial disturbance would cause transition to occur

at $Re = 8.5 \times 10^5$. If the apparent shear is reduced, the flow would proceed to transition along a path corresponding to an effectively lower initial disturbance amplitude. In the example shown in Figure 2, the apparent shear was reduced so that the transition process proceeded along a path of 0.1% initial disturbance level. The transition Reynolds number can be seen to increase by 15%. The opposite is true when the apparent stress shear is reinforced.

The main element of active control is the actuator used to produce the desired perturbations in the boundary layer. The first, and most popular, device used to input laminar instability waves into the boundary layer, is the vibrating ribbon developed by Schubauer and Skramstad (1947). In this technique, a metal ribbon is suspended laterally in the boundary layer (normal to the flow direction) and close to the plate wall in which a permanent magnet is installed. A sinusoidally varying current is passed through the ribbon to electromagnetically oscillate the ribbon, thus introducing controlled disturbances into the boundary layer. Another method was developed by Loehrke (1970) in which a thin resistance wire is stretched in tension laterally across the plate in the boundary layer. An electric current is used to heat the wire, thus changing the strain. Periodic heating of the wire, dubbed the "tickler",

creates mechanical oscillations of the wire which input disturbances within the boundary layer.

Both methods described above cannot excite arbitrary disturbance waveforms, due to the mechanical limitations imposed by the finite inertia and resonant modes of the system. This, in addition to the inherent inability to readily control the spanwise phase, limits the vibrating ribbon and "tickler" techniques primarily to the studies of single frequency, two-dimensional laminar instability waves. (Saric et al. (1979) were able to excite two frequencies with a single vibrating ribbon, although the frequency range was limited by the vibrational modes of the ribbon). The ribbon and "tickler" also have the undesirable characteristic of being intrusive in the flow, even when not operating.

An ideal activator would be nonintrusive at all times, capable of inputting arbitrary waveforms, and capable of exciting controlled three-dimensional disturbances. Local active surface heating, using flush-mounted thin-film heaters, was selected as a means to fulfill the above criteria. A single strip heating element, with low thermal inertia, is capable of actively controlling a wide range of naturally occurring T-S waves.

The effect of heating at the wall may be illustrated by noting that the term $\frac{d\mu}{dT}\left(\frac{\partial T}{\partial y}\right)_w\left(\frac{\partial u}{\partial y}\right)_w$ in the x-momentum

equation can be interpreted as a nonvanishing $\rho v_w \left(\frac{\partial u}{\partial y}\right)_w$ at the plate wall:

$$\left[-\frac{d\mu}{dT}\left(\frac{\partial T}{\partial y}\right)_w + \rho v_w\right]\left(\frac{\partial u}{\partial y}\right)_w = 0 \ . \tag{10}$$

Consequently, periodic heating of a surface strip can be compared to small oscillations normal to the surface. The magnitude of the equivalent surface oscillation velocities can easily be estimated. From Equation (10), the effective wall displacements are

$$v_{w,eff} = -\frac{1}{\rho}\frac{d\mu}{dT}\left(\frac{\partial T}{\partial y}\right)_w \ . \tag{11}$$

Using the relations

$$\delta \sim \left(\frac{\nu x}{U_\infty}\right)^{\frac{1}{2}} \ , \tag{12a}$$

and

$$\theta \sim \left(\frac{\kappa x}{u_\theta}\right)^{\frac{1}{2}} \ , \tag{12b}$$

where δ and θ are the velocity and heater-induced thermal boundary layer thicknesses respectively, and u_θ is the velocity within the boundary layer at the thermal boundary layer thickness height. Making the usual approximation that $u \sim y$ near the wall, one finds from Equation (11) that

$$\left(\frac{v_w}{U_\infty}\right)_{eff} \propto \frac{Pr^{\frac{1}{3}}}{Re^{\frac{1}{2}}} \left(\frac{x_s}{\Delta}\right)^{\frac{1}{3}} \frac{d\log\mu}{d\log T} \frac{\Delta T}{T} , \qquad (13)$$

with a constant of proportionality of order unity. Therefore, the effective normal wall velocity is linearly related to the overheat. This is an important consideration when one is seeking a simple relation between the input heater waveform and the resulting perturbations.

The velocity boundary conditions at the plate wall are $u = v = 0$. The "effective" normal wall velocity perturbations, due to periodic surface heating, are introduced as physical velocity fluctuations in the boundary layer. This happens through periodic changes in the slope and curvature in the velocity profile at the surface of the strip heater. The result is a velocity perturbation in the boundary layer in the vicinity of the strip heater. Thus, the net effect of active heating is to input velocity perturbations into the boundary layer which evolve into laminar instability waves.

The local heat flux from the heating element, q, into the boundary layer may be related to the effective normal wall velocity. The Fourier heat conduction law

$$q = - k \frac{\partial T}{\partial y} , \qquad (14)$$

may be substituted into Equation (11), to give

$$\left(\frac{v_w}{U_\infty}\right)_{eff} \propto Pr \frac{d\log\mu}{d\log T} \frac{q}{\rho U_\infty c_p T} . \qquad (15)$$

The total heat flux from the strip heater may be calculated using Lighthill's relation for the heating supplied to the boundary layer from a two-dimensional strip on the wall. Brown (1967) suggests that if the width of the strip is small compared to its position on the plate, i.e.

$$\frac{\Delta}{x_s} << 1 , \qquad (16)$$

then an isothermal "top hat" temperature distribution on the strip may be assumed. Imposing the narrow strip condition, the total heat transfer rate from a heated strip in a Blasius boundary layer is

$$Q = - 0.53\ k\ b\ (\Delta T)\ Pr\ Re^{\frac{1}{2}} \left(\frac{\Delta}{x_s}\right)^{\frac{2}{3}}, \qquad (17)$$

where b is the strip heater spanwise length.

The average effective normal wall velocity may be related to the total heating power supplied by the strip using Equations (13) and (17). Therefore, assuming that all of the heat generated by the strip is transferred into the fluid,

$$\left(\frac{v_w}{U_\infty}\right)_{eff} \propto Re^{-1} \frac{d\log\mu}{d\log T} \frac{Q}{kbT} \frac{x_s}{\Delta} , \qquad (18)$$

with a constant of proportionality of order unity.

The total heat flux, Q, may be put in the nondimensional form of a Stanton number, St, based on the ambient fluid temperature, where

$$St \equiv \frac{Q}{\rho U_\infty C_p T(b\Delta)} . \qquad (19)$$

The depth of penetration into the boundary layer of the thermal and velocity perturbations from the strip heating element is shallow compared to the velocity boundary layer thickness. A characteristic disturbance penetration depth may be taken to be θ, which can be compared to the boundary layer thickness, δ. From Equation (12), for Blasius flow,

$$\frac{\delta}{\theta} \approx \left(Pr \frac{x_s}{\Delta}\right)^{1/3} . \qquad (20)$$

The critical layer is defined as being the layer in the boundary layer where the phase velocity of the instability waves is equal to the local mean velocity. In general, the critical layer is in the vicinity of the displacement thickness height, δ^*, a considerable distance from the wall.

Thus, to input perturbations in a region where they would rapidly begin to amplify, the strip heater must be wide compared to the displacement thickness, i.e.

$$\frac{\Delta}{\delta^*} > 1 \quad . \tag{21}$$

Equation (21) is essentially an empirical condition which is discussed more fully in Chapter 4. Even though the heater is relatively wide in comparison to the local boundary layer thickness, spatial phase control of the perturbations is maintained due to the limited streamwise range of influence of the heater near the critical layer.

The frequency used to excite laminar instability waves, f, is typically expressed as a nondimensional frequency, F, where

$$F = \frac{2\pi f \nu}{U_\infty^2} \quad . \tag{22}$$

Equations (18), (21), and (22) form the basis of the scaling relations for active heating. An example of how these relations may be applied to general flat plate flows, and some typical values of the parameters, are given in Appendix A.

The technique of active surface heating to excite laminar instability waves was developed in the present experiments. The method was used to demonstrate the princi-

ples of linear superposition of two sets of forced waves. A downstream heater was used to both cancel and reinforce waves input by an upstream heater. Finally, with wall shear probes as nonintrusive sensors, and a computer controlled feedback system, the use of a single strip heater to modify the amplitude of naturally occurring waves was investigated.

2 Experimental Apparatus

2.1 Initial Considerations

A flow of very high quality is required in studies of boundary layer stability and transition. Such a flow was obtained in the GALCIT High Speed Water Tunnel as discussed by Ward (1976). Although this was the prime facility used for the actual experiment, an open channel was used for preliminary experiments on a testbed flat plate that was built to verify design concepts and construction techniques.

The investigation involved two experimental phases: passive boundary layer control (steady heating) and active control (nonsteady local heating). Both aspects of the work were accomplished using a single flat plate. Initially, the plate was built with internal heaters and the necessary instrumentation for the passive control experiments. Later, the plate was reconfigured with additional instrumentation and surface-mounted heaters for the active control experiments.

2.2 High Speed Water Tunnel

The GALCIT High Speed Water Tunnel (HSWT), Figure 3, is a pressurized, vertical, closed-circuit facility. Either a two-dimensional or an axisymmetric test section may be

installed in the upper leg. The axisymmetric test section has an internal diameter of 35.6 cm (14 inch) compared to the 15.3 cm (6 inch) width of the two-dimensional section. The axisymmetric test section was chosen because it can be freely rotated through 360°. This feature was essential in the study of buoyancy effects at several different plate orientations. Edge contamination effects were also reduced by the larger diameter of the axisymmetric test section. The static pressure in the test section was variable from 0.2 bar to nearly 6 bar absolute. This feature is mainly used to trigger or suppress cavitation. Air released during cavitation is reabsorbed under pressure into solution in the resorber chamber, a large volume tank extending 25.9 m (85 ft) below the level of the test section. Since cavitation was not a concern in the experiment, the test section pressure was generally set near atmospheric. Slight pressure adjustments were used to control the flow rate of dye into the model.

Prior to conducting the boundary layer experiments, the freestream turbulence level at U_∞ = 3.1 m/sec (10 ft/sec) was measured with a conical hot film probe (TSI Model 1231). The intensity was near 0.1% on the centerline and 1.0% 5 cm (2 inch) from the test section wall (open symbols, Fig. 4). The relatively high turbulence level was primarily due to the absence of screens and the deteriora-

tion of the honeycomb in the turbulence-management section upstream of the nozzle. The test section, nozzle, and turbulence management section were stripped, sanded smooth, and refinished with epoxy paint. A new stainless steel honeycomb and 40 mesh screens were installed. The turbulence intensity was then measured to be less than 0.04% at the centerline and 1.0% 1.9 cm (0.75 inch) from the wall, as shown by the solid symbols in Figure 4. The velocity distribution (Fig. 5) in the test section is quite uniform with the velocity boundary layer confined to within 1.9 cm (0.75 inch) from the wall.

2.3 Flat Plate Model

The flat plate model consisted of an elliptical leading edge, constant thickness plate, and a trailing edge flap. The plate is 102 cm (40 inch) long, 35 cm (13.75 inch) wide, and 2.5 cm (1.0 inch) thick. The model was constructed by sandwiching five resistance pad heaters (each 15 cm (6 inch) long, 30 cm (12 inch) wide and 1.3 mm (0.050 inch) thick) between two 1.2 cm (0.47 inch) thick type 304 stainless steel flat plates, 84 cm (33 inch) long and 35 cm (13.75 inch) wide. Dow Corning silicon oil was used to ensure adequate thermal contact between the pad heaters and the plates. One plate was instrumented with an array of type J iron-constantan thermocouples and flush

mounted hot film wall shear probes (TSI Model 1268W). The thermocouples were mounted in pairs to determine local mean heat transfer rates and wall overheats. Three pairs were mounted laterally at the center of each pad heater (at the middle and at each side to determine the heating uniformity of each pad). Thus, in total, 15 thermocouple pairs were installed. Nine hot film probes were mounted flush with the plate surface as shown in Figure 6. Photographs of the interior of the plates are seen in Figure 7. The lower plate in the figure carries the thermocouple pairs and the hot film probes (the probe holders are the circular plate inserts). The exterior surfaces of both plates were ground and polished to a 10^{-5} cm rms (four micro-inch) finish. The surface waviness was less than one part per thousand with wavelengths less than 2.5 cm (1.0 inch).

The leading-edge profile is a 4:1 ellipse. Both a high quality stainless steel leading edge and a second lucite leading edge were fabricated. The latter, shown in Figure 8, was instrumented with five static pressure taps on the upper surface and a single pressure tap on the lower surface of the leading edge. In addition, two independent dye injection manifolds, with eight dye ports each, were installed in the leading edge for flow visualization. The pressure taps were connected to a fast switching Scanivalve (Datametrics model W1260) whose output was fed into a dif-

ferential pressure sensor (Datametrics model 511-10) via a water isolater (Datametrics model 552). The electrical output of the pressure transducer was converted to a pressure reading by a Barocell electric manometer (Datametrics model 1173). The static pressure upstream of the model in the test section served as the reference pressure. Passive red and blue colored dyes were bled into the boundary layer on the leading edge at a point upstream of the critical Reynolds number. The eight dye ports from each manifold were offset from each other by 0.050 in. laterally to create two color dye streak pairs. By observing these streaks one could determine the onset of three-dimensionality in the boundary layer as well as judge overall flow characteristics.

A trailing edge flap was used to position the stagnation point on the leading edge,thus varying the pressure gradient. The flap had a chord length of 15 cm (6 inch) and was made of 2024 aluminum. It was held in place with stainless steel pins which served as the rear plate supports in the HSWT test section. They also functioned as hinges for the flap. The flap was adjustable with an external arm through a flap angle, δ_f, range of +/- 6°.

The 0° flap setting was found by varying the flap angle until the stagnation point was at x = 0. This was accomplished by monitoring the pressure on the leading edge

with a single pressure tap on the lower surface and a corresponding pressure tap (at the same x location) on the upper surface. The stagnation point was defined to be at x = 0 when the pressure from the two taps was equal. The pressure distribution at $\delta_f = -5°$ is shown in Figure 9. The plate blockage ratio was 10% which assisted in keeping the velocity overshoot to a low value.

2.4 Plate Modifications for Active Surface Heating

After the completion of the passive heating experiments, flush surface mounted strip heaters were added to the plate for use in the active heating experiments. The heaters were metal ribbons 2.5 mm (0.1 inch) wide, 0.051 mm (0.002 inch) thick, spanning the width of the plate. Nichrome was used in the initial tests, but, due to bonding and corrosion difficulties, stainless steel was substituted. The resistance of the strip heaters was typically 1-2 ohms. This kept the heater voltages quite low (less than 25V), even for substantial power outputs. Since the strip heaters were in direct contact with the flow, low voltages were necessary for safety and to minimize the effects of electrolysis. A low output impedance power amplifier was designed to drive the heaters (Section 2.6).

Initially, a single strip heater was mounted on the lucite leading edge at x = 5.1 cm (2 inch) (Fig. 8). Two

additional strip heaters were subsequently flush mounted on a lucite insert (Fig. 10) downstream of the leading edge at x = 7 cm (2.75 inch) and x = 9.5 cm (3.75 inch). A spot heater, for use in preliminary three-dimensional excitation experiments, was formed by coating all but the central 1.3 cm (0.5 inch) of the back of a strip heater with a thick layer of solder. This effectively created a local region of relatively high resistance on the strip. This heater was mounted between the two strip heaters of the lucite insert at x = 8.3 cm (3.25 inch). The insert, in turn, was flush mounted on the plate.

2.5 Flat Plate Assembly and Installation

An O-ring and gasket seal between the upper and lower plates were used to provide water isolation for the internal heating pads. The thermocouple and hot film leads were taken to the side of the plate via thin slots (visible in Figure 7). The leads exited the plate through a slot in the side wall which joined a mating slot in a hollowed out pin. The pin served to locate and hold the plate in the test section. Water isolation for the wire leads was provided by the pin. The heating pad wires were grouped together on the opposite side of the plate and left the plate through a similar mating pin arrangement. The design ensured that water did not contact the internal heating pads. The sur-

face strip heater leads and the dye manifold and pressure tap lines exited through the bottom of the plate and left the test section near the rear of the plate. Care was taken in routing the wires and tubes so that this slight blockage on the lower (noninstrumented) side of the plate would not affect the flow adversely.

2.6 Heater Power Supplies

The five passive heating pads were powered by individual variable transformers. Each pad could operate at voltages up to 240V rms AC. This, however, created a strong electric field in the vicinity of the probe leads, inducing electrical noise. High-power rectifier and filter circuits were constructed to provide low-ripple DC to the heaters. This, along with some internal shielding (visible on the right side of the lower plate in Figure 7), cured the noise pickup problem.

In preliminary active heating experiments, commercial power amplifiers were used to drive the surface mounted strip heaters. All of the amplifiers had problems operating at frequencies below 10 Hz (necessary for the experiment) and/or delivering sufficient power to the low impedance heaters. To resolve these difficulties, a two channel 300 watt/channel true-DC power amplifier with a two ohm output impedance was designed and built. The initial active con-

trol experiments involved sinusoidal heating. Since Joule heating is quadratic in input voltage, it was necessary to drive the heaters at half the desired frequency. This method worked well when sinusoidal waveforms were input to the heaters at half the desired excitation frequency. In general, the technique would not work with complex waveforms. An input signal preprocessor was built in which the square-root was taken in real time of a general, DC-offset input waveform. Once amplified, the heater then squared the signal back to its original form with an inconsequential DC offset. This method allowed the input of arbitrary forcing waveforms to the flow without any distortion.

2.7 Thermocouple and Hot Film Instrumentation

The general thermocouple layout is shown in Figure 11. The thermocouples were mounted in pairs, each pair comprised of two thermocouples separated 1.3 cm (0.5 inch) laterally. One thermocouple was mounted 0.13 cm (0.050 inch) from the inner plate wall while the other was mounted 0.076 cm (0.030 inch) from the outer wall of the plate. RTV adhesive and silicon grease were used to ensure good thermal contact and electrical isolation from the plate. The heat transfer was assumed to be uniform and one-dimensional in the vicinity of each thermocouple pair. Heat fluxes and wall overheats were therefore easily determined.

Each thermocouple had two cold junctions, formed by joining the iron-constantan leads to copper wires. The cold junctions were placed inside a silicon-oil-filled test tube. The test tubes were immersed in an ice bath which was kept in a styrofoam jacketed Dewar with an inner diameter of 20 cm (8 inch). The Dewar was able to accommodate 60 reference junctions. The copper leads emerging from the Dewar were soldered onto the copper traces of the thermocouple amplifier printed circuit boards. This prevented any stray thermoelectric potentials. As shown in Figure 12, the circuit had a differential input and amplifier stage with variable gain and offset followed by a 10 Hz low pass output filter. The overall gain and offset were adjusted for linear operation (10 mv/°C) in the region of interest, 20° to 35°C. The thermocouple amplifier outputs were multiplexed in pairs to digital voltage panel meters and the readings were recorded manually.

Hot film wall shear probes were the main diagnostics used in the passive and active heating experiments. Without varying the freestream velocity, wall shear measurements could be made at five Reynolds numbers. Four wall shear probes were mounted off the centerline to measure boundary layer two-dimensionality. Transition was defined to occur when wall shear turbulent intermittency reached 50%.

Hot-film-probe calibration runs were performed at the beginning and end of each experimental session. Benchmark runs were repeated throughout the test period. In many cases, qualitative results were obtained from uncalibrated probes. For low frequency (<80 Hz) wall shear fluctuations below 5%, the probe response was nearly linear. In turbulent flow high frequencies were encountered. Brown (1967) showed that the effective streamwise length of the probe would be reduced to the measured length due to nonsteady heat transfer from the probe in the unsteady boundary layer. Although this was an easy correction, it was not made due to the qualitative nature of the turbulent wall shear recorded in the experiments. All turbulent signals plotted in this report are uncalibrated. Intermittency data were not sensitive to probe calibration.

The hot film sensors were potted flush (Elmers Hand Moldable Epoxy along with Duro Epoxy Cement and Filler) in stainless steel probe holders which were then flush mounted in the plate. They were oriented in such a way that they would resolve τ_x on the wall. Figure 13 shows a closeup of the leading probe holder, the only one having two hot films mounted in tandem. This probe arrangement was used to determine the local phase speed of the laminar instability waves.

A hot film constant temperature anemometer circuit was designed (Fig. 14). The overheat was adjusted to give a hot film operating temperature of 65°C. A standard intermittency meter design was used which employed a band-pass filter, rectifier, level detector and retriggerable one-shot. The intermittency output was a TTL digital signal. Nine complete anemometer and intermittency circuits were fabricated on individual printed circuit boards.

The nine channels of the analog wall shear signals were multiplexed to an oscilloscope and DVM. The analog data were also digitized and stored on magnetic tape (Section 2.8). The digital intermittency signals were multiplexed into a digital intermittency meter. The meter was designed to display the percent of time the wall shear was turbulent per variable unit time.

2.8 Data Acquisition

A general-purpose microprocessor-based controller system was designed for use in the experiment. It functioned as a data acquisition system, active feedback controller, and general purpose laboratory front-end instrument. The heart of the system was an Intel 8085A microprocessor. The 8085A was interfaced over the system bus to four analog to digital (A/D) converters, four digital to analog (D/A) converters, a waveform synthesizer circuit, and

a parallel processor with an arithmetic processing unit. The block diagram of the system is shown in Figure 15. Programming was accomplished by direct entry of 8085A machine code instructions using a front panel keyboard. The programs were stored in 8 kbytes of Eraseable Programmable Read Only Memory (EPROM). Data and intermediate results were temporarily stored in Random Access Memory (RAM).

Four Analog Devices eight-bit A/D converters (AD 570) were used to digitize the four channels of hot film signals simultaneously at 1 kHz. The active control experiments involved the real time analysis of the digitized wall shear data in order to synthesize input forcing waveforms used to activate the surface strip heaters. The feedback control algorithm (discussed in Section 4.6 and Appendix C) made use of the waveform synthesizer circuit to generate signals which were output to the power amplifiers via one of the four Motorola (MC3410) D/A converters. The other three D/A converters were generally connected to the x, y, and z, inputs of a Hewlett Packard 1741A oscilloscope to create a vector display of the data. This allowed multiple channels of data to be simultaneously displayed on a single oscilloscope screen. The parallel processor section used an Intel 8231 Arithmetic Processing Unit integrated circuit and 4 kbytes of RAM along with a second 8085A microprocessor, which was independent of the main system 8085A. The paral-

lel processor was available for on-line number crunching applications (i.e. spectrum analysis, data correlations, digital filtering, etc.) which would proceed in parallel with the data acquisition. A brief description of the CPU, keyboard/display, waveform synthesizer, D/A, and A/D hardware is given in Appendix B.

The entire system was interfaced to an Advanced Electronics Design 6200 LD dual 8 inch floppy disk drive unit used for intermediate mass storage of the data. The floppy disks were formatted to be directly compatible with the GALCIT HYDRA 0 computer system. This computer has a PDP 11/44 CPU and is used for general purpose data processing. The HYDRA 0 system is equipped with hard and floppy disk drives, line and daisy wheel printers, a magnetic tape unit, a vector graphics display unit, and an eight color plotter. The operating system is RT-11. The data acquired by the 8085A system were written as RT-11 files on the floppy disks, and were transferred from the floppy disks to magnetic tapes once a day during the experiment.

3 Passive Boundary Layer Control

3.1 Basic Plan

The plate was initially mounted horizontally with the heated side up. To establish the baseline transition characteristics, wall shear measurements were made of the unheated boundary layer. This determined the transition Reynolds number, $Re_{x;tr}$; in addition, it documented the laminar-turbulent transition process. The five heating pads were then run independently at varying heat fluxes. The input power levels required for various wall temperature distributions were then determined. The effect of passive heating on transition was found for two temperature distributions.

To investigate possible buoyancy effects, the test section was rotated 90° so that the plate was vertical. The heat stabilization tests were then repeated. The plate was then rotated 90° so that the instrumented side of the plate was face down. Finally, the plate was rotated an additional 90°. The instrumented side was then 180° from its initial vertical position. This was done to see if there were any asymmetries present in the plate or in the flow.

3.2 Natural Transition

The wall shear history of the transition process was recorded, beginning with steady laminar flow at $Re_x = 5 \times 10^4$. Figure 16 shows the effect of a progressive increase in the Reynolds number. T-S waves are clearly visible at $Re_x = 2.5 \times 10^5$ (Fig. 16b). The laminar instability waves undergo slow amplification for quite some distance until the onset of nonlinear wave behavior. The spikes shown in Figure 16d are characteristic of this behavior. Transition was defined to occur at $Re_x = 1.25 \times 10^6$ where the intermittency is 50%. Unit Reynolds number effects were small, but present. These were presumably due to background disturbances whose amplitudes varied with the freestream velocity. The farthest downstream probe, P6, indicated that transition occurred at $Re_{x;tr} = 1.4 \times 10^6$. The upstream probe, P0, gave a value of $Re_{x;tr} = 1.15 \times 10^6$. Probe P2, a compromise, was used in reporting transition numbers. The physics of the transition process was not discernibly altered by the slight unit Reynolds number effect.

3.3 Plate Temperature Distributions

Throughout the passive heating experiments the wall temperature distribution was observed to exhibit hysteresis effects. This was attributed to the high heat transfer

rates encountered in the turbulent boundary layer, as compared to the relatively low rates of heat transfer present in the laminar boundary layer. The transition Reynolds numbers obtained were dependent on the procedure used to set-up the wall overheat distribution under test. To standardize the startup procedure, a "laminar path" was followed in which the flow was maintained laminar at all times up to the point used to record transition. This was done by gradually increasing tunnel velocity and wall overheat to slowly approach the test conditions. Should transition occur upstream of the probe, the high turbulent heat transfer rates would prevent the wall from attaining the desired overheat, resulting in a much lower transition Reynolds number. The hysteresis effect was most notable when the laminar path was followed in the startup procedure. The heaters were shut down and then restarted after the plate had cooled. Without lowering the tunnel velocity (or varying the pressure gradient), it was impossible to reach the transition Reynolds number obtained by following the laminar path. The same effect was seen by Barker and Jennings (1977) in transition studies of the axisymmetric heated flow tube discussed in Chapter 1.

The first wall temperature profile studied was the case of constant heat flux. Two wall overheat distributions, resulting from heater power fluxes of 2.17 and

3.88 w/cm^2 (U_∞ = 3.4 m/s (11 ft/sec); plate horizontal, instrumented side up) are shown in Figure 17. At 2.17 w/cm^2 the wall overheat value fell from a value of 4°C at x = 46 cm (18 inch) to 0.5°C downstream of that point. The flow had become turbulent resulting in higher heat transfer rates and a cooler wall. Up to the point of transition, the wall temperature distribution is nearly linear. In a flat plate boundary layer, the wall overheat increases parabolically with x for constant heat flux. The plate used in this study had a slightly adverse pressure gradient which may, in part, account for the linear temperature distribution. A linear fit of the data was made that had the form:

$$T_w = T_a + \Delta T(x/L_{tr})$$

where the subscripts a and w refer to the ambient and wall temperatures respectively, ΔT is the wall overheat at transition, and L_{tr} is the transition length. The above form allows comparison with the flow tube data taken by Barker for the case of linearly increasing overheat along the length of the tube.

The second case studied was that of isothermal heating. Two overheats (4° and 8°C; plate horizontal, instrumented side up) at U_∞ = 3.4 m/s (11 ft/sec) are plotted in Figure 18. In all cases, the scatter in the Reynolds number measurements was approximately 15%.

3.4 Transition Reynolds Numbers with Heating

A reading of 50% intermittency at a hot film probe was used as an indication of transition to turbulence. As noted in Section 3.3, a drop in wall overheat also signaled transition in the uniform heating experiments. In addition, flow visualization was used as a qualitative transition indicator. Still photographs and movies were taken looking down from the top, of the plate and of the dye streaks that were bled into the boundary layer at the leading edge. The dye rapidly diffused in the turbulent region and was visible only in the laminar zones. The dye was injected into the laminar boundary layer on the leading edge at a point below $Re_{x;cr}$ where the pressure gradient was favorable. Wall shear and temperature measurements showed no significant change in the transition process when dye was injected into the boundary layer.

The effect of uniform heating on transition is shown in Figure 19. Transition is delayed by a factor of 2.5 ($Re_{x;tr,heat} = 3.1 \times 10^6$) with a wall overheat of 8.5° C at transition. There is no discernible trend for the data to differ in the three plate orientations (instrumented side up, down, and vertical). The flow tube results of Barker and Jennings (1977) show a slightly greater delay in transition, at a given overheat.

The results of isothermal heating on transition are plotted in Figure 20. There is a stronger effect on delaying transition for a given ΔT than there is when the flow is heated uniformly. A 5.5°C overheat is necessary to delay transition by a factor of 2.5 compared to a 9°C overheat at transition required by uniform heating. Once again, there is no apparent buoyancy effect introduced by varying the plate orientations. Barker and Jennings' flow tube results show the same overall trends in the data. As in the previous case of uniform heating, transition occurs later in the flow tube than it does on the flat plate for the same overheat.

3.5 Comparison with Theory

The experimental results are compared to the theory of Wazzan and Gazley (1978) which predicts transition Reynolds numbers for various Falkner-Skan wedge flows in water with isothermal heating. To account for the slight adverse pressure gradient on the plate, the Falkner-Skan parameter, β , was computed on the plate from the measured pressure distribution. The theoretical predictions are plotted (Figs. 19 and 20) for an average $\beta = -0.05$ on the

plate. The measurements show slightly lower transition Reynolds numbers than were predicted, however the overall agreement with theory is good. Barker and Jennings' flow tube had a small favorable pressure gradient ($\beta = +0.07$). Their measurements agree well with the theory up to a 5°C overheat. Since the main difference between the flat plate and flow tube experiments was the pressure gradient, the somewhat greater effectiveness of the flow tube in delaying transition for a given overheat may possibly be attributed to a favorable pressure gradient.

3.6 Discussion and Conclusions

The experiments clearly demonstrate the effects of passive heating in delaying transition to turbulence in water up to 10°C. For relatively low overheats (<4°C), there is little difference between uniform heating and a uniform temperature distribution. Above 4°C, transition is delayed by a greater amount with isothermal heating than with uniform heating. The power required to maintain a specified constant wall overheat is roughly twice that needed by uniform heating to produce the same overheat at transition. The additional power supplied to the boundary layer in the isothermal heating experiments above 4°C accounts, in part, for the lower wall temperatures required to delay transition by the same amount as achieved by uni-

form heating. Therefore, uniform heating is more efficient in producing moderate increases (<75%) in transition Reynolds number than is a uniform temperature distribution. The net power expenditure is roughly equal in both cases when transition is delayed more than 75%.

There is no indication in the present measurements that buoyancy effects had a significant role in affecting transition at moderate overheats. Wazzan et al. (1968) neglected the effects of buoyancy-driven instabilities in their theory. It was anticipated that the present experiments would show the occurrence of slightly greater transition Reynolds numbers when the boundary layer was heated from above than from any other direction. The buoyant fluid in the boundary layer would be stabilizing in this orientation, adding to the effects of passive heating. As shown in Figures 19 and 20, comparison of the data from the three orientations does not give a clear indication that any buoyancy-induced effects on transition are present. The reason may be that in the plate vertical orientation, the estimated buoyant crossflow velocities in the boundary layer were, on the average, three orders of magnitude less than the freestream velocities. Since the transit time of a fluid element in the boundary layer was short, buoyancy-induced crossflow stability effects would be expected to be minimal at the overheat and velocity configurations employed in the experiments.

The Richardson number (ratio of buoyancy to inertial forces),

$$Ri = \frac{-g\left(\frac{\partial \rho}{\partial y}\right)}{\rho\left(\frac{\partial u}{\partial y}\right)_w^2} \quad ,$$

is often taken to be an indication of the amount of density stratification present in a boundary layer flow. For the case of the boundary layer heated from above, the maximum estimated Richardson number encountered in the experiments was $Ri = 2 \times 10^{-5}$. As discussed by Schlichting (1968), stabilizing buoyancy effects may be neglected when $Ri < 5 \times 10^{-3}$ which was the case in the present experiments.

When the boundary layer is heated from below, buoyancy effects are destabilizing. Wu and Cheng (1976) predicted that buoyancy induced instability effects could be neglected when

$$(Gr_x/Re_x^{1.5}) < 100 \, ,$$

where Gr_x is the local Grashof number (ratio of the buoyancy to viscous forces),

$$Gr_x = \frac{g \Lambda \Delta T x^3}{\nu^2} \quad ,$$

and Λ is the coefficient of thermal expansion. This was experimentally verified by Gilpin et al. (1978). In the recent experiments, the maximum value of this parameter was found to be

$$(Gr_x/Re_x^{1.5}) = 2 \ ,$$

which indicates that flow stability would not be appreciably affected by buoyancy.

Barker and Jennings (1977) speculate that the difference between theory and their measurements may be due to several factors in addition to buoyancy-induced effects. They note that one such factor is that the "e^9 transition criterion may become increasingly incorrect as the unit Reynolds number is increased and the region of linear growth of disturbances vanishes". Unit Reynolds numbers in their experiments were typically 3 - 5 times greater than in the present work. Barker and Jennings also note that the Rayleigh number, based on thermal boundary layer thickness at the downstream end of their flow tube, is on the order of 1400, which may indicate that a destabilizing crossflow in the tube was present.

In conclusion, passive heating has proven to be an effective method of delaying transition on a flat plate in

water. The theory developed by Wazzan et al is successful in predicting transition Reynolds numbers under uniform temperature distributions with overheats below 5°C. Thus, for this range of overheats, the lack of observable buoyancy induced shifts in measured transition Reynolds numbers seems to justify the omission of the effects of density stratification in the theory.

4 Active Boundary Layer Control

4.1 General Approach

The technique of using surface mounted strip heating elements to excite controlled boundary layer disturbances on a flat plate in water was developed. The linearity of the instability waves was studied by artificially exciting two sets of T-S waves. One set of waves, forced by an upstream strip heater, was cancelled by a second set of downstream waves which were properly phase locked to the upstream waves. Experience gained from the forced cancellation experiments, where frequency, phase, and amplitude were known a priori, was used to plan a first attempt at active feedback control of natural T-S waves. In this stage the effect that attenuation of T-S waves had on transition was observed.

4.2 Active Surface Heating

In the Introduction (Chapter 1) it was suggested that boundary layer perturbations could readily be input if the heater width Δ was larger than the displacement thickness δ^* (Eqn 21). Velocity fluctuations input near the wall would rapidly perturb the flow in the region near δ^* which is in proximity to the critical layer (where the most unstable

waves begin to amplify). If Δ is very large, phase control would be difficult. A suggestion of a comfortable range (experimentally determined) of the parameter Δ/δ^* is given at the end of this section.

The leading strip heater, H0, was mounted on the leading edge at x = 5.1 cm (2 inch); at U_∞ = 1.2 m/sec (4 ft/sec), Δ/δ^* = 7.4. The placement of this heater relative to the neutral stability curve at U_∞ = 1.2 m/sec (4 ft/sec) is shown in Figure 21. The heater is in a slightly stable region. Also shown in Figure 21 are the locations of the two downstream strip heaters (H1 and H2) and the centerline probes (P0, P0A, P2, P4, and P6). The pair of leading probes are separated in x by 0.38 mm (0.150 inch) and are indicated by the intensified dashed line. The leading probe is P0 with P0A just behind. This is the pair used in most T-S wave phase speed determinations.

As an initial test of active heating, T-S waves were excited at the nondimensional frequency F = 1.55. At 1.2 m/sec (4 ft/sec) in water, f = 40 Hz. The instability waves travel from H0 to P0 at a constant F, which is a horizontal path on the stability diagram shown in Figure 21. The frequency F = 1.55 yields the largest integrated growth of the waves between P0 and H0 at 1.2 m/sec (4 ft/sec). The results of steady sinusoidal excitation using active heating

are shown in Figure 22. All wall shear signals and computed spectra were digitally band-pass filtered between 15 and 100 Hz unless otherwise noted. The lower trace is the square-root sine wave signal sent to the strip heater. The total rms power input to the strip heater is 25 watts ($St = 1.7 \times 10^{-5}$; the Stanton number for this experiment is defined in Equation 19). The middle trace is the wall shear response, with rms fluctuations of approximately 1%. The maximum u' velocity perturbations in the boundary layer are estimated to be 0.3% based on calculated eigenfunctions of the Orr-Sommerfeld equation. The upper trace is the unforced steady wall shear signal. The spectra of the forced and unforced cases are compared in Figure 23. Relatively weak natural waves at 46 Hz are present in both the forced and unforced cases.

Thermocouple measurements of strip heater overheats (on the testbed flat plate in the open channel) show that the maximum overheat is estimated to be 2° to 3°C. The wall temperature perturbation was immeasureable (i.e. < 0.1°C) 5Δ (1.3 cm (0.5 inch)) downstream of the heater, which is consistent with the work of Brown (1967). Brown demonstrated, analytically and experimentally, that the overheat produced by a strip heating element in a laminar boundary layer would only be significant within 2Δ of the heating strip. This is due to diffusion, and heat transfer back to the plate.

Therefore, the wall shear probes, mounted far (>50Δ) downstream of the heaters, would not be directly sensitive to the thermal activity of the strip heaters. To verify this, an experiment was conducted in which the heater was operated at constant power through a range of frequencies between 27 and 54 Hz. At both ends of this range, stability theory predicted that the waves would decay by the time they reached the leading hot film probe. The wall shear signals in Figure 24 show that the forced waves amplify at 42 Hz, and damp at 27 and 54 Hz, as predicted by theory. Since the strip heater overheat was constant throughout the range of input frequencies, the lack of response of the hot film probes at 27 and 54 Hz indicates that the probes were responding only to velocity (not thermal) perturbations in the boundary layer.

The adaptability of this technique to forcing complex waveforms is indicated in Figure 25. Sinusoidally amplitude modulated wave packets were input (lower signal, square-root waveform) by the heater. The packets are evident in the wall shear response. The experiment was repeated with varying input frequencies. Spectral analysis of the (squared) input signal to H0, and the wall shear measured by P0, indicated linear behavior of the boundary layer for moderate forcing levels (<100 watts; $<St = 7 \times 10^{-5}$). Some nonlinearity in growth and harmonic content of the waves,

due to the behavior of the boundary layer, was experienced at input levels above 125 watts. The rms wall shear fluctuations $(\tau'/\overline{\tau})_{rms}$ were 5% at the onset of nonlinear behavior. The nature of surface heating precludes the difficulties encountered with heretofore conventional techniques.

Several runs were made with H1 and H2 to determine their response in a slightly thicker boundary layer. The freestream velocities and input frequencies corresponded to those set in the H0 experiments. Even though H1 and H2 were located in a less stable region (closer to the neutral curve) than was H0, the required forcing level for the same wall shear response obtained with H0 was substantially higher. This indicated that the parameter Δ/δ^* was quite critical in choosing heater width and location. It was found from experience, with the two different flat plates operating at various unit Reynolds numbers in two facilities, that a comfortable range of Δ/δ^* is

$$2 < \Delta/\delta^* < 10 .$$

When working in this range, T-S waves were easily excited without excessive wall overheats.

4.3 Modification of Forced T-S Waves

The first application of the active heating technique was the modification of forced T-S waves with a second set of forced waves. A strip heater, H0, was used to force T-S waves. A second downstream strip heater (H1 or H2) input waves phase-locked to the upstream heater. Linearity of the T-S waves was investigated by operating the downstream heater in a manner to superpose waves in and out of phase with those driven by the upstream heater. Amplitudes of the resulting T-S waves were measured with the probes: P0, P1, and P2.

Individual responses of the upstream and downstream strip heaters were determined experimentally under identical flow conditions. H0 was operated at 12 w to input single frequency (31 Hz) T-S waves. The upper trace of Figure 26 is the wall shear signal of the waves recorded by P2. The response of H1, operating at 31 Hz, was also studied. It was found that at 30 w, H1 drove waves which grew to the same amplitude at P2 as those previously input by H0 (middle trace, Figure 26).

Waves input by the upstream and downstream heaters were superposed by operating both heaters (H0 and H1) at 31 Hz simultaneously, H0 at 12 w and H1 at 30 w. The case of in-phase reinforcement was set-up by adjusting the phase of H1, relative to H0, to maximize the amplitude of the wall

shear fluctuations at P2. The results are plotted in Figure 27. The phase relation of the input waveforms to H0 and H1 can be determined from the lower traces of Figure 27. The phase shift between H0 and H1 is $\Delta x/c_r$, where Δx is the distance between H0 and H1, and c_r is the T-S phase velocity. It happens that Δx is nearly equal to λ, the excited T-S wavelength. This accounts for the apparent in-phase relation of the input signals to the heaters. As predicted by linear theory, the amplitude of the reinforced waves is approximately double that of the waves forced by H0 alone.

Heaters H0 and H1 were run at the same frequency and power levels required for reinforcement, but with a phase shift of 180°. Figure 28 shows the result of the experiment in which probe P2 recorded nearly complete cancellation of waves input by H0. The cancelled waves result in a wall shear signal comparable to that obtained in the unforced boundary layer. The results of the forced wave interaction experiments are summarized in Figure 29 in which the spectra of the time domain signals, shown in Figures 27 and 28, are plotted. The four cases (no forcing, H0 alone, H0 + H1, H0 - H1) are normalized by the amplitude of the spectral peak corresponding to forcing with the upstream heater, H0, alone.

Experiments were also carried out using heater H2 to cancel waves input by H0. The results were similar to the previous experiments, but the power required by H2 to effect cancellation was 80 watts. The prime reason for the downstream heaters requiring greater power is that they must force waves equal in amplitude to waves already having undergone exponential growth. Also, since all of the heaters have the same width,

$$\left(\frac{\Delta}{\delta^*}\right)_{H0} > \left(\frac{\Delta}{\delta^*}\right)_{H1} > \left(\frac{\Delta}{\delta^*}\right)_{H2},$$

which indicates a decrease in the effectiveness of the downstream heaters.

4.4 Two-Dimensionality of T-S Waves

It is essential that the naturally occurring laminar instability waves are primarily two-dimensional if a single strip heater is to be effective in controlling the waves. The first line of laterally spaced probes (P1, P2, and P3) was used to determine the two-dimensionality of the natural and forced T-S waves. The probes were each spaced 7.6 cm (3 inches) apart in span, which corresponds to a separation of 5λ, where λ is the wavelength of the most unstable waves. This spacing was sufficient for an accurate indication of the T-S wave spanwise uniformity. Figure 30 illustrates the two-dimensionality of naturally occurring waves. The upper

two traces are the wall shear signals recorded by P1 and P2. The spanwise uniformity of the waves is evident from the cross correlation (lower trace, Figure 30) of the signals which are highly correlated at zero time. The two-dimensionality inherent in forced waves (excited by H0) is seen in Figure 31. The degree of spanwise correlation of the forced waves is slightly higher than in the unforced case. Both natural and forced waves are highly phase coherent, as well as two-dimensional, as shown in Figures 30 and 31.

4.5 The Active Control Approach

A single strip heater, H0, and a single hot film probe, P0, were used to actively control the naturally occurring T-S waves. In active control terms, the heater was the actuator and the hot film probe was the sensor. Since the sensor was downstream of the actuator, the arrangement could be thought of as a feed-forward control system. A traditional approach would have involved the probe being placed upstream of the heater for direct feedback. Due to the requirement that the heater be within the suitable range of Δ / δ^*, it was located in a slightly stable region (figure 32). The natural waves were quite weak at this location, requiring an extremely sensitive hot film anemometer. This necessitated the placement of the

probe in the unstable region where larger amplitude waves would be present.

The overall layout of the feedback control loop is depicted by the block diagram of Figure 33. The probe and hot film anemometer produced a wall shear signal which was passed to the 8085 microprocessor controller and data acquisition computer system. The computer digitized the analog wall shear input and, using a feedback control algorithm, synthesized an input signal for the strip heater. This signal was fed into the power amplifier which drove the heater. The waves driven by the heater were superposed with the naturally occurring T-S waves. The probe, acting as an error sensor, measured the modified wall shear, thus closing the loop.

4.6 The Feedback Algorithm

The algorithm developed for use in the feedback control experiments was intuitively based, and met the criteria of stability, simple structure, and easy implementation. No effort was made at formulating an optimal control algorithm for the first attempt at active control. In the approach taken, it was assumed that the natural T-S waves were two-dimensional and linear. The waves were taken to be somewhat band-limited, (i.e. the full width half maximum of the spectral peak was less than 0.1 octave) due to the process by

which waves selectively amplify in the boundary layer. The initial tunnel disturbance spectrum was rather broad band with no strong peaks. The integrated growth of the waves from H0 to P0 was such that only a limited range of frequencies were selectively amplified by the time the waves reached P0. It was further supposed that the wave amplitude fluctuations were small (peak fluctuations less than 25% of the mean amplitude) and that the mean flow parameters were invariant during a given active control run. All of the above assumptions, with the exception of linearity, were verified in previous experiments. This approach allowed the natural T-S waves to be treated as having a single frequency component, constant amplitude, and slowly varying phase.

Simply put, the feedback algorithm determined the mean frequency and amplitude of the natural waves measured by a single probe (P0). A strip heater (H0), upstream of the probe, was used to force waves at the same mean frequency and amplitude as the naturally occurring waves. Phase lock between the forced and natural waves was maintained by periodic impulsive phase updates.

To attenuate the natural waves, the phase of the forced waves, input by H0, was maintained 180° out of phase with the natural waves at H0. To reinforce the natural waves, the phase of the forced waves was maintained in phase with the natural waves.

The detailed steps of the feedback algorithm are listed below.

Step 1. The forcing input amplitude required to excite waves equal to the mean amplitude of the naturally occurring T-S waves was experimentally determined. This was accomplished by first measuring the amplitude of the natural waves and then sinusoidally forcing waves near their frequency. A beat pattern resulted due to the linear superposition of the forced and natural waves. The amplitude of the driving signal was varied manually until the maximum amplitude in the beat pattern was twice that of the unforced waves (indicating 100% reinforcement). The minimum amplitude in the beat signal would then be near zero indicating occasional cancellation. The forcing amplitude, A_0 , to achieve this condition was recorded.

Step 2. The 8085 microcomputer system determined the mean frequency , $\bar{\omega}$, of the natural waves. This was done by counting zero crossings of the digitized high pass filtered wall shear signal. (After the experiments reported here were concluded, a Fast Fourier Transform (FFT) algorithm was incorporated into 8085 microcomputer for on-line spectral analysis). The phase speed, c_r, of the waves was determined using probes P0 and P0A. Probe P0A was used only to determine c_r (which does not vary significantly between

the heater and probe), and not as an error sensor in the feedback loop.

Step 3. The wavelength, λ, of the T-S waves was computed from the values obtained in Step 2. The total phase shift, Φ, between the actuator and probe was obtained;

$$\Phi = \frac{2\pi L}{\lambda} = 2n\pi + \phi$$

where L is the distance between H0 and P0 (6 inches) and $\phi < 2\pi$.

Step 4. An input wave, $A_0 \sin \bar{\omega} t$, was then synthesized at arbitrary initial time with strip heater H0.

Step 5. The naturally occurring waves at P0 were reconstructed by subtracting the synthesized input signal (with suitable amplitude and phase corrections) from the output of P0 which was the summation of the forced and natural waves. This subtraction was initially performed using analog circuitry designed for the task. The feedback algorithm was subsequently modified so that the subtraction would be accomplished digitally; however, this modification was not implemented during the experimental runs reported here. Typically, six positive going zero crossings of the reconstructed natural waves were counted, which formed the delay in the loop.

Step 6. As the last zero crossing was sensed, the phase of the input signal to the strip heater was set to $\pi - \phi$ for cancellation (or $2\pi - \phi$ for 100% reinforcement).

Step 7. Step 5 was then performed.

The feedback loop was comprised of Steps 5 and 6. The loop delay built into Step 5 allowed the modified waves to propagate from H0 to P0 so that the effect of the previous phase update could be judged at one time. The phase of the natural waves generally varied less than $\pi/6$ radians during the loop delay period. This variation did not significantly affect the feedback control experiments.

Note that Figure 32 has an open circle on the solid vertical line, corresponding to the position of H0, and a horizontal arrow pointing towards a left brace spanning a portion of the dashed line (P0). The brace indicates the range of naturally occurring waves measured at P0. The open circle signifies the single forcing frequency input by the heater, and the rightward pointing arrow portrays the path of the forced waves from H0 to P0. A brief description of the algorithm implemented by the 8085 microcomputer system, along with the 8085 assembly language listing, is given in Appendix C.

4.7 Active Control of Laminar Instability Waves

Naturally occurring T-S waves were recorded at sensor P0 at U_∞ = 4 ft/sec, Re^* = 850. The waves are seen in the lower trace of Figure 35a. The amplitude fluctuations

are small and the waves are band-limited. The waveform satisfies the feedback control requirements set forth in Section 4.6. The upper trace in Figure 35a is the input voltage to the strip heater. Since this is the unforced case, the signal is a straight line. The strip heater power required to force waves equal in amplitude to the naturally occurring waves was experimentally determined to be 10 watts.

The initial experiment was the attempt to cancel naturally occurring waves. The microprocessor computer was programmed with the feedback algorithm to maintain the forced waves 180° out of phase with the natural waves. The results are presented in Figure 35b. The upper trace is the synthesized square-root sine-wave input signal to H0. The impulsive phase updates occur every six periods. The lower trace is the total wall shear signal recorded by P0. A marked decrease in the wall shear is evident by comparison with Figure 35a. The average rms wall shear fluctuations are a factor of 2 - 3 lower than the perturbations due to the natural waves. The feedback control system was completely stable, with runs typically lasting five minutes.

Amplitude modulation of the waves is present in the signal. These wave packets were due to two effects:

a) After a phase update for cancellation, the control signal phase did not change for six subsequent wave peri-

ods. During this time the phase of the natural waves drifted slightly creating a beat waveform.

b) The boundary layer had a slight response to the impulse introduced by the rapid phase shift.

A brief experiment was conducted to investigate the impulse response of the boundary layer. Exploiting the low thermal inertia of the strip heaters, an impulse 5 ms wide was input to H0. The peak impulse power was set at 200 watts, which was much greater than the effective impulse power levels present (due to impulsive phase updates) during the active feedback control experiments. The boundary layer response is seen in Figure 34. The four wall shear traces form an x-t diagram of the boundary layer response. The impulse is input at t = 0, indicated by the heavy vertical arrow at the origin. The lower trace is the wall shear recorded by P0, the error sensor probe used for active control. A very weak wave packet is formed starting at t = 0.3 sec. (The power levels of the impulsive phase updates encountered in the feedback control experiments were an order of magnitude less than the 200 watts used in this experiment). The upper three traces in Figure 34 record the subsequent nonlinear growth of the packet which eventually forms a turbulent spot.

The second active control experiment was the attempt to reinforce the naturally occurring waves. The feedback

controller was programmed for in-phase forcing. The amplitude of the natural waves was measured to be the same as in the cancellation experiments; the power was again set at 10 watts. The lower trace of Figure 35c is the wall shear signal of the reinforced waves. The average amplitude of the reinforced waves is approximately twice that of the natural waves.

The effect of attenuating the amplitude of the natural waves on transition was demonstrated using flow visualization. Dye was injected at the leading edge into the boundary layer. One-second time exposures were taken of the optically dense dye streaks against the light planform background of the plate. Any unsteadiness in the boundary layer, as well as turbulent diffusion, would prevent the streaks from registering on the film. Transition was said to occur on the plate at the point where the dye streaks were no longer visible. Photographs, looking down on the plate, are shown in Figure 36. The flow is left to right, and the flow conditions are identical to those in the feedback control experiments discussed above. Figure 36a shows natural (unforced) transition at $Re_{x;tr} = 8 \times 10^5$. Figure 36b corresponds to the case of active natural T-S wave attenuation with a 25% increase in transition length. Active reinforcement of the waves decreases the transition length by 25% (Figure 36c).

4.8 Conclusions

The idea of active surface heating has appeared, from conception through development, and on to initial applications as a highly desirable technique for use in the laboratory environment. The prime reasons for choosing this technique (nonintrusiveness, the property that arbitrary temporal and spatial disturbances may be input, and ease of use) have since been borne out by experience in the lab. The method of active surface heating allowed active control to be used, for the first time, in a turbulence related problem.

To summarize the results of the active heating experiments, periodic surface heating by thin flush mounted heating elements was used to input perturbations into the boundary layer. The strip heating elements were used to input sinusoidal and complex temporal waveforms, as a demonstration of the flexibility of the surface heating technique. Sinusoidally excited waves, as well as naturally occurring laminar instability waves, were shown to be highly two-dimensional and phase coherent. An experiment was performed in which two strip heaters, one upstream of the other, were operated simultaneously. It was shown that by properly phasing the waves excited by the two strip heaters, it was possible for the downstream heater to reinforce, or cancel, the waves input by the upstream heater by simple

linear superposition of the waves. Finally, a single strip heater and probe were used in a computer controlled feedback loop to actively attenuate naturally occurring laminar instability waves. This resulted in a significant delay of boundary layer transition to turbulence.

The active-control approach gave the opportunity to investigate the effects on transition of attenuating the developing perturbations in the boundary layer. The previous attempt to delay transition using passive heating (Chapter 3), in which the mean velocity profile was modified, required 1900 watts ($St = 1.3 \times 10^{-3}$) to achieve a 25% increase in $Re_{x;tr}$. Under identical flow conditions, the same delay in transition was accomplished with active control using only 10 watts ($St = 7 \times 10^{-6}$) of power. Thus, in dealing with the instability mechanism alone, over two orders of magnitude less power was needed to obtain the same result.

A preliminary experiment was conducted to utilize the capability of a surface spot heater to introduce controlled three-dimensionality into the boundary layer. The spot heater, discussed in Section 2.3, and located at $Re_x = 1 \times 10^5$, was used to excite turbulent spots. Flow visualization, along with wall shear measurements, verified that spots were fully formed at $Re_x = 7 \times 10^5$. Preliminary wall shear data analysis indicated that oblique waves

were present in the boundary layer, upstream of the spots. A natural application of active surface heating would be the use of discreet heating elements in arrays, both linear and two-dimensional. Arrays would be useful to excite and modify three-dimensionality in the laminar and turbulent boundary layers. Such arrays are presently under development.

An obvious use of active heating is its use as a transition fixing, or boundary layer tripping device. It has been repeatedly demonstrated in the present experiments that open loop forcing on the flat plate lowers the transition Reynolds number throughout a wide range of freestream velocities and pressure gradients. Artificially generated T-S waves have been noticed by others to have a transition Reynolds number lowering effect, but the excitation methods used were mechanical. Active surface heating is, at present, unique in its ability to be readily engaged, with no effect on the flow while disengaged. In addition, it is a highly quantitative technique, as opposed to various intrusive mechanical methods. These advantages circumvent many of the difficulties encountered with boundary layer tripping devices found on flat plates, airfoils, and other bodies. The use of active heating, mainly as an experimental tool, seems quite attractive in a wide variety of flows.

REFERENCES

Barker, S. J., and C. Jennings (1977) On the Stability of the Water Boundary Layer in a Heated Tube, "Proc. of the NATO - AGARD Symp. on Laminar-Turbulent Transition", Copenhagen.

Blasius, H. (1908) The Boundary Layers in Fluids with Little Friction, NACA TM 1256.

Brown, G. L. (1967) Theory and Application of Heated Films for Skin Friction Measurement, Proc. of the 1967 Heat Transfer and Fluid Mech. Inst., 361 - 381.

Burgers, J. M. (1924) The Motion of a Fluid in the Boundary Layer along a Plane Smooth Surface, Proc. 1st Int. Cong. Appl. Mech., Delft, 113.

Dryden, H. L. (1934) Boundary Layer Flow near Flat Plates, Proc. 4th Int. Cong. Appl. Mech., 175.

Heisenberg, W. (1924) On Stability and Turbulence of Fluid Flows, NACA TM 1291.

Gilpin, R. R., H. Imura, and K. C. Cheng (1978) Experiments on the Onset of Longitudinal Vortices in Horizontal Blasius Flow Heated from Below, J. Heat Transfer, vol. 100, 71 - 77.

Klebanoff, P. S., K. D. Tidstrom , and L. M. Sargent (1962) The Three-Dimensional Nature of Boundary-Layer Instability, J. Fluid Mech., vol. 12, 1 - 34.

Liepmann, H. W. (1943) Investigation of Boundary Layer Transition on Curved Boundaries, NACA rep. 3H30.

Liepmann, H. W., and G. H. Fila (1947) Investigations of Effects of Surface Temperature and Single Roughness Elements on Boundary Layer Transition, NACA Rep. 890.

Liepmann, H. W., G. L. Brown, and D. M. Nosenchuck (1982), Control of Laminar Instability Waves Using a New Technique, J. Fluid Mech., vol. 118, 187 - 200.

Liepmann, H. W., and D. M. Nosenchuck (1982), Active Control of Laminar-Turbulent Transition, J. Fluid Mech., vol. 118, 201 - 204.

Lin, C. C. (1945) On the Stability of Two-Dimensional Parallel Flows, Pt. 1 General Theory, Q. Appl. Math, vol. 3, 117 - 142.

Loehrke, R. I. (1970) Stimulated Temperature and Velocity Perturbations in a Laminar Boundary Layers, Ph.D. Thesis, Illinois Institute of Technology.

Lowell, R. S. (1974) Numerical Study of a Heated Water Boundary Layer, Ph.D. Dissertation, Case Western Reserve University.

Orr, W. M. F. (1907) Proc. R. Irish Acad., vol. 27, 1 - 138.

Prandtl, L. (1921) Bemerkungen uber die Entstehung der Turbulenz, Z. Angew. Math. Mech., vol. 1, 431 - 436.

Pretsch, J. (1942) The Excitation of Unstable Perturbations in a Laminar Friction Layer, NACA TM 1343.

Rayleigh, Lord (1880) "Scientific Papers", vol. 1, Dover, New York.

Saric, W. S., G. A. Reynolds, D. L. Weber, and P. Konstadinopoulos (1979) Dynamic Response of a Vibrating Ribbon for Boundary Layer Stability Experiments, V.P.I. and S.U. rep. no. VPI-E-29.29.

Schlichting, H. (1932) Ann. Phys. Leipz., vol. 14, 905 - 936.

Schlichting, H. (1968) "Boundary Layer Theory", 6th ed., McGraw Hill, New York.

Schubauer, G. B., and H. K. Skramstad (1947) Laminar Boundary Layer Oscillations and Stability of Laminar Flow, J. Aero. Sci., vol 14., 68 - 78.

Sommerfeld, A. (1908) Atti. Fourth Congr. Int. Math., Rome, vol. 3, 116 - 124.

Smith, A. M. O. (1957) Transition, Pressure Gradient, and Stability Theory, Proc. 9th Int. Congr. on Appl. Mech., Brussels, vol. 4, 234.

Strazisar, A. J., E. Reshotko, and J. M. Prahl (1977) Stability of Heated Laminar Boundary Layers, J. Fluid Mech., vol. 83, 225 - 247.

Stuart, J. T. (1979) Stability and Transition, Some Comments on the Problems, in: "Laminar - Turbulent Transition", (R. Eppler and H. Fasel, eds.), IUTAM Symposium, Stuttgart, 1 - 13.

Tollmien, W. (1929) The Production of Turbulence, NACA TM 609.

Ward, T. M. (1976) The Hydrodynamics Laboratory at the California Institute of Technology - 1976, Trans. ASME, December 1976, 740 - 748.

Wazzan, A. R., and C. Grazley, Jr. (1978) The Combined Effects of Pressure Gradient and Heating on the Stability and Transition of Boundary Layers in Water, The Rand Corp., rep R-2175-ARPA.

Wazzan, A. R., T. Okamura, and A. M. O. Smith (1968) The Stability of Water Flow Over Heated and Cooled Flat Plates, J. Heat Transfer, vol. 90, No. 1, 109 - 114.

Wazzan, A. R., T. Okamura, and A. M. O. Smith (1970) The Stability and Transition of Heated and Cooled Incompressible Laminar Boundary Layers, Proc. Heat Transfer, Int. Heat Transfer Conf., Versailles, vol. 2.

White, F. M. (1974) "Viscous Fluid Flows," McGraw Hill, New York.

Wu, R S., and K. C. Cheng (1976) Thermal Instability of Blasius Flow along Horizontal Plates, Int. J. of Heat and Mass Transfer, vol. 19, 907 - 913.

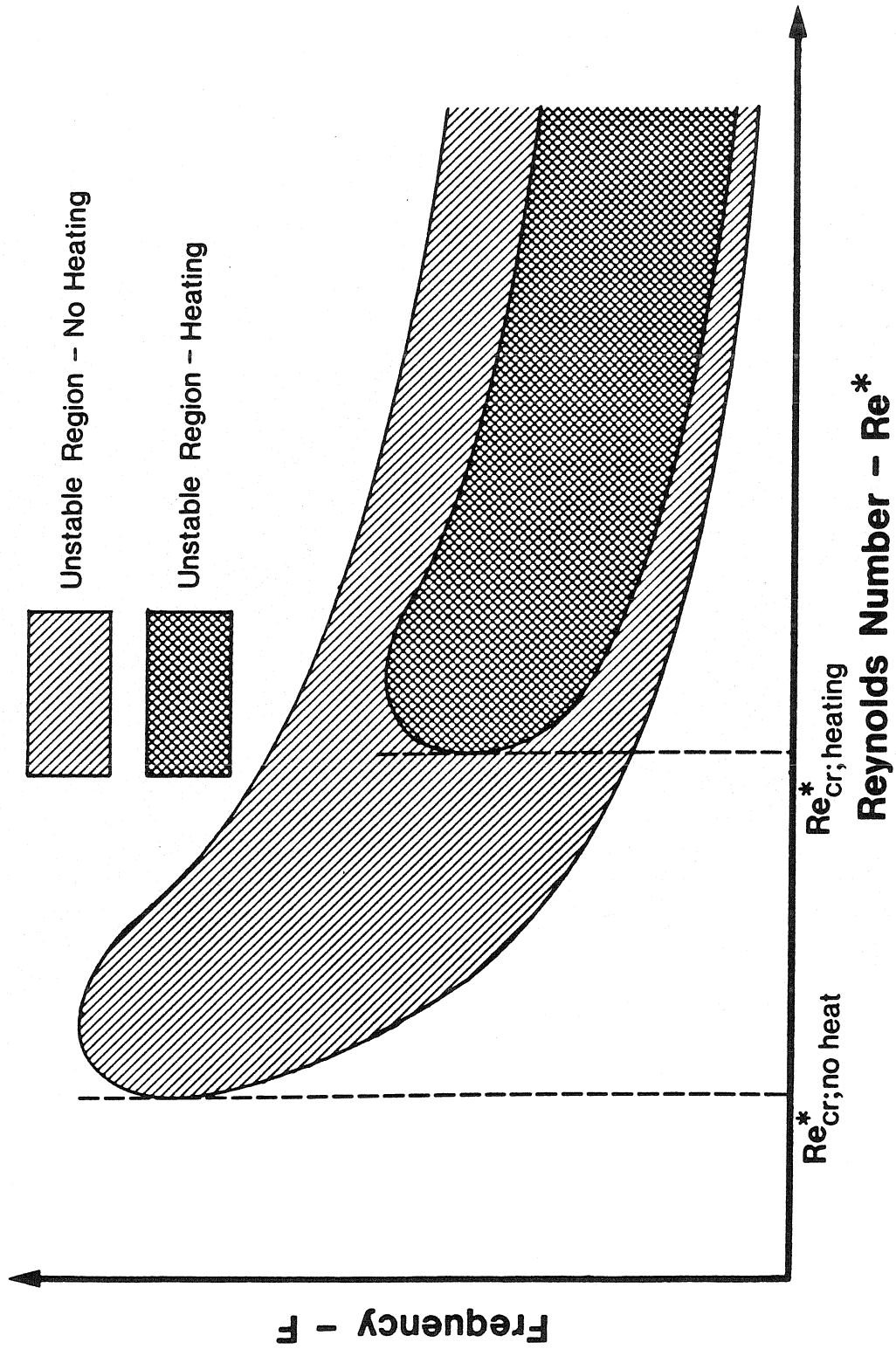

Figure 1. Effect of Passive Heating in Water on Boundary Layer Stability

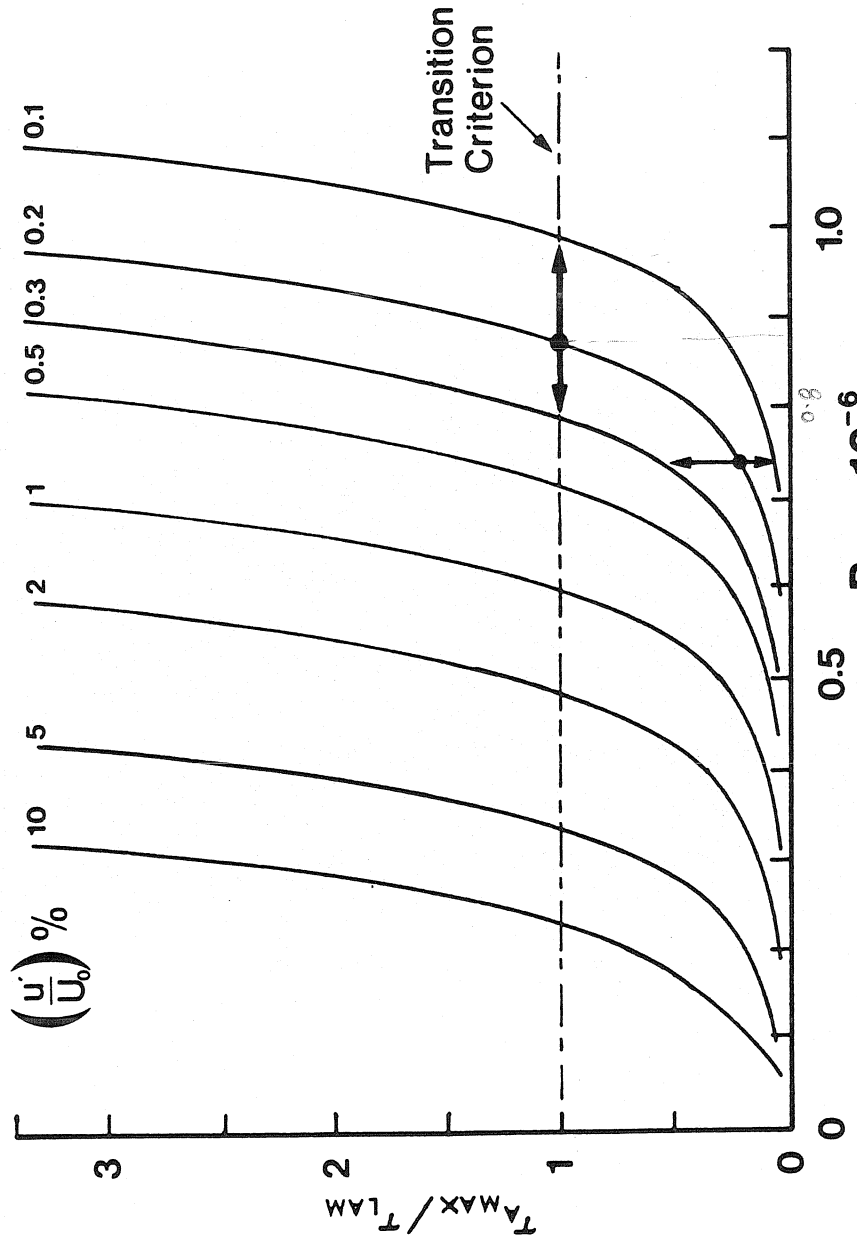

Figure 2. Effect on Boundary Layer Transition of Controlling the Amplitude of the Laminar Instability Waves

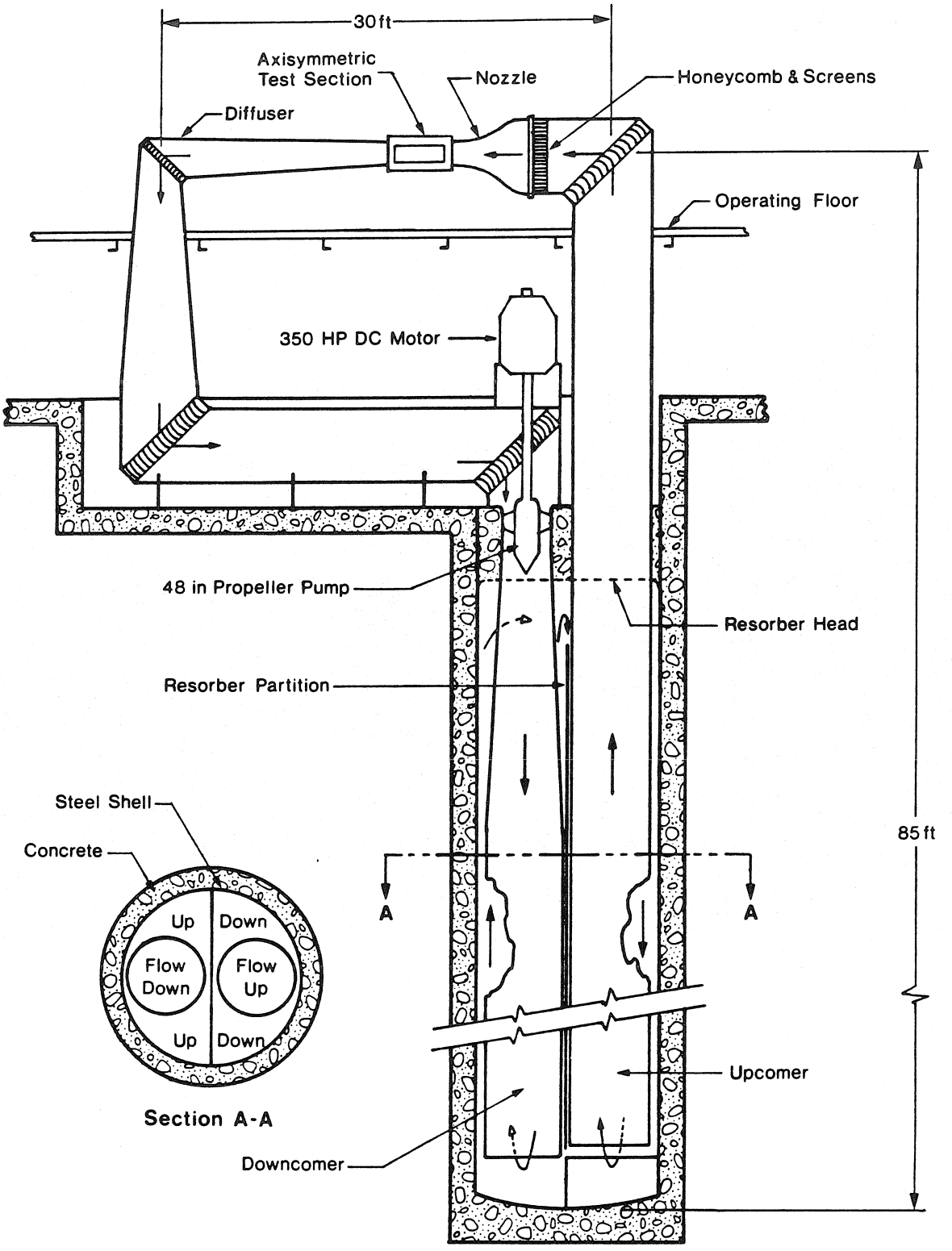

Figure 3. HSWT Layout

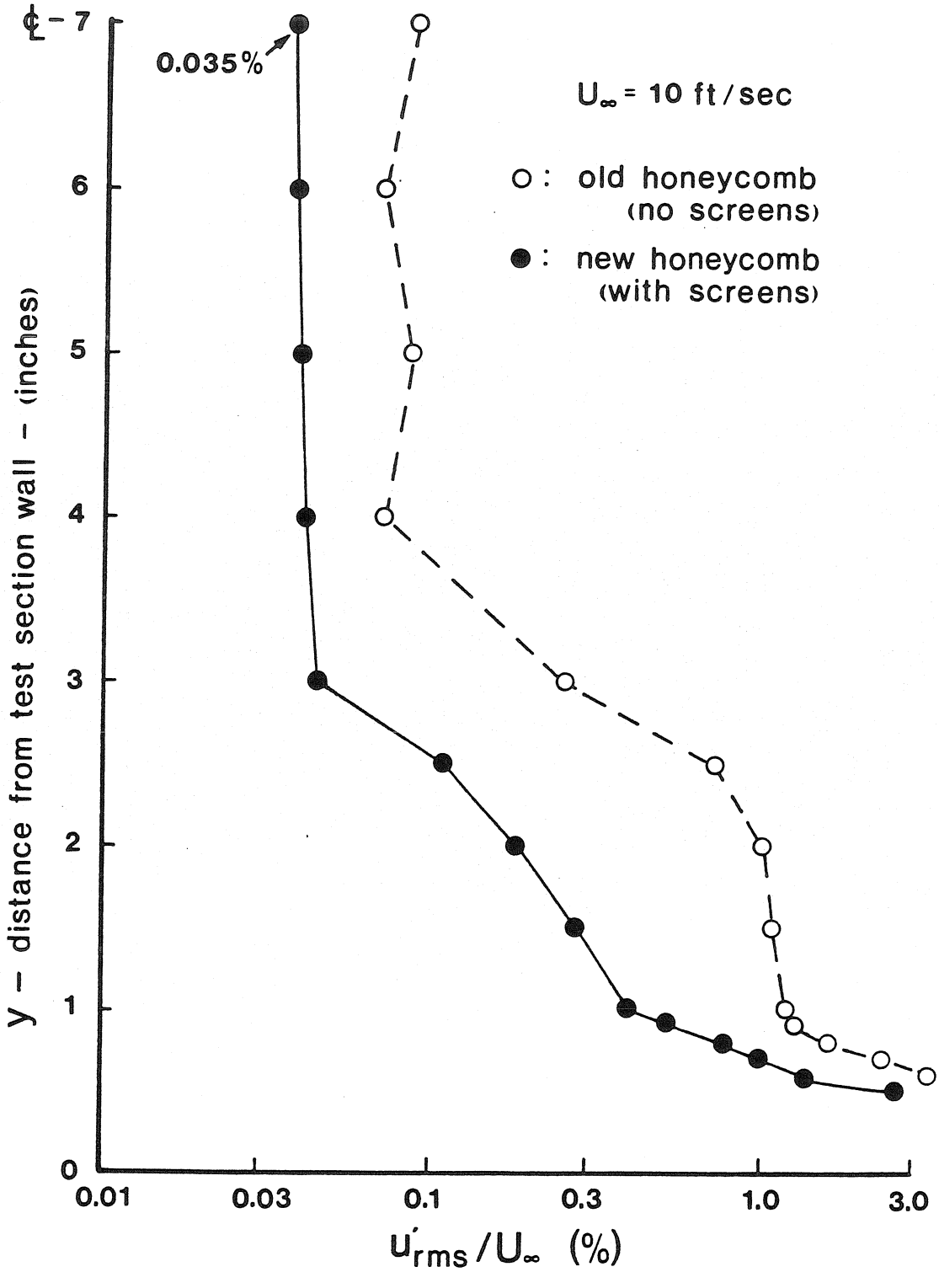

Figure 4. HSWT Turbulence Intensity Distribution in the Axisymmetric Test Section

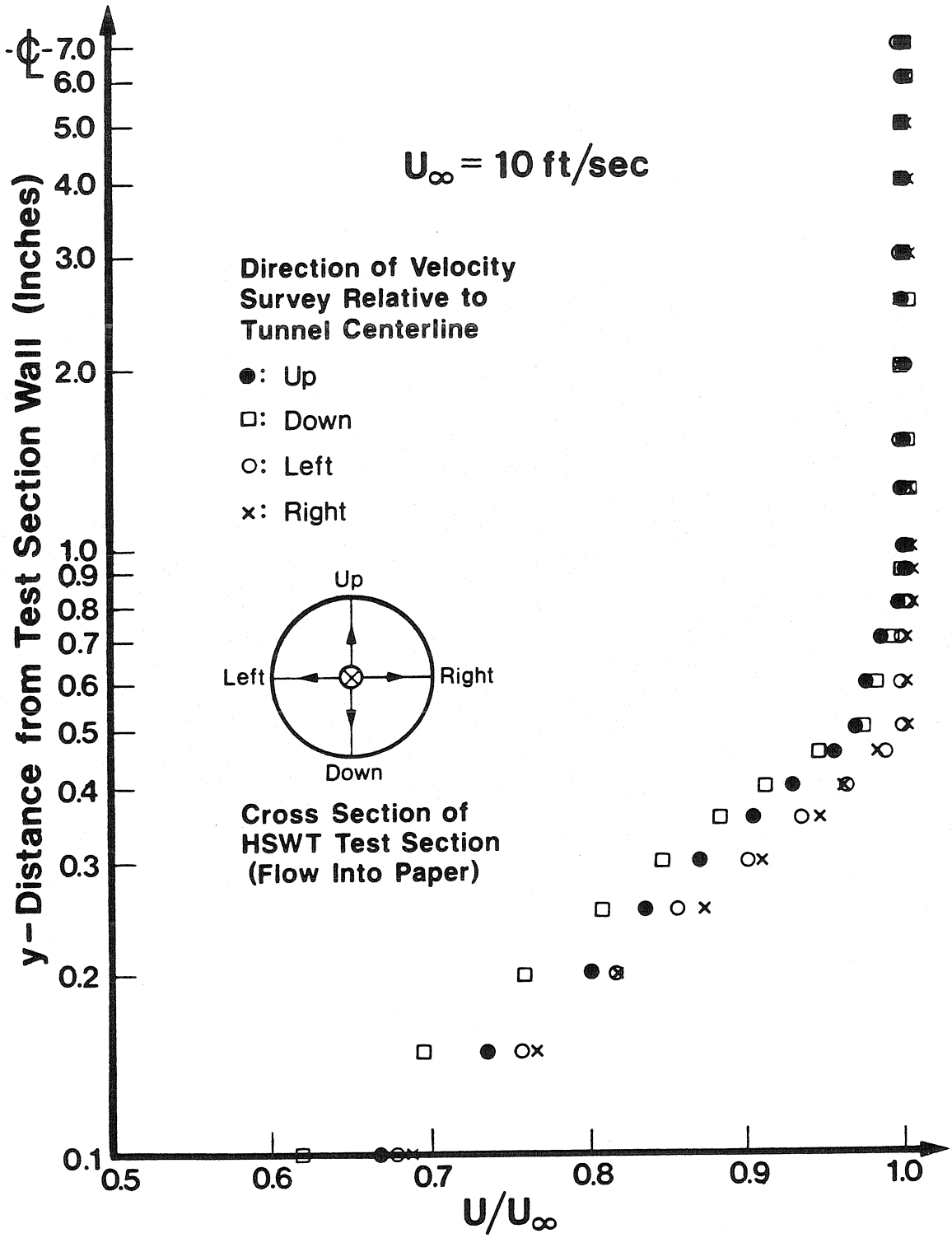

Figure 5. HSWT Velocity Distribution in the Axisymmetric Test Section

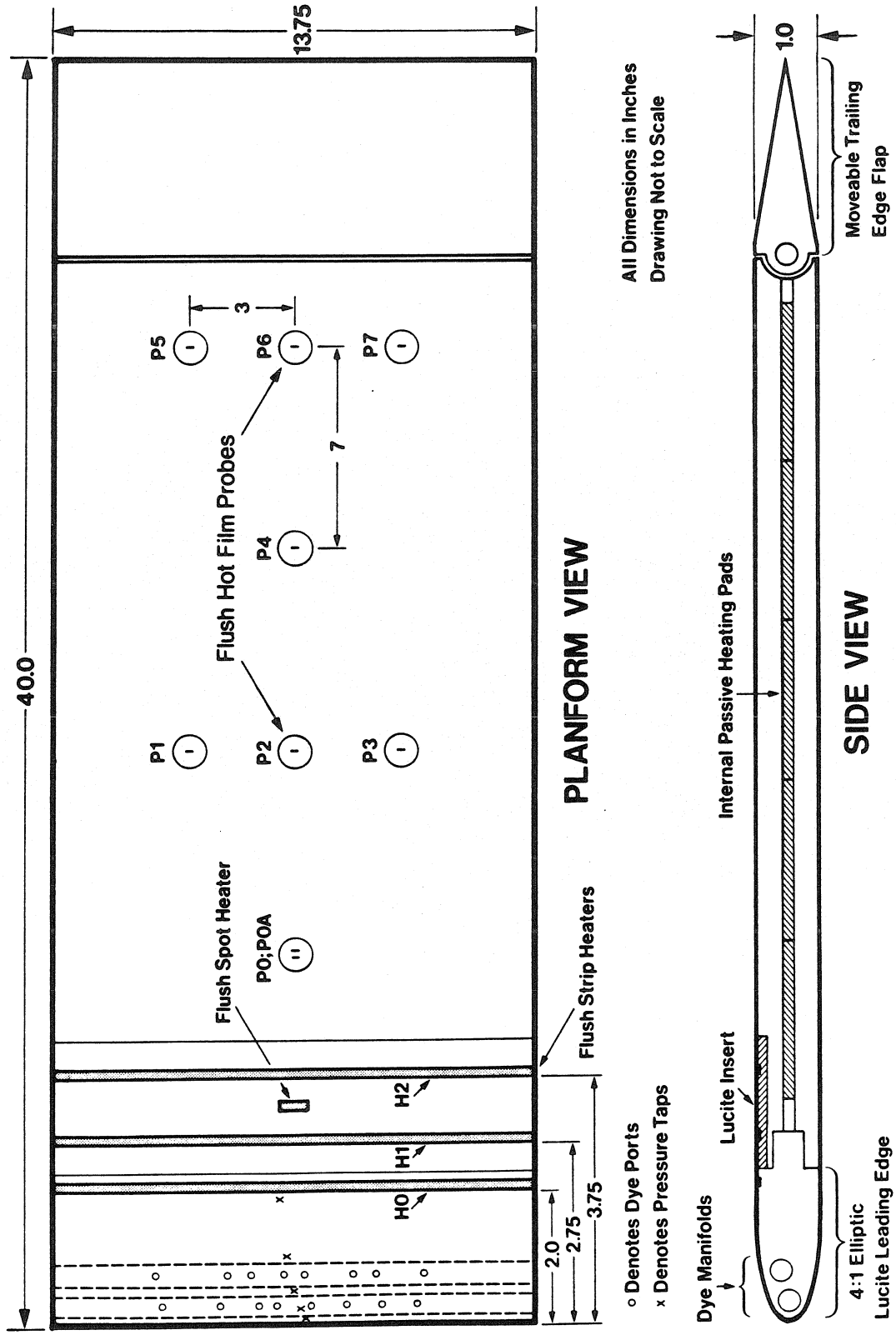

Figure 6. Flat Plate and Hot Film Probe Array Layout

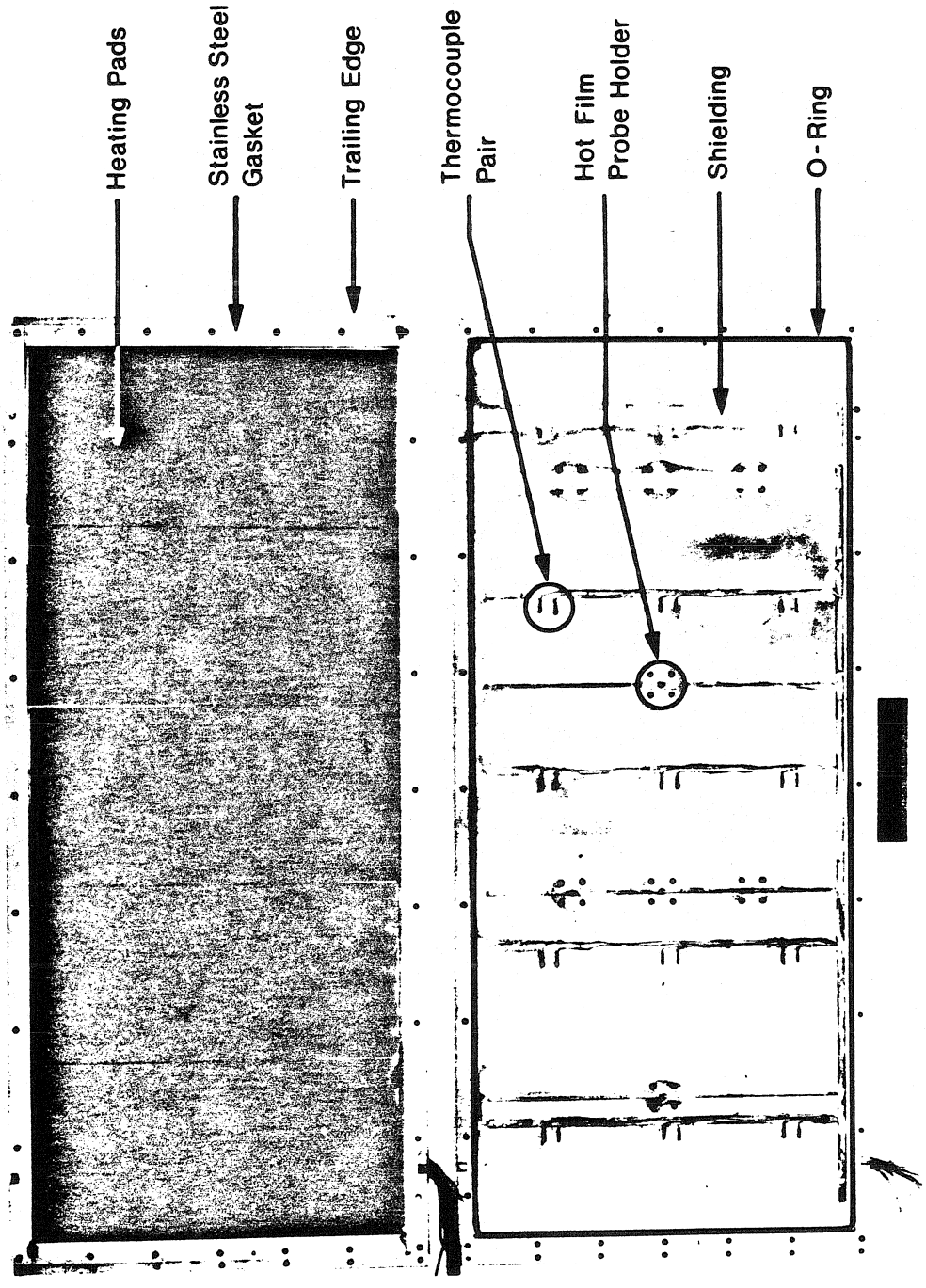

Figure 7. Interior Photograph of Disassembled Plate

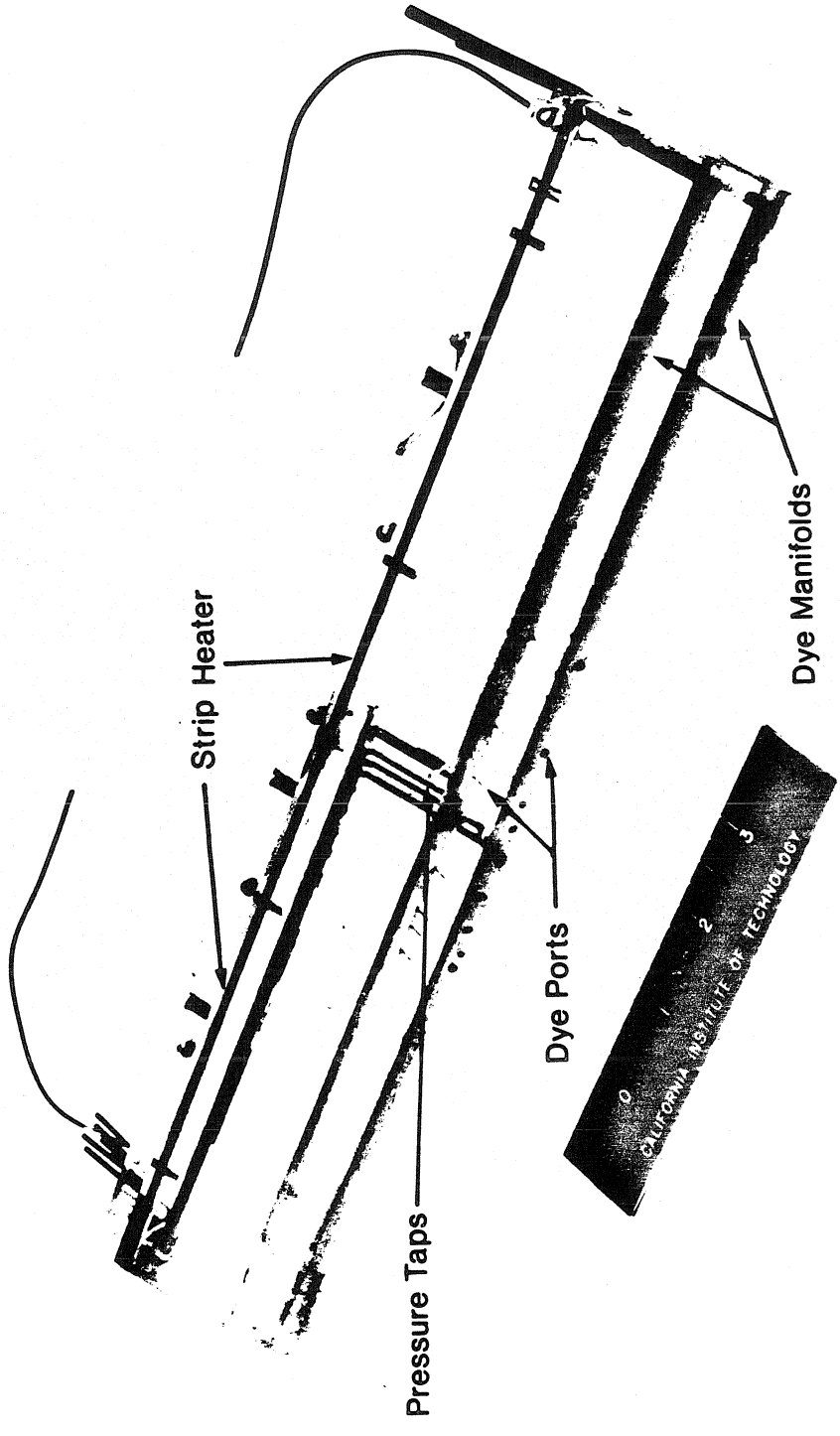

Figure 8. Lucite Leading Edge

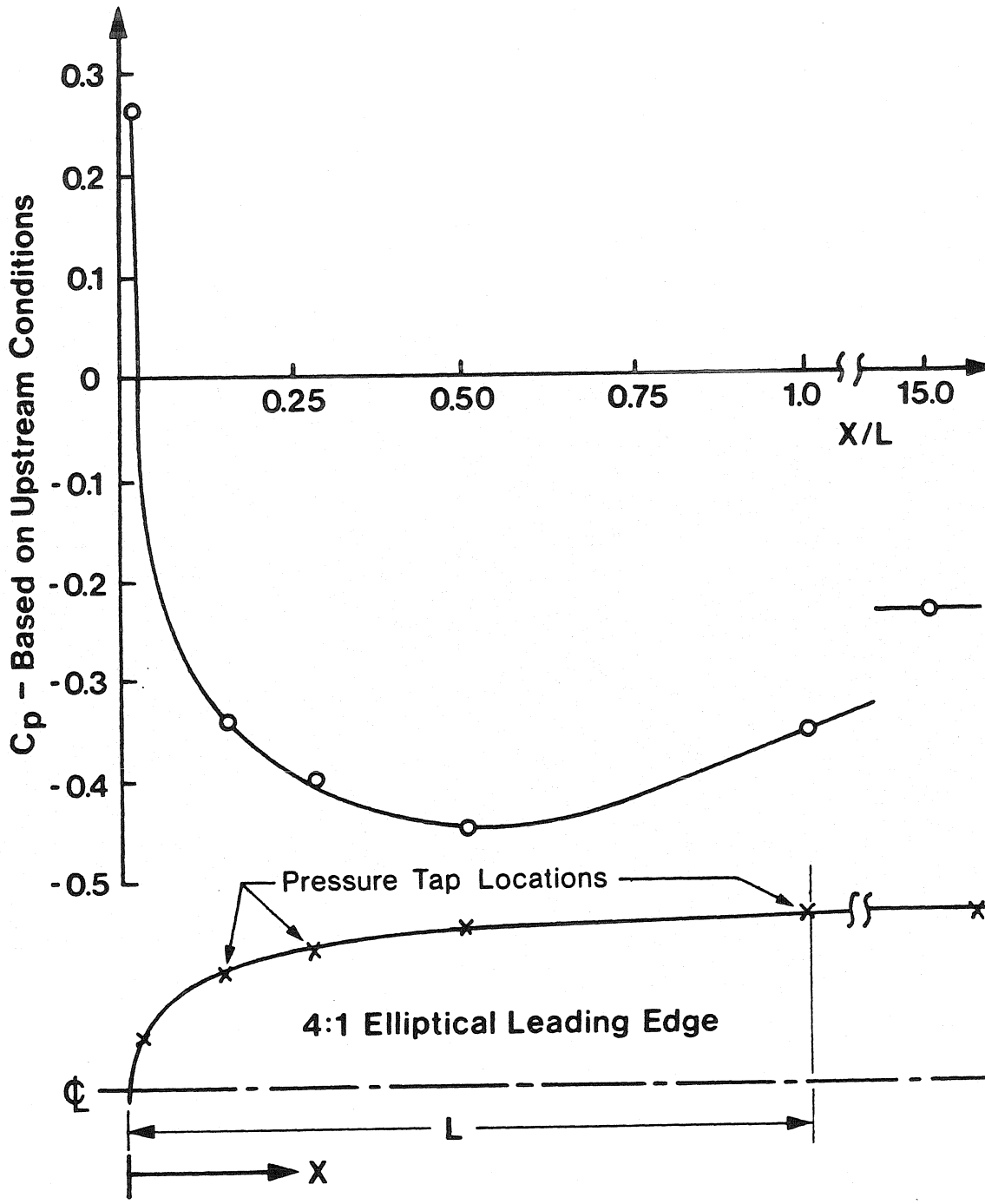

Figure 9. Static Pressure Distribution

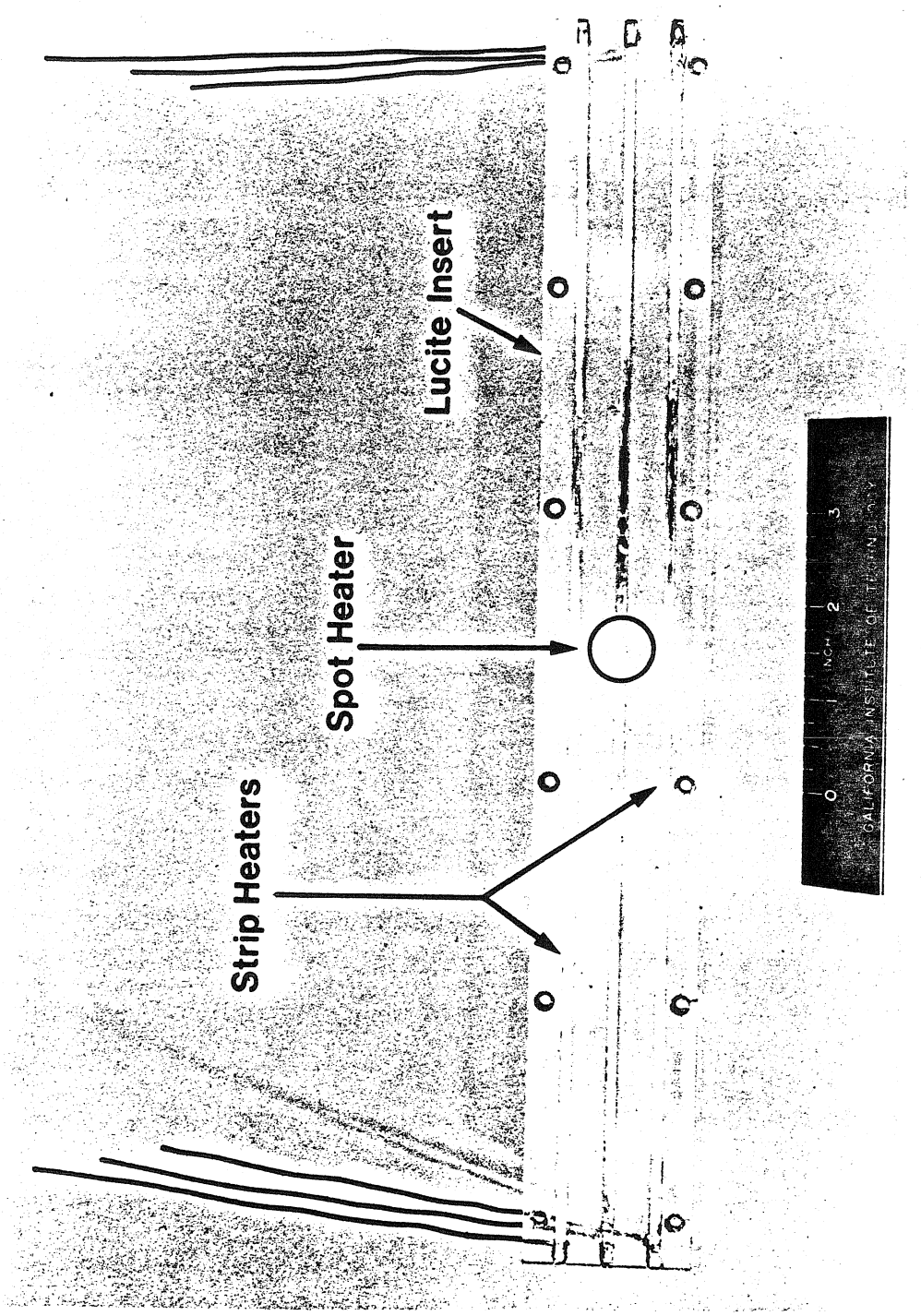

Figure 10. Strip Heater Insert

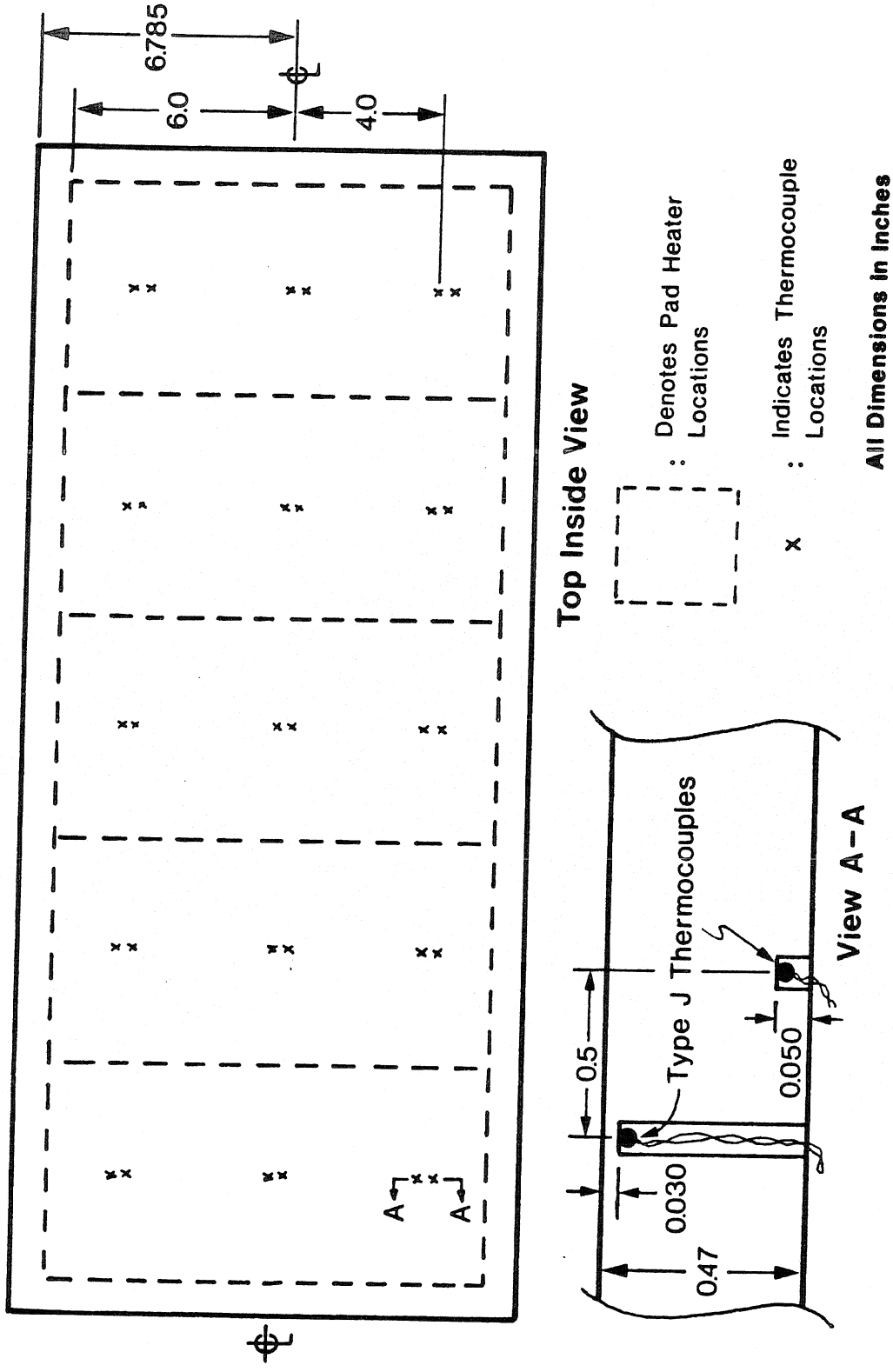

Figure 11. Thermocouple Array Outlet

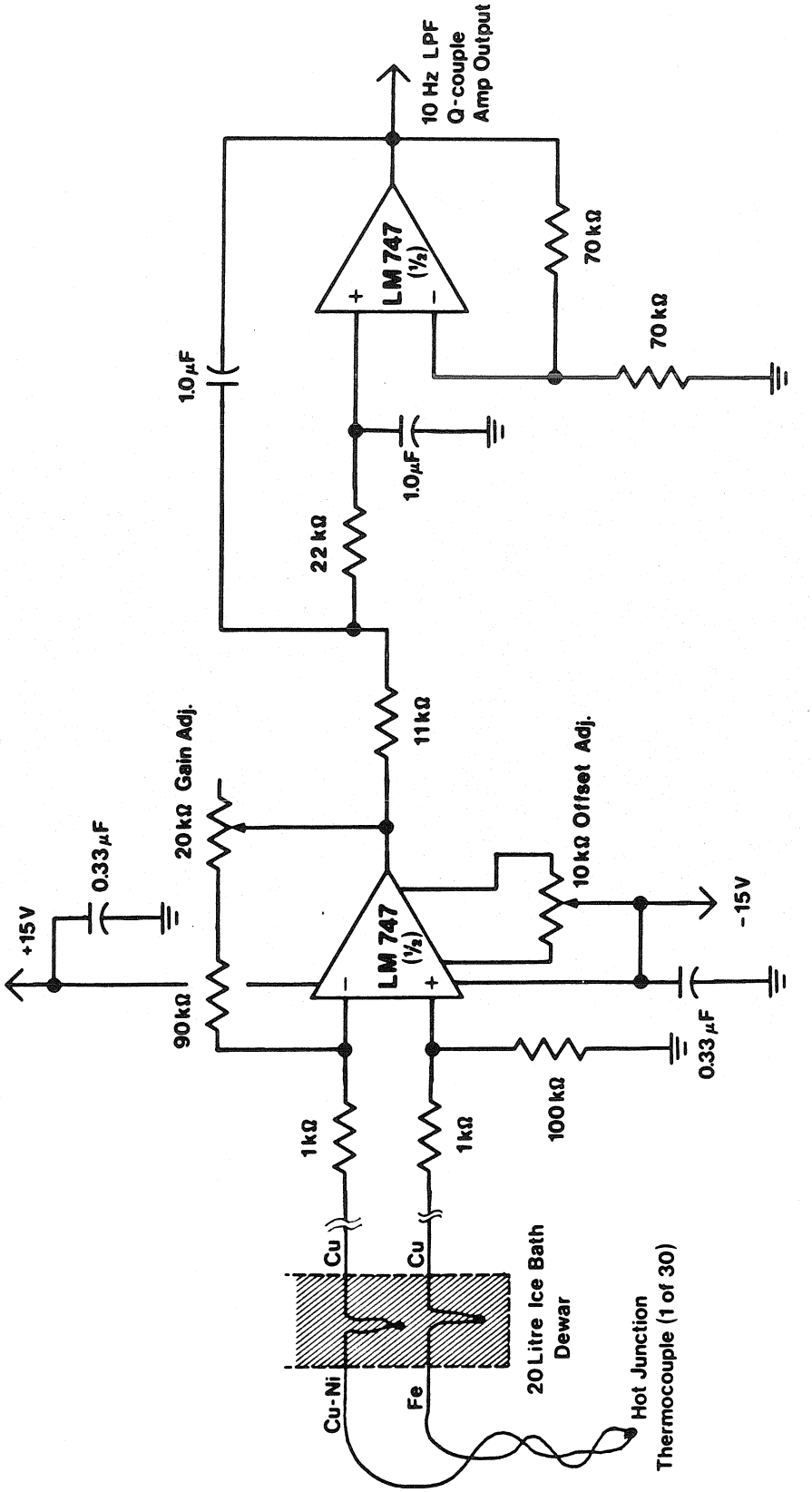

Figure 12. Thermocouple Amplifier Circuit

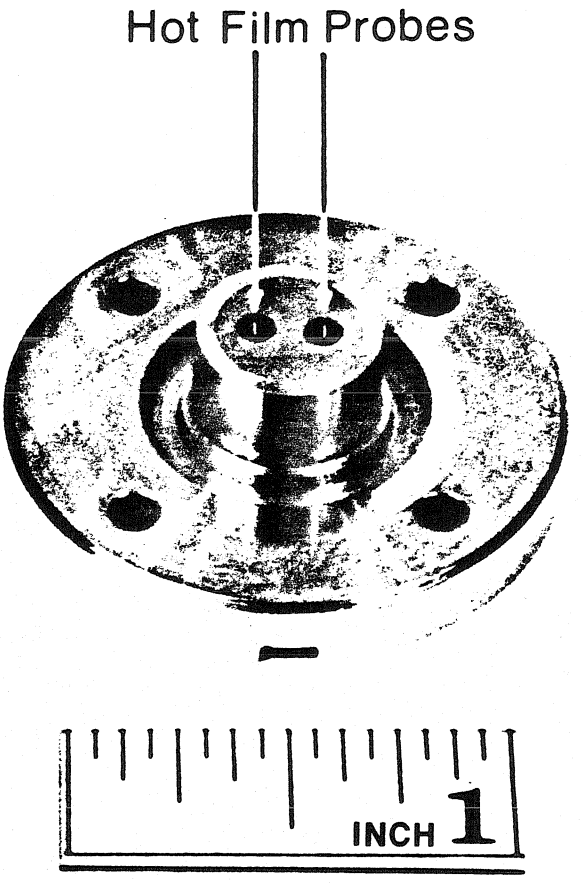

Figure 13. Flush Mount Hot Film Probe Holder

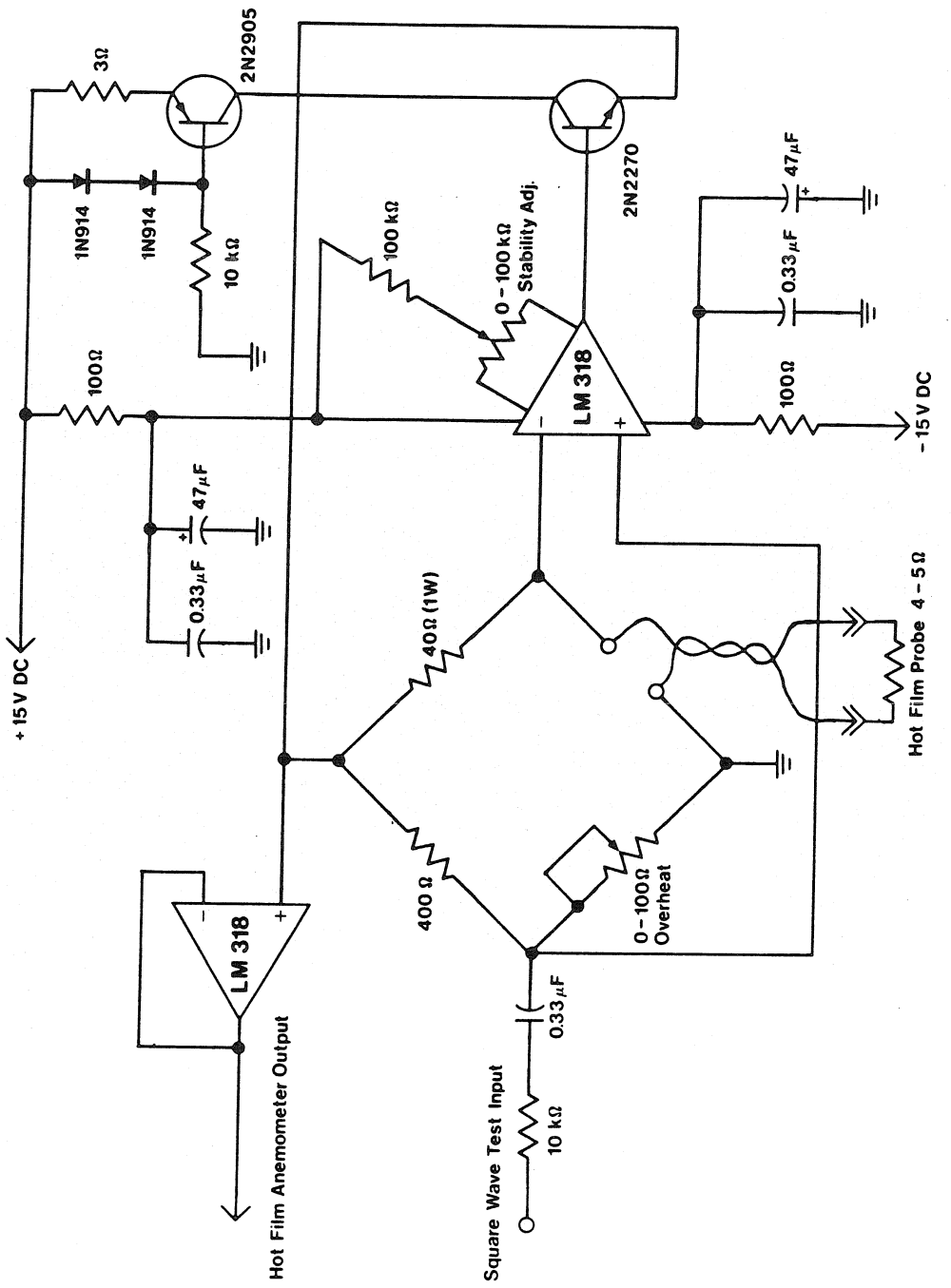

Figure 14. Hot Film Anemometer Circuit

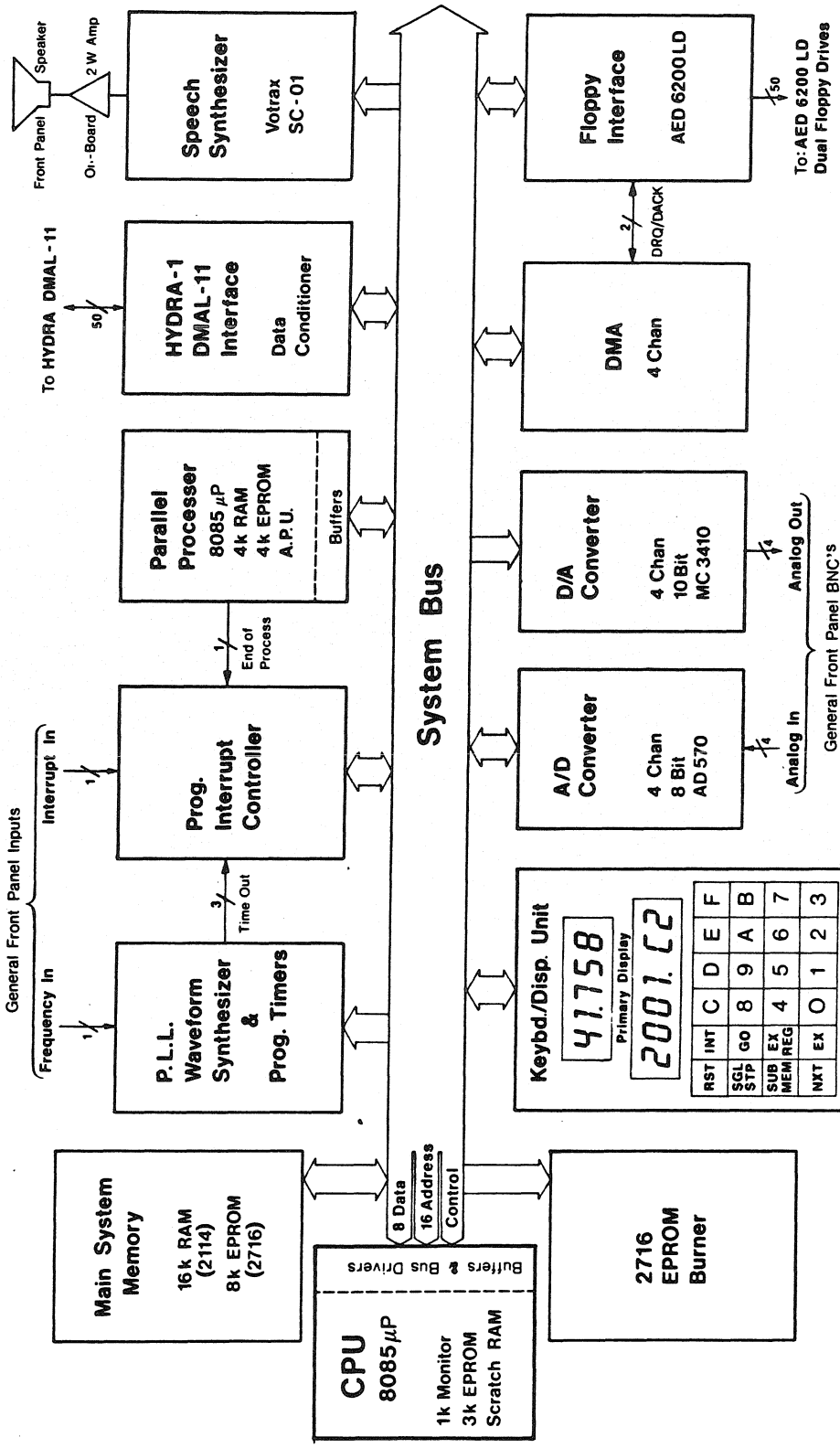

Figure 15. Block Diagram of Data Acquisition and Feedback Control Electronics

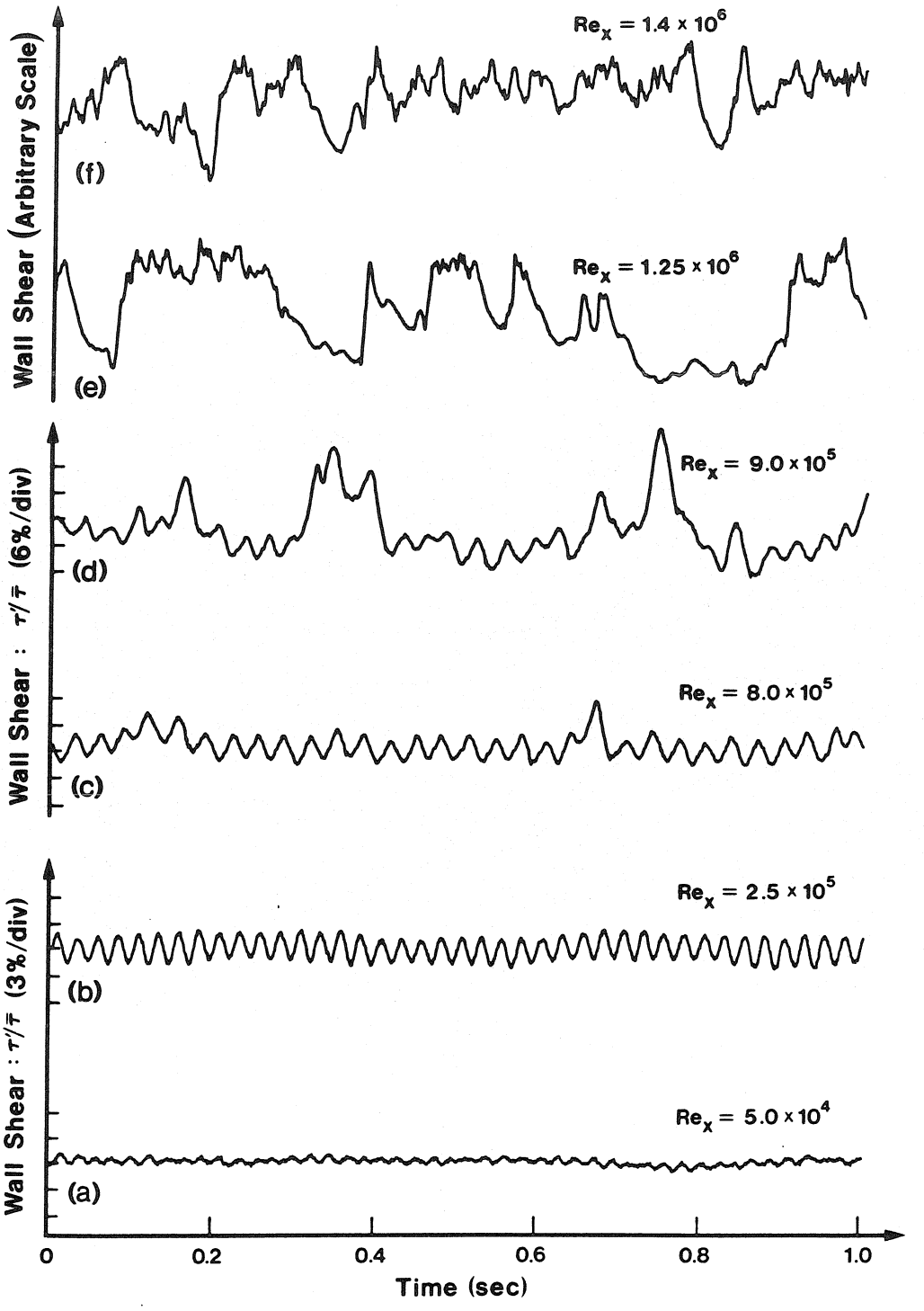

Figure 16. Wall Shear History of the Natural Transition Process

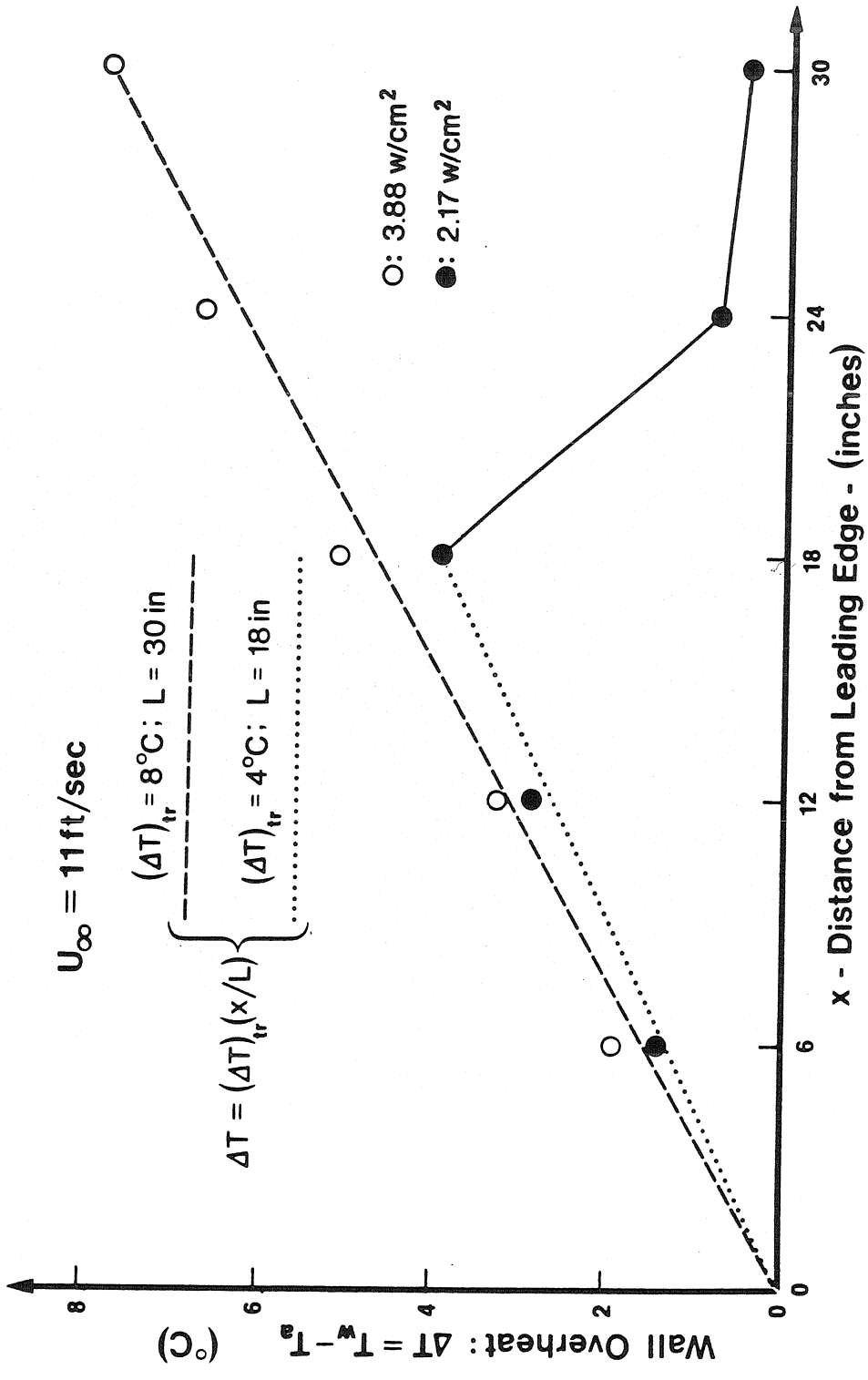

Figure 17. Plate Temperature Distributions Under Uniform Heating

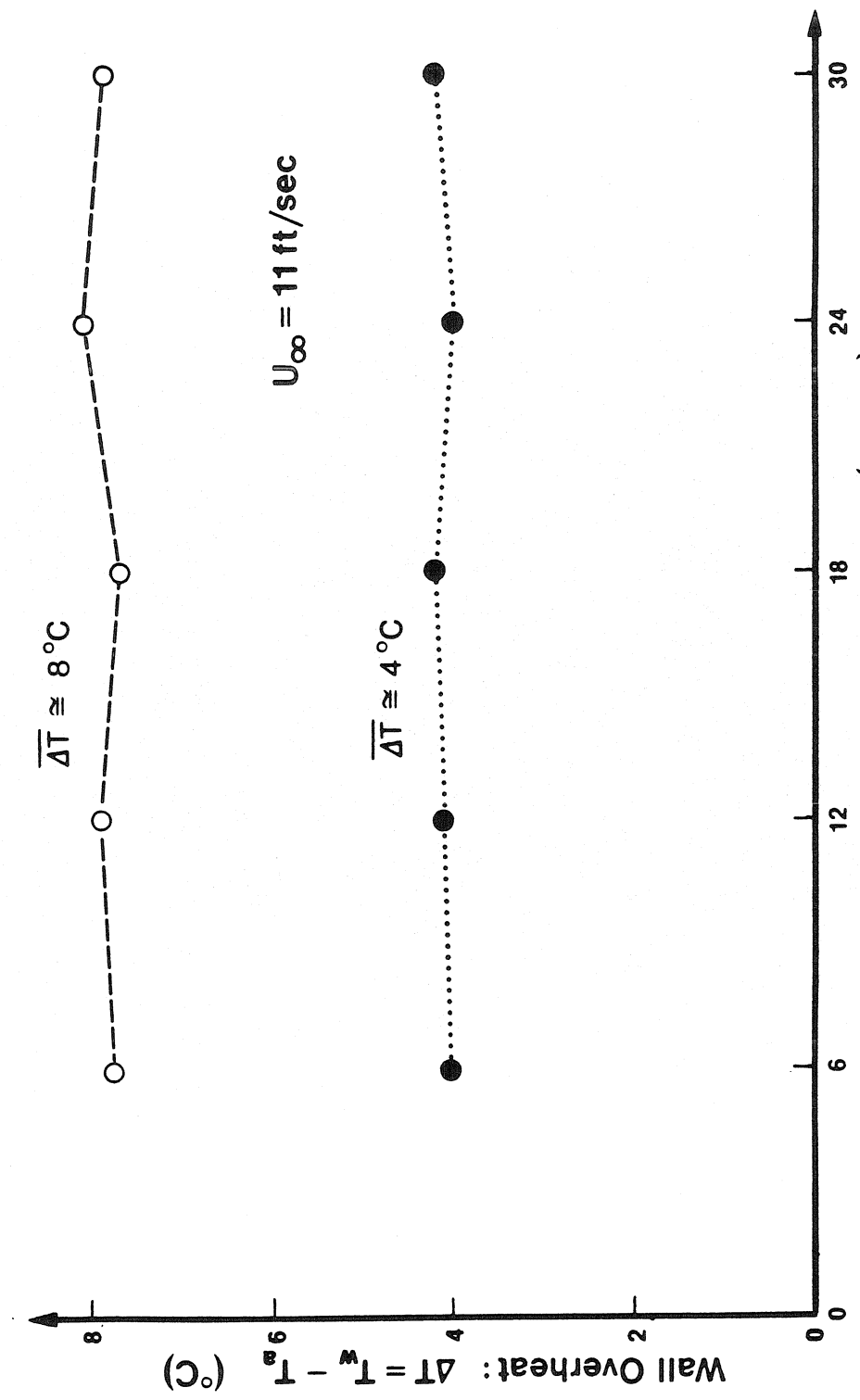

Figure 18. Plate Temperature Distributions for Isothermal Heating

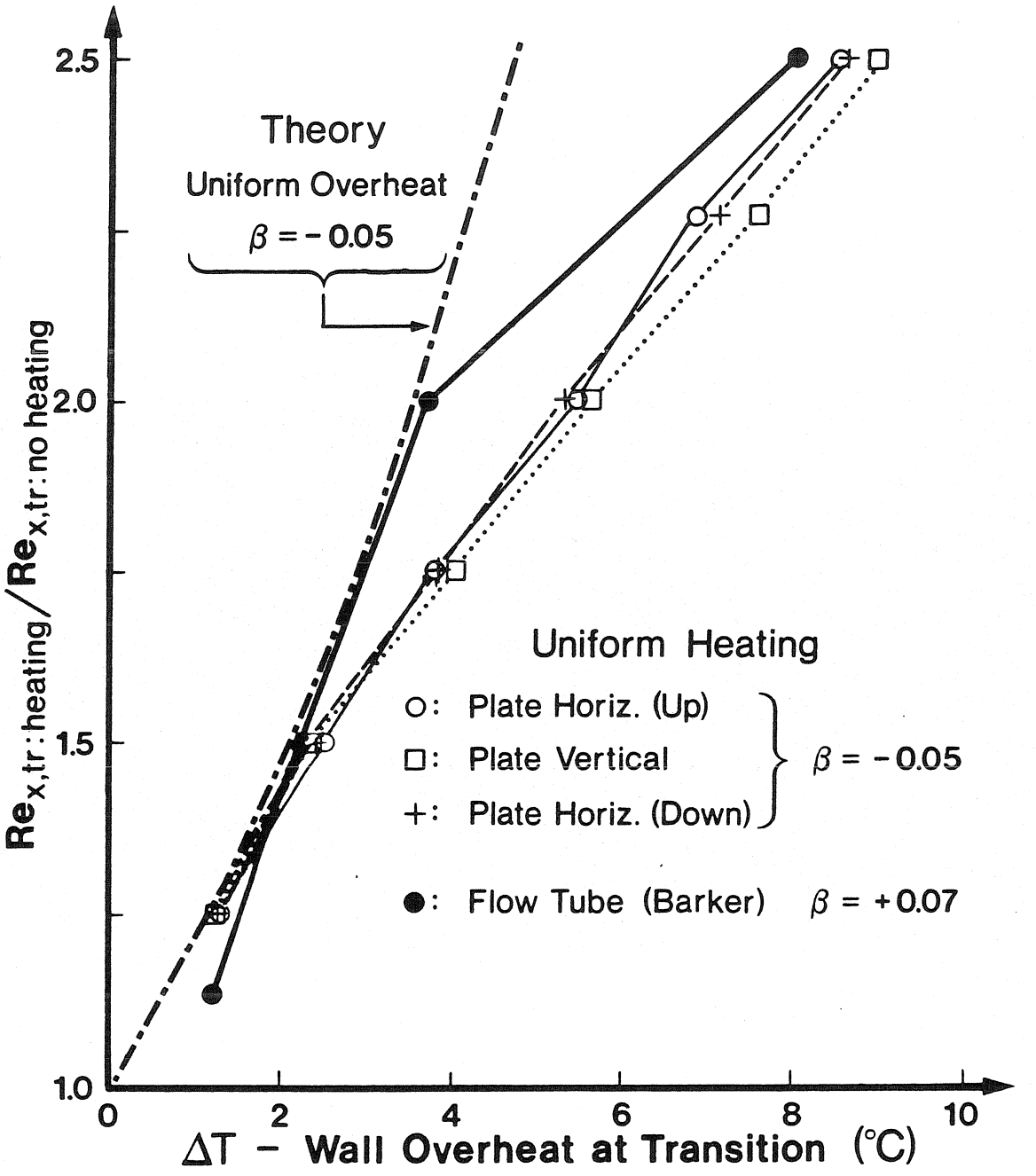

Figure 19. Effect of Passive Uniform Heating on Transition

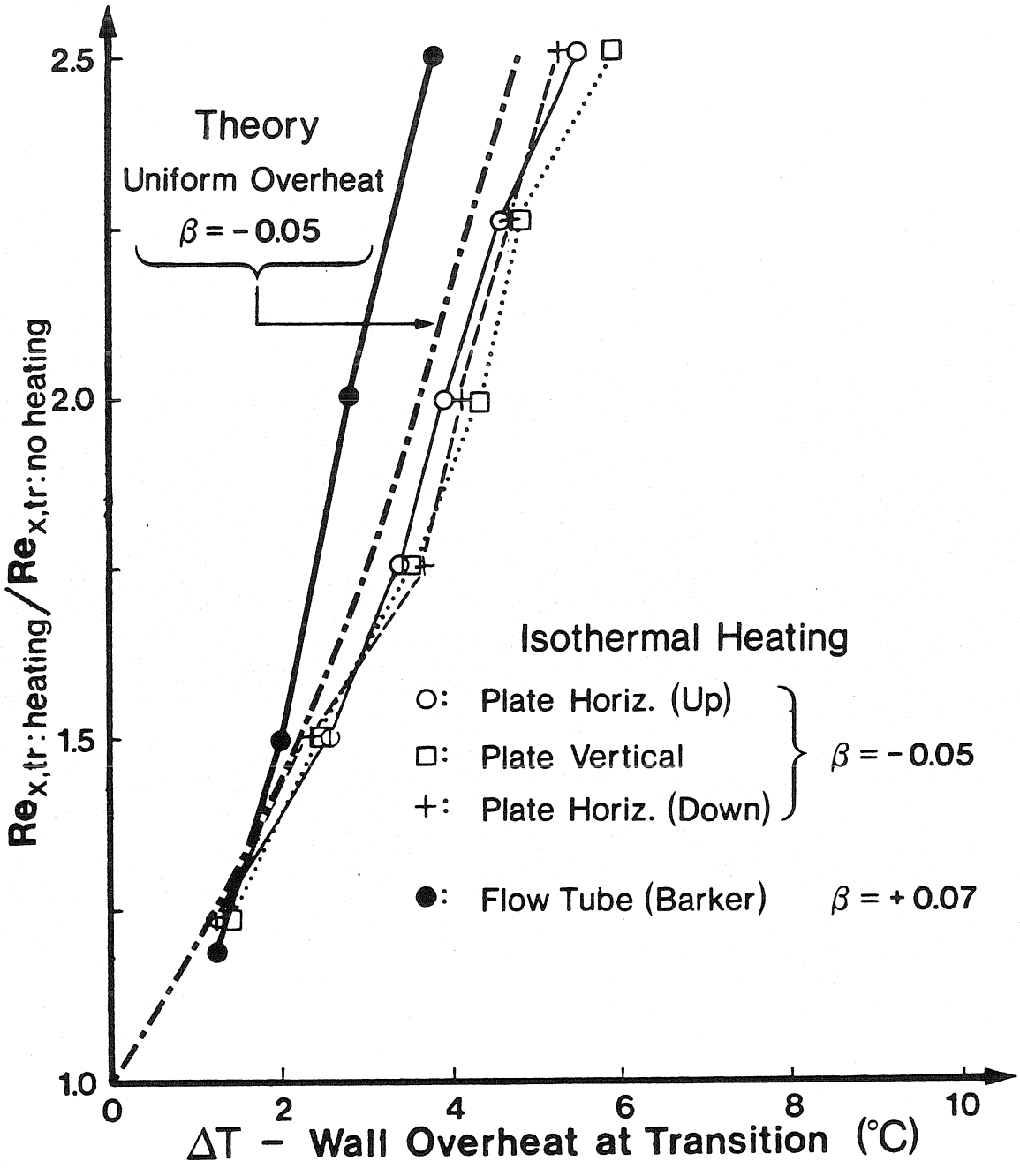

Figure 20. Effect of Passive Isothermal Heating on Transition

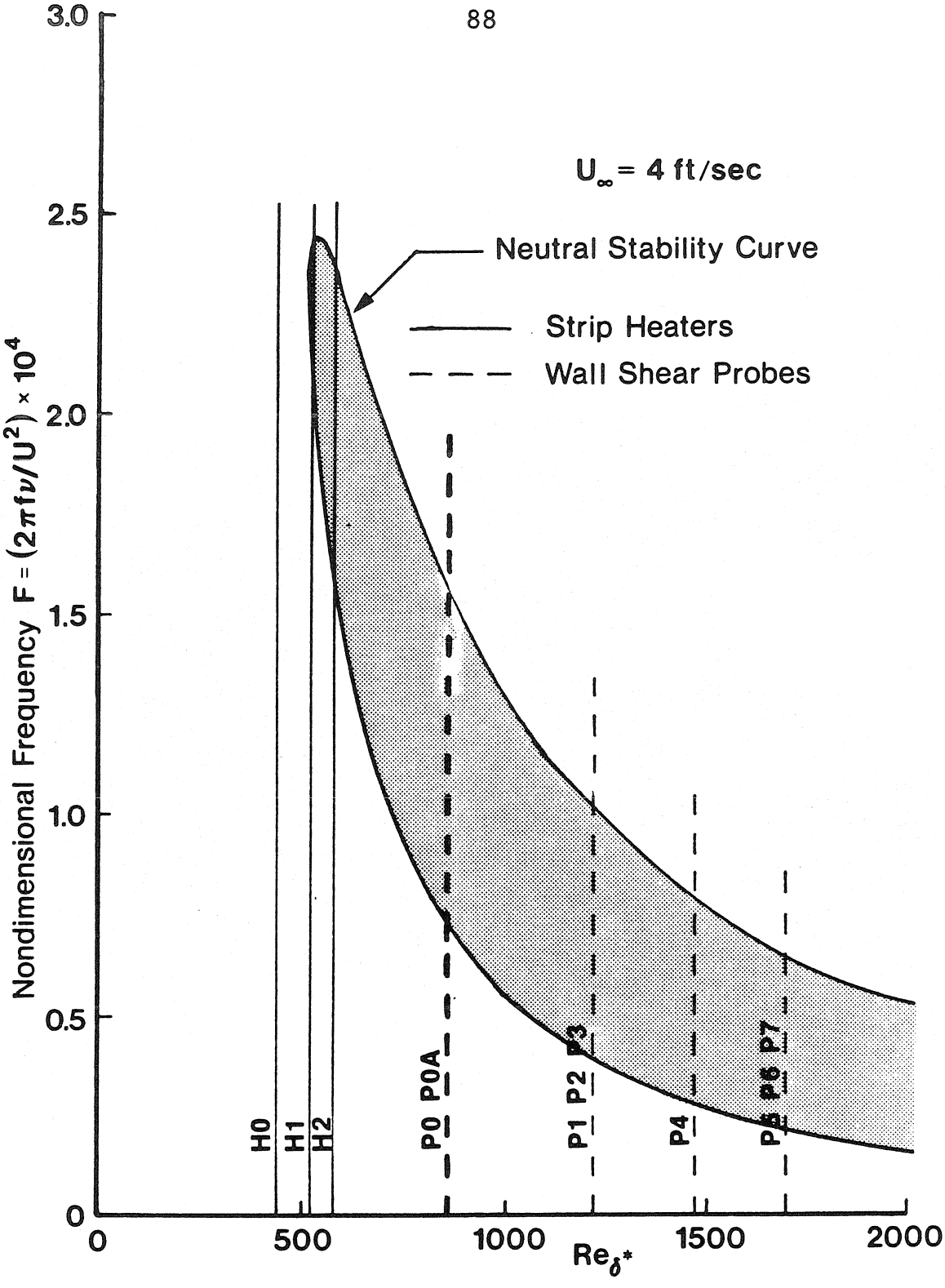

Figure 21. Strip Heater and Probe Positions Relative to the Neutral Stability Curve

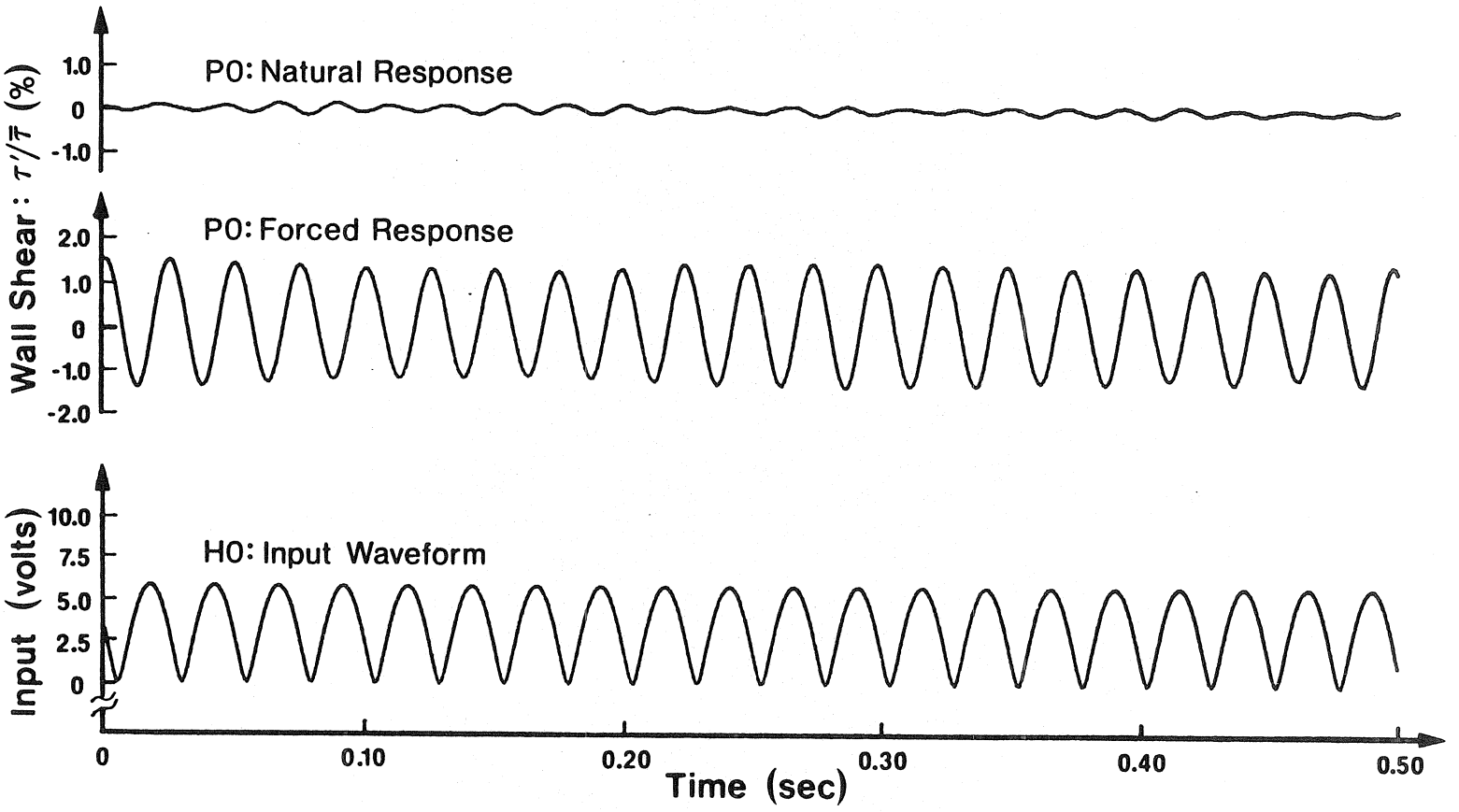

Figure 22. Continuous Sinusoidal Forcing

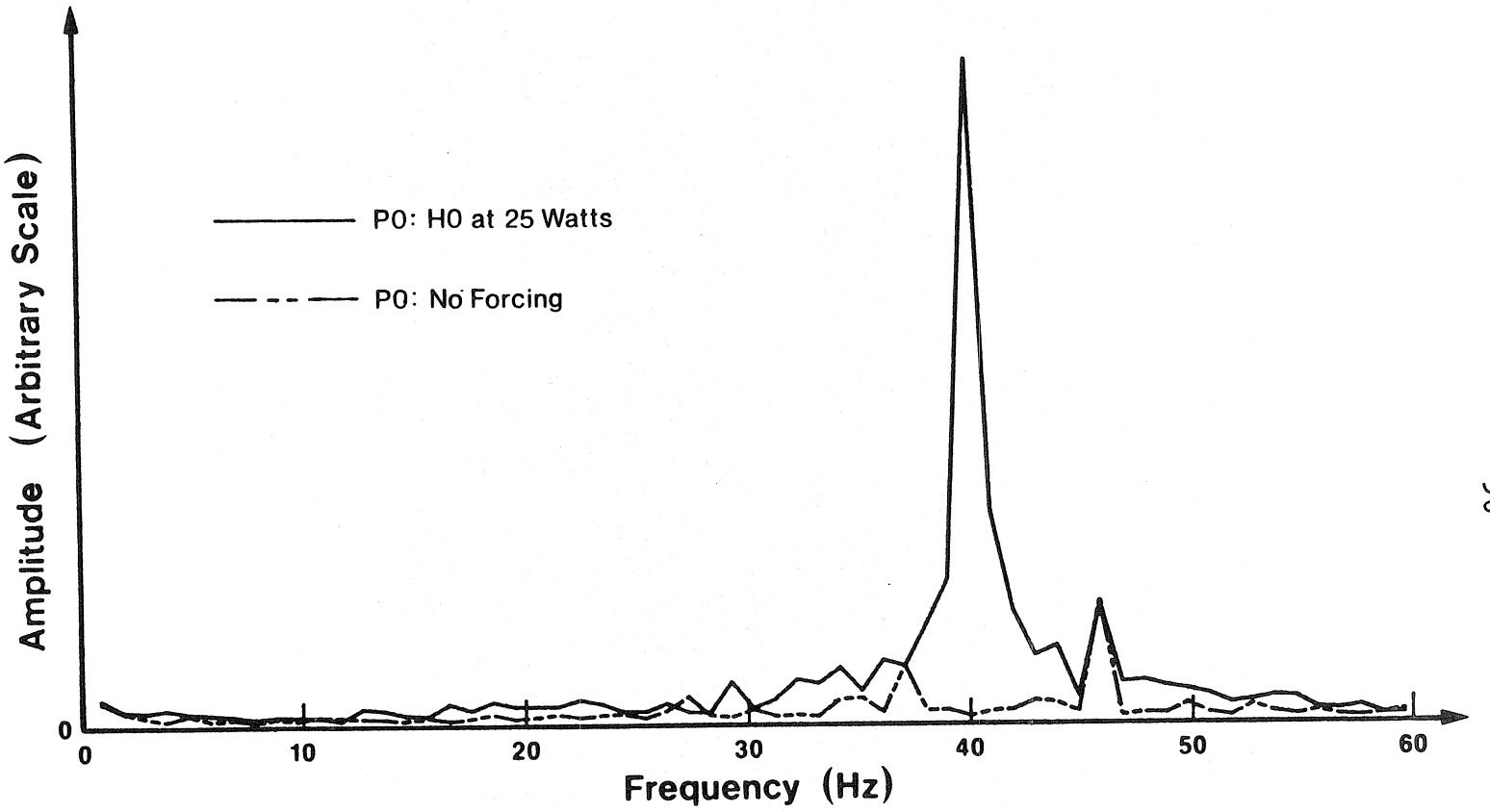

Figure 23. Spectrum of Continuous Sinusoidal Forcing

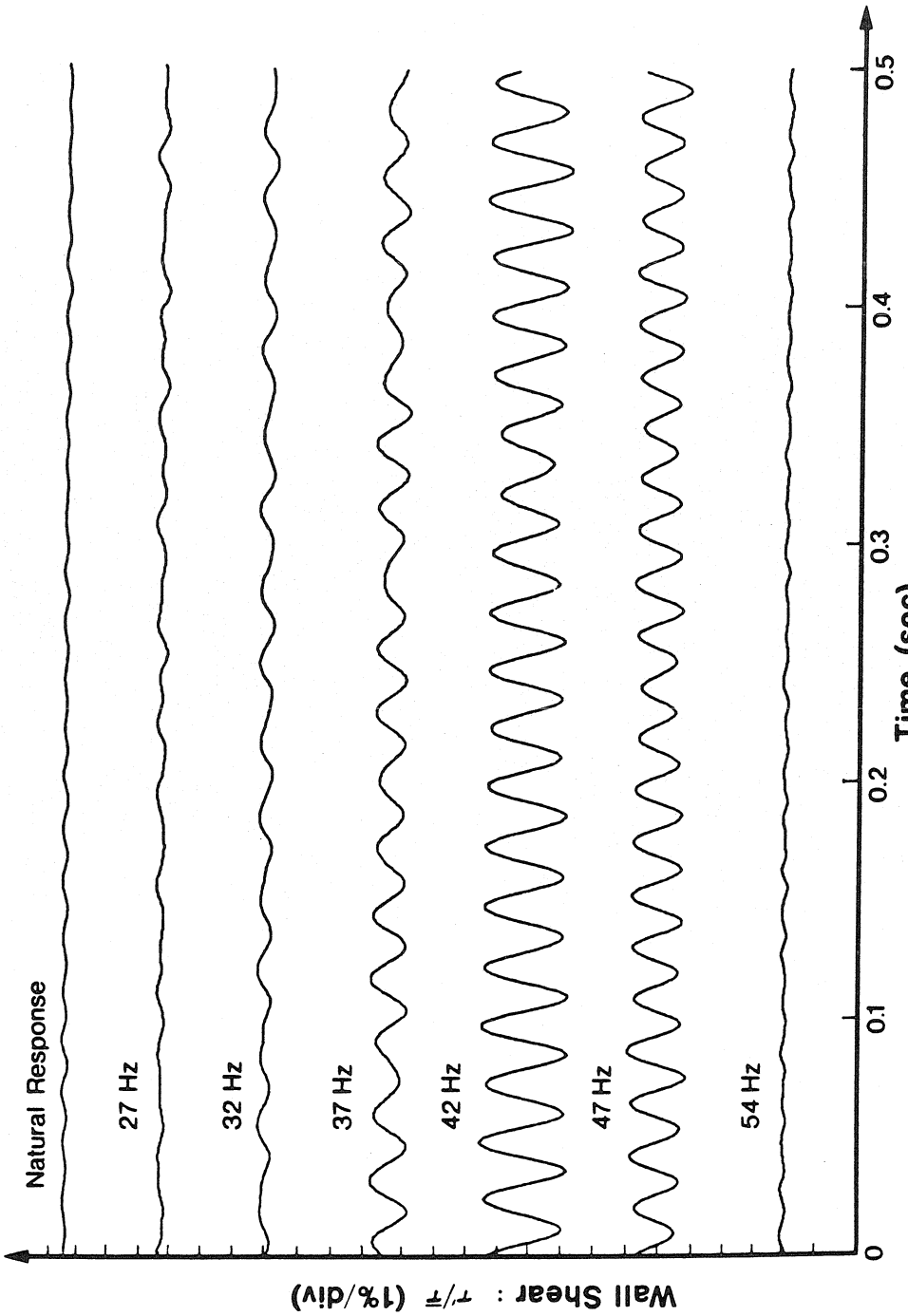

Figure 24. Effect of Varying Forcing Frequency

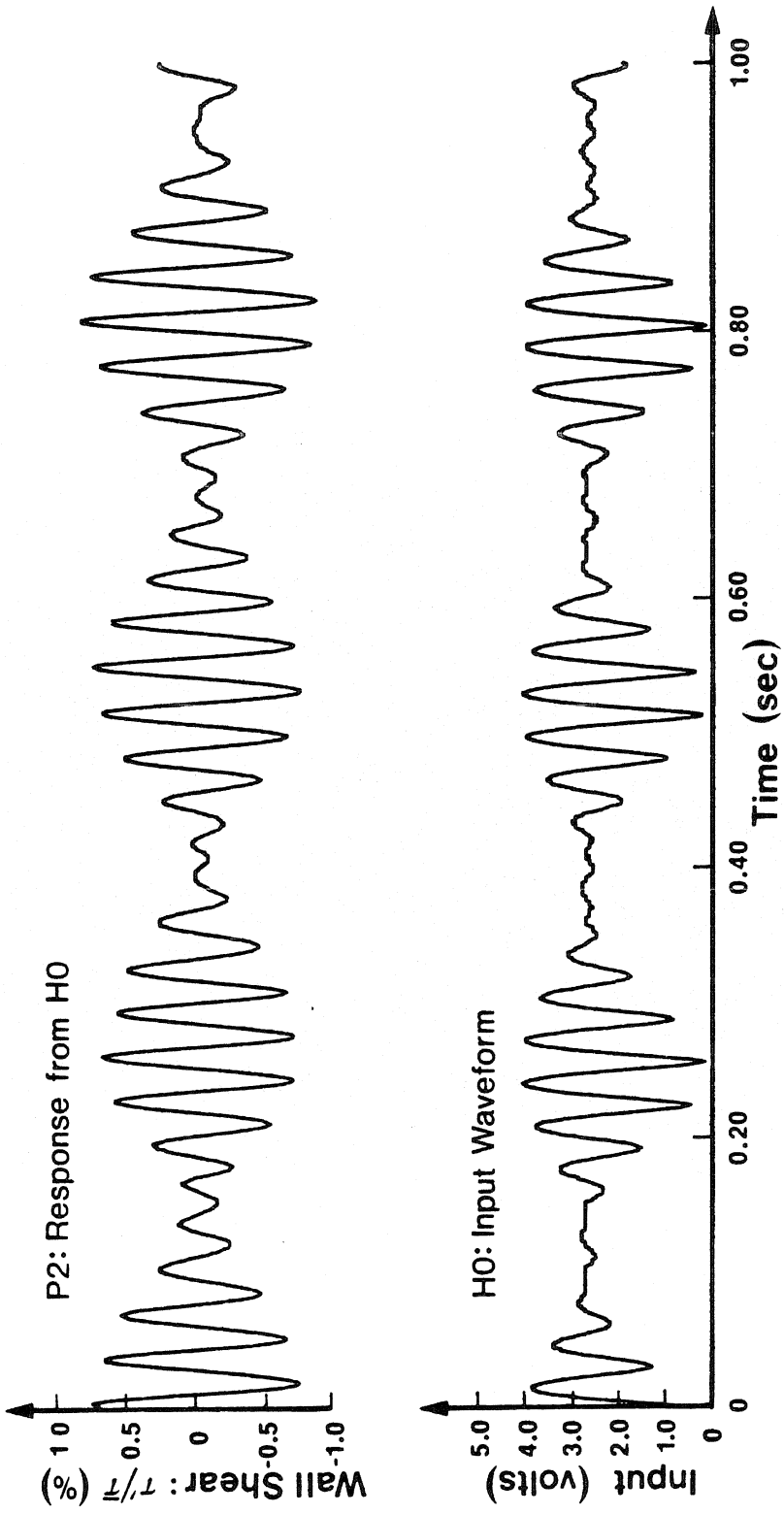

Figure 25. Amplitude Modulated Forcing

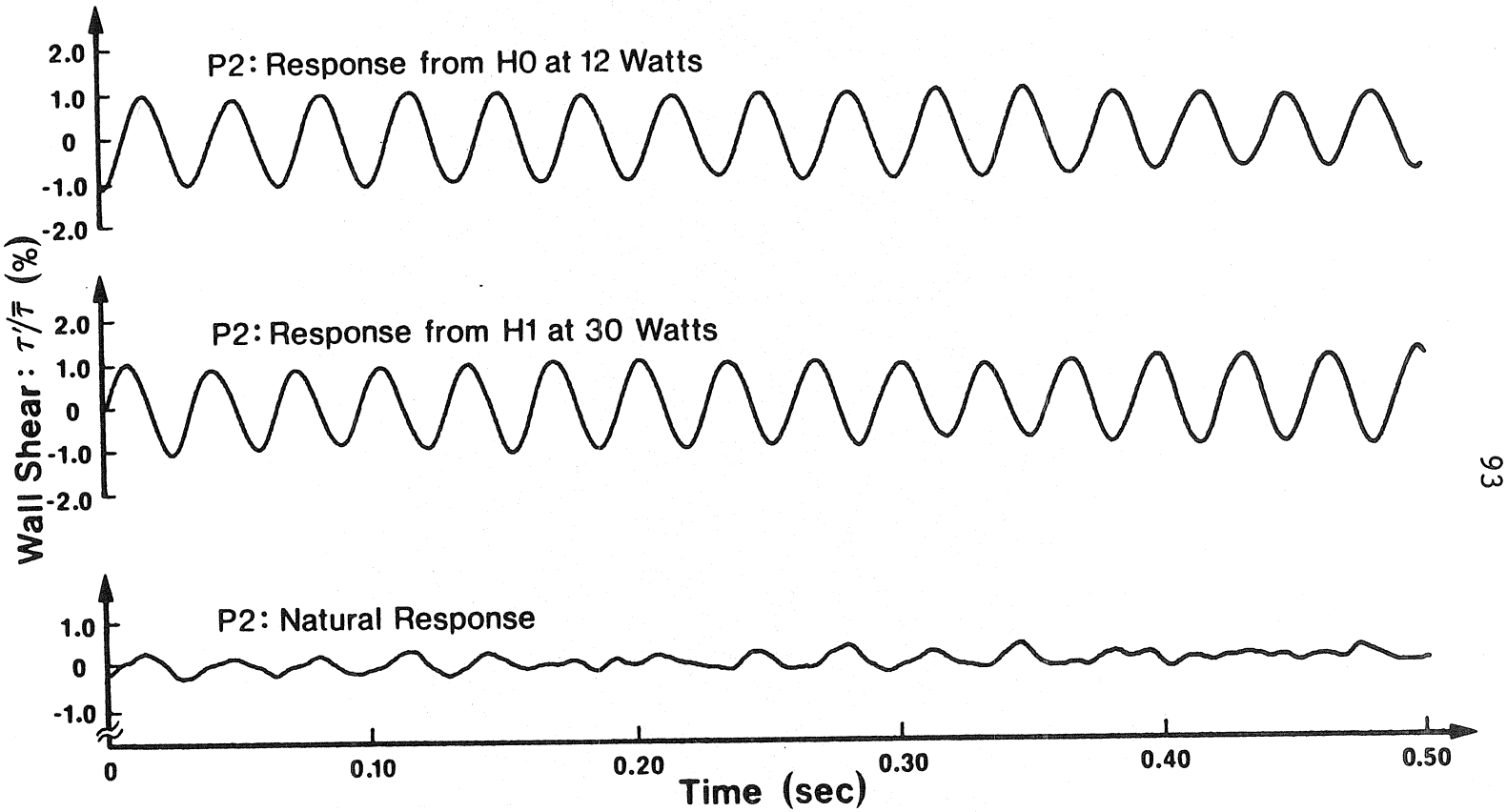

Figure 26. Individual Response of Upstream and Downstream Heaters

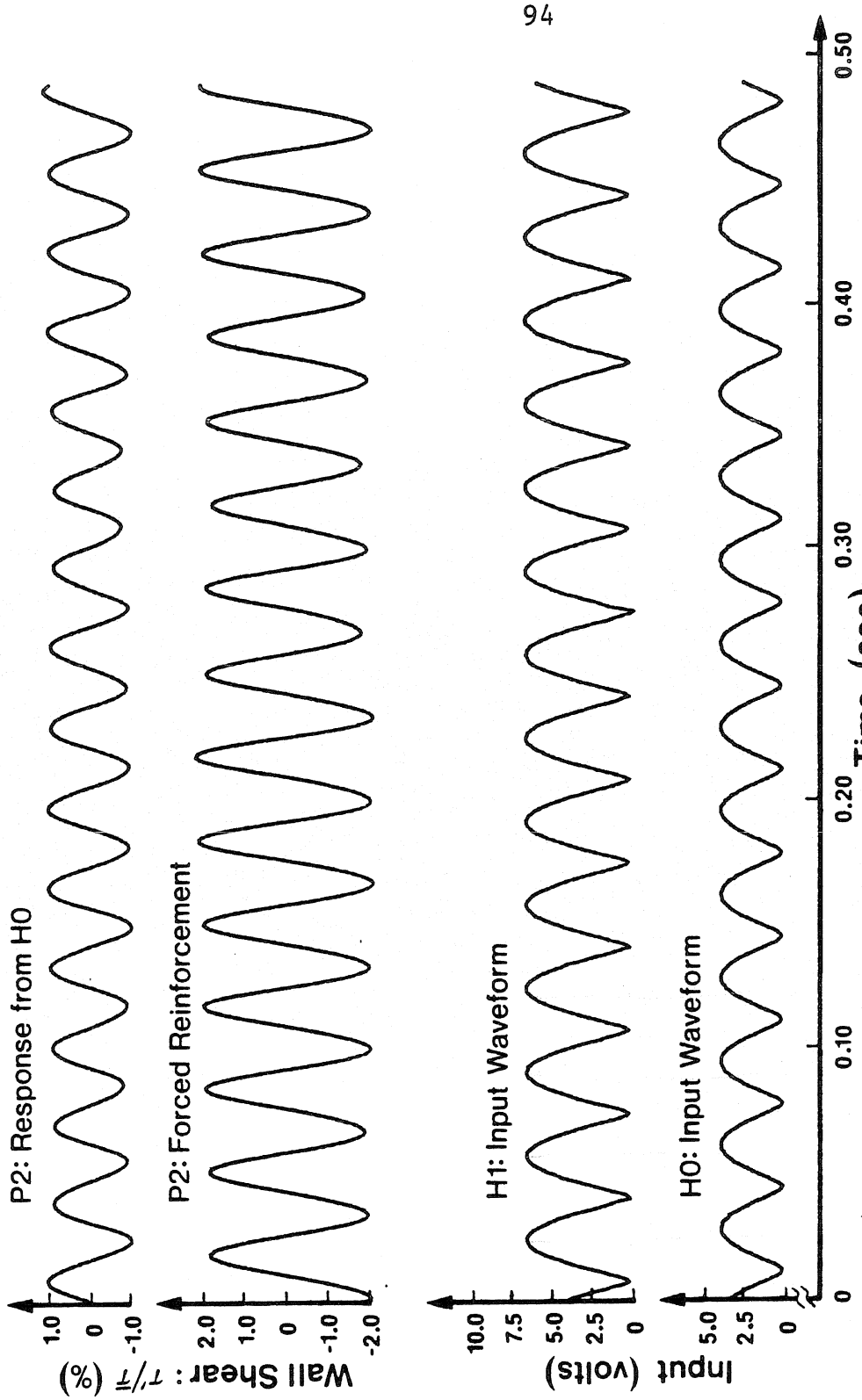

Figure 27. Reinforcement of Forced T-S Waves

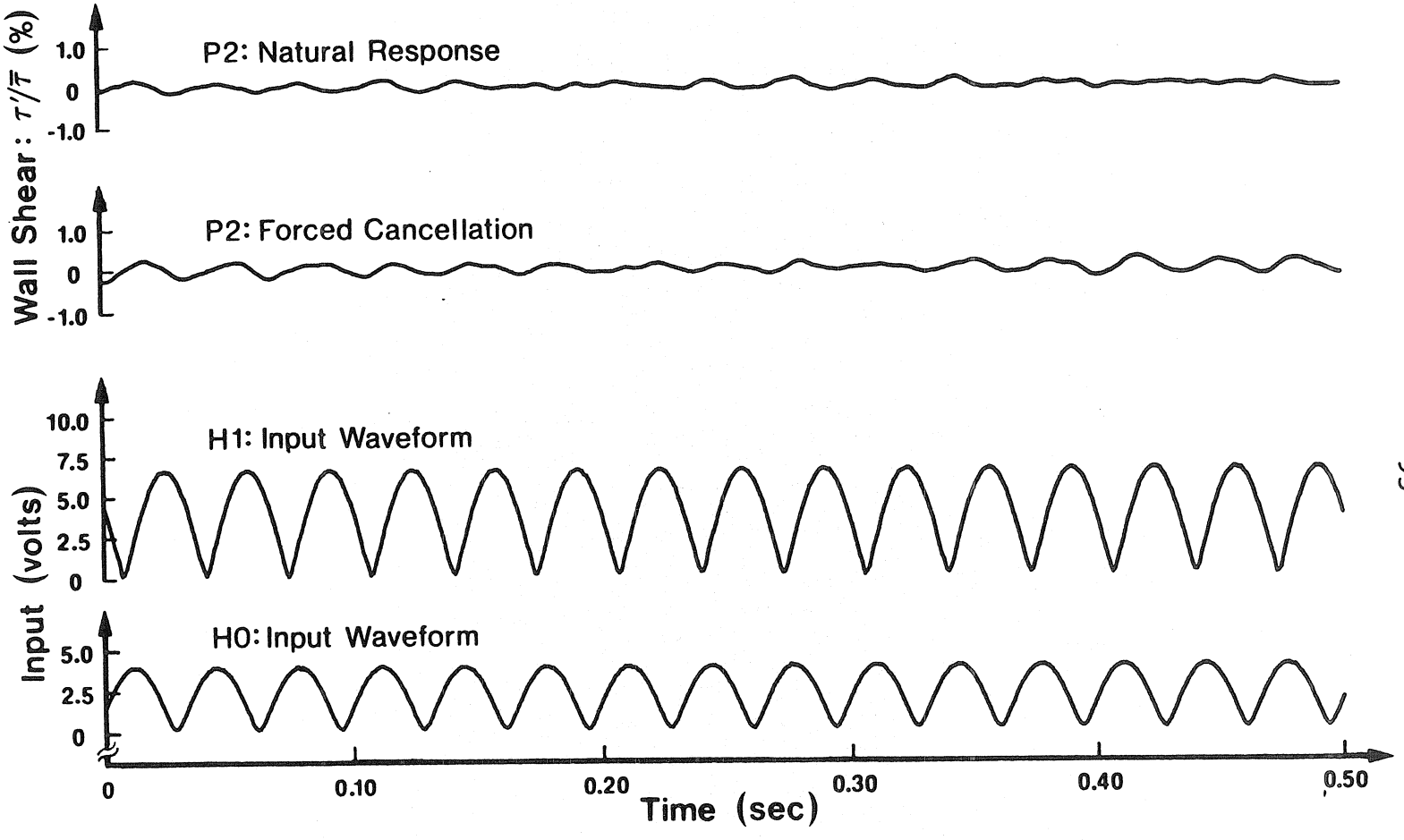

Figure 28. Cancellation of Forced T-S Waves

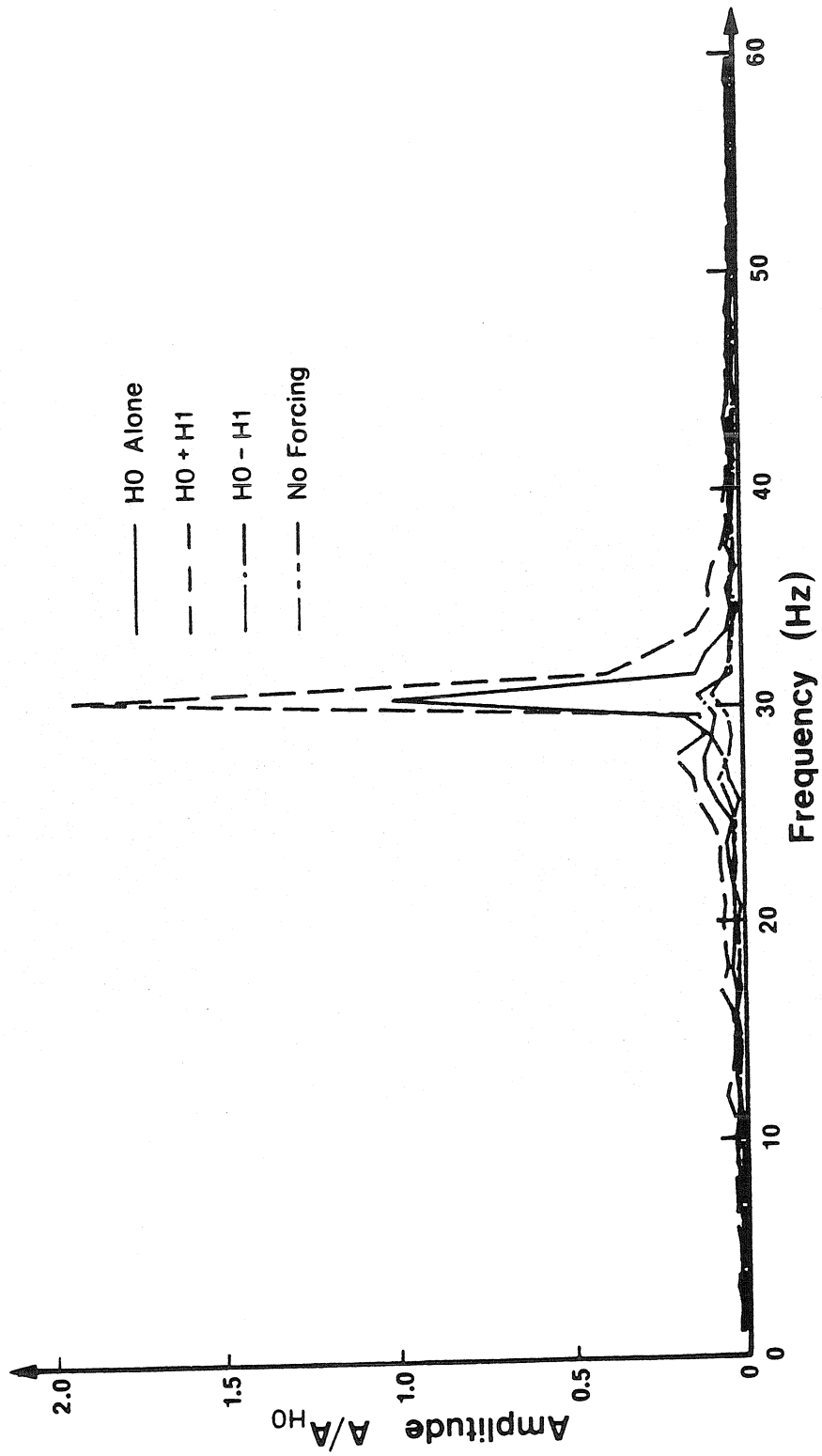

Figure 29. Spectra of Forced T-S Wave Interactions

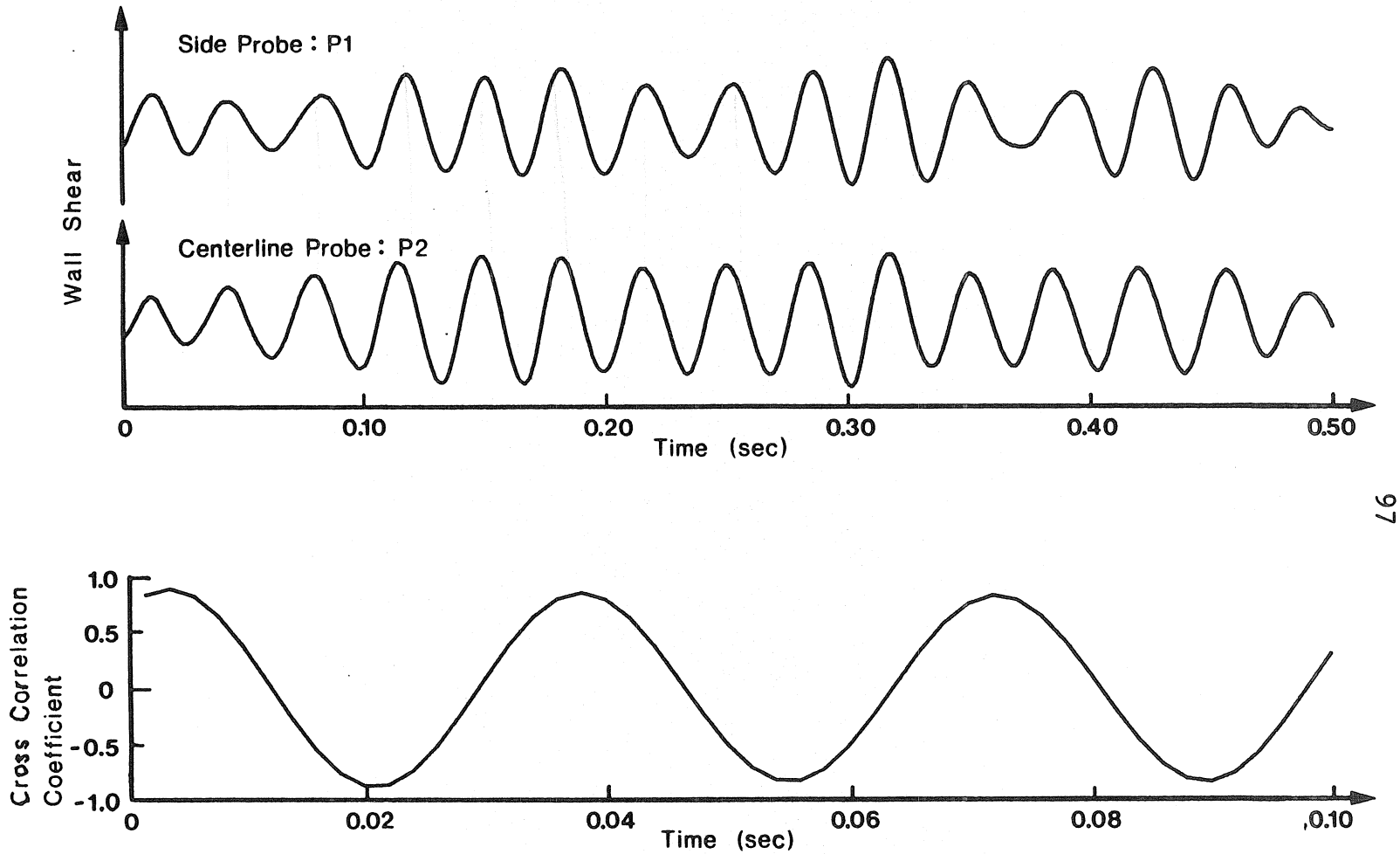

Figure 30. Two-Dimensionality of Naturally Occurring T-S Waves

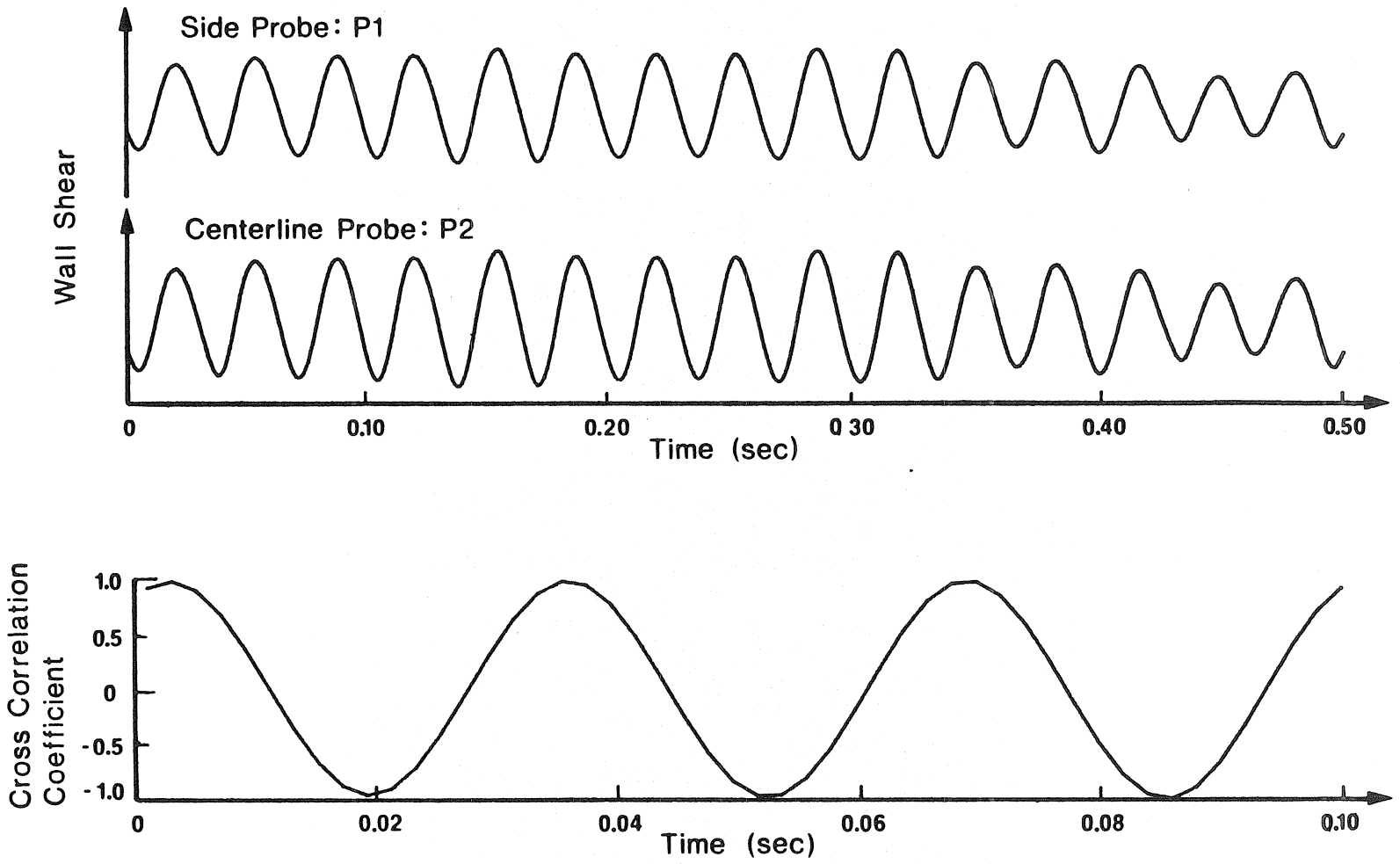

Figure 31. Two-Dimensionality of Forced T-S Waves

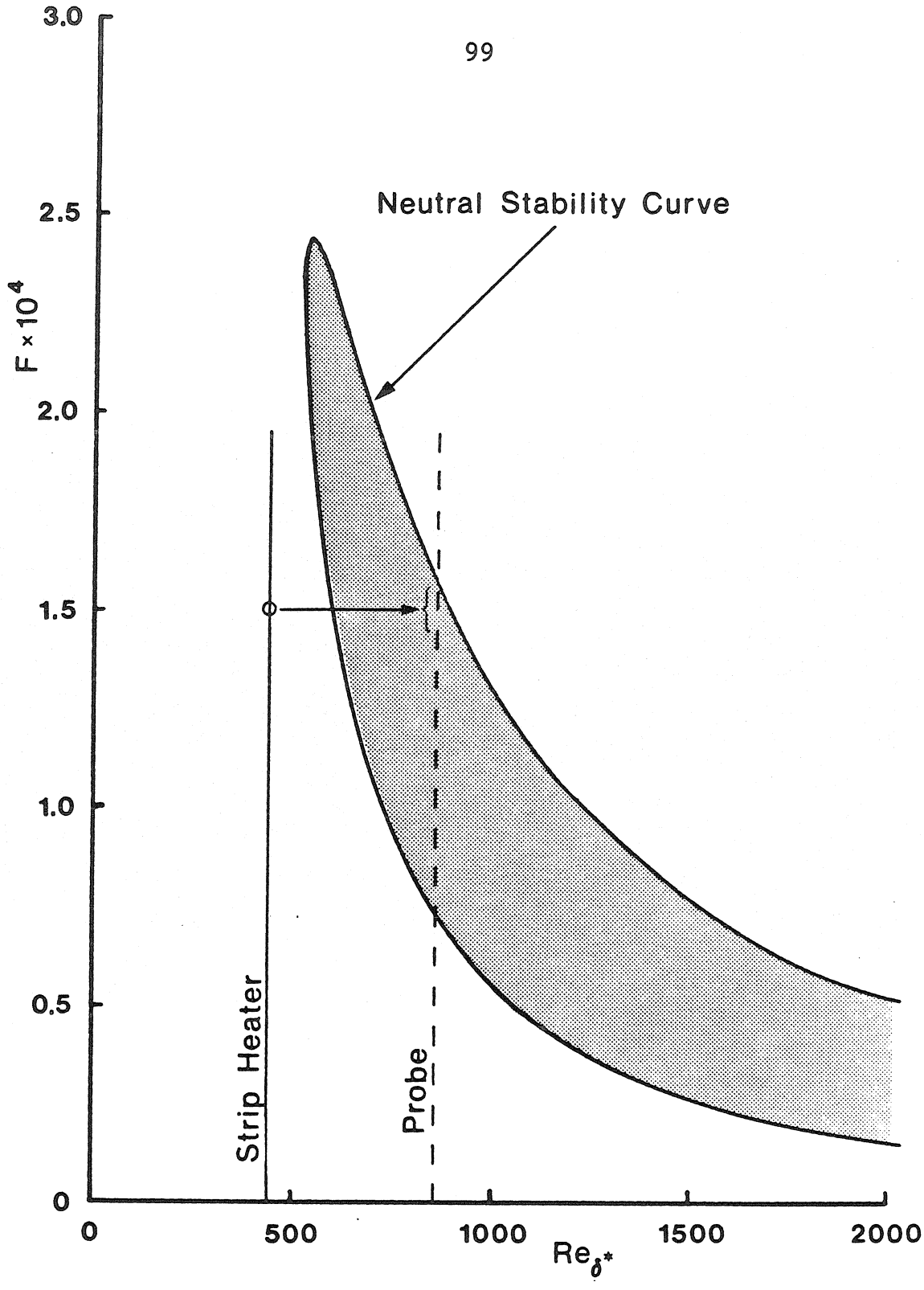

Figure 32. Strip Heater and Probe Placements Relative to Neutral Curve for Natural T-S Wave Cancellation Experiments

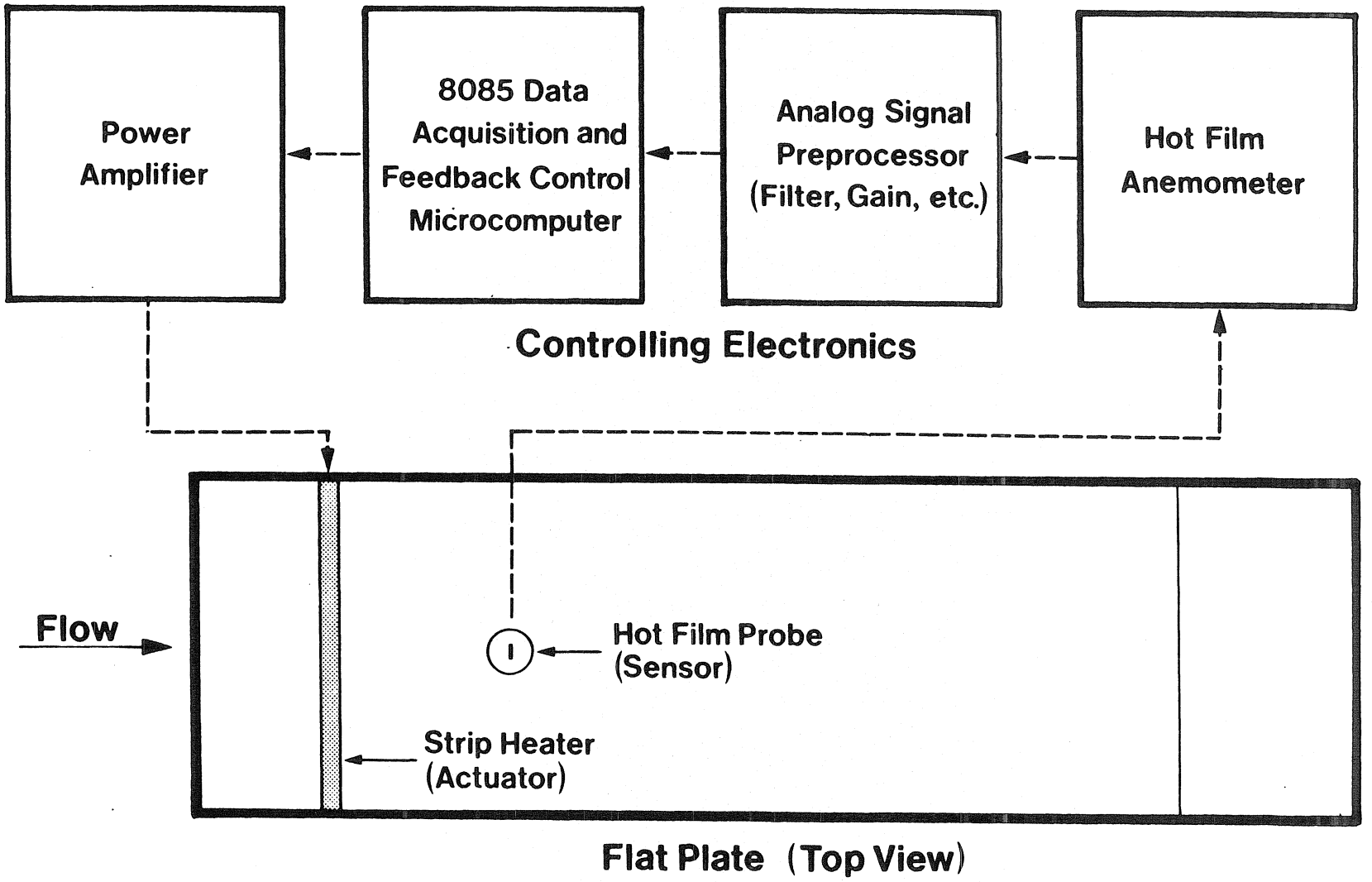

Figure 33. Active Feedback Control Layout Diagram

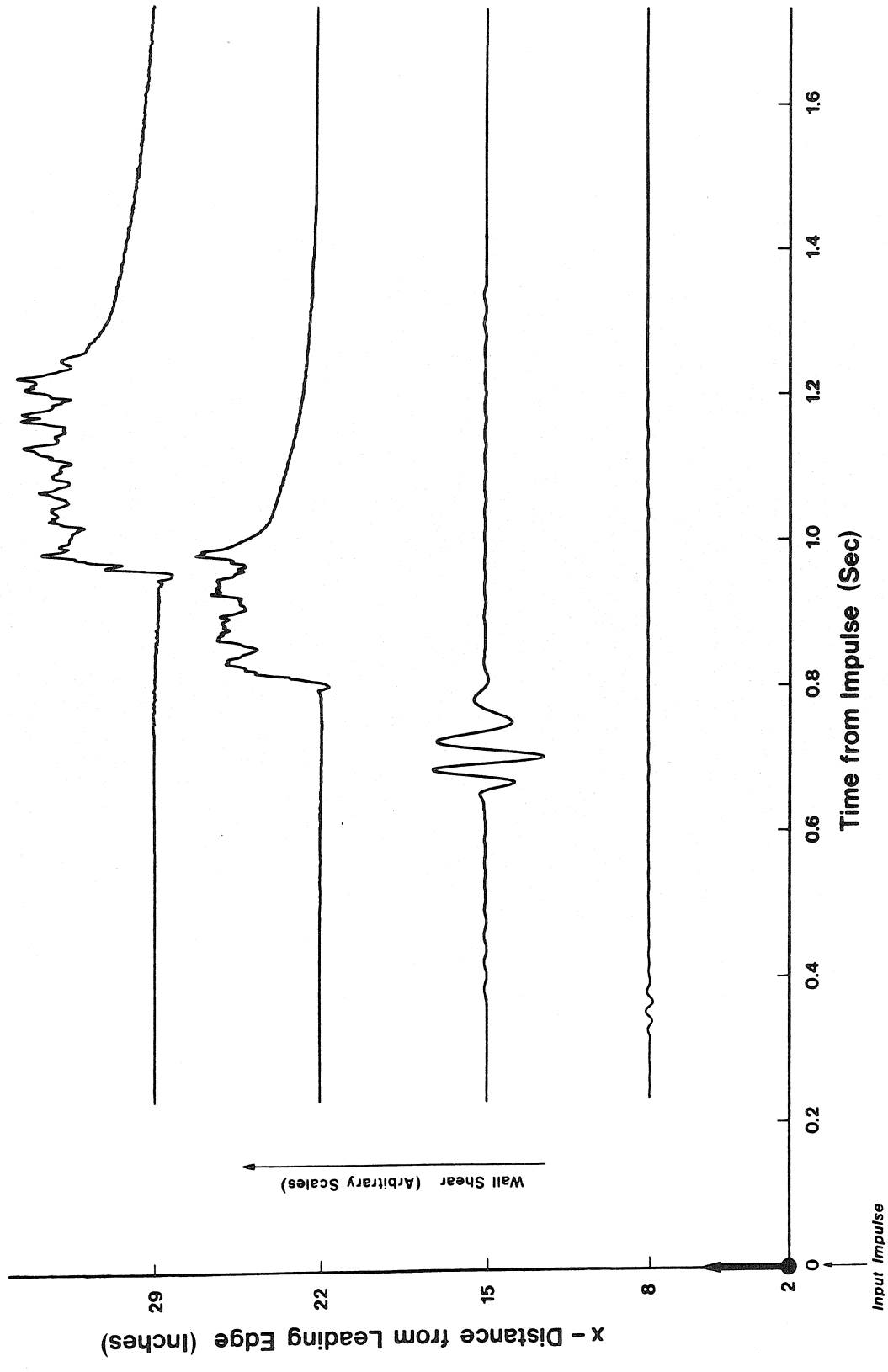

Figure 34. Two-Dimensional Impulse Response of Laminar Boundary Layer

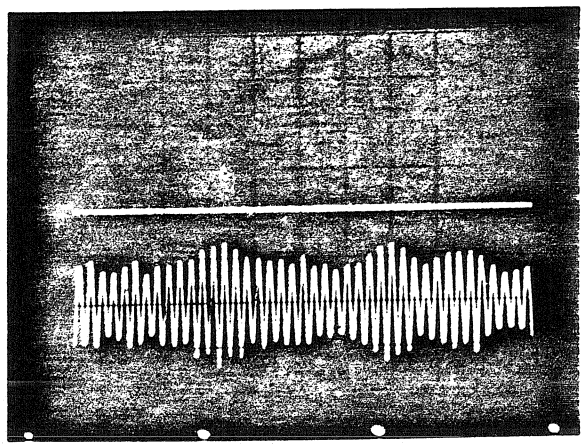

(a) Feedback OFF

"Naturally Occurring" T-S Waves

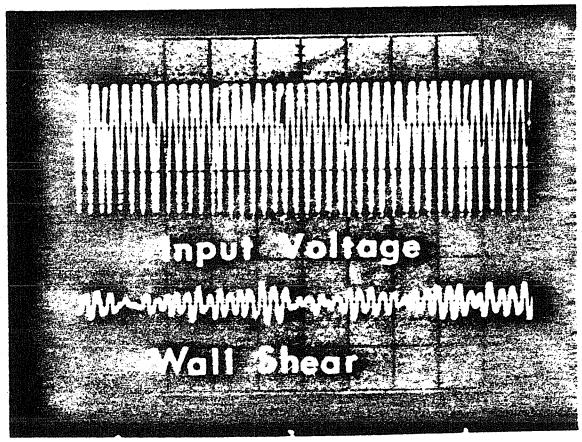

(b) Feedback ON

Out-of-Phase Cancellation

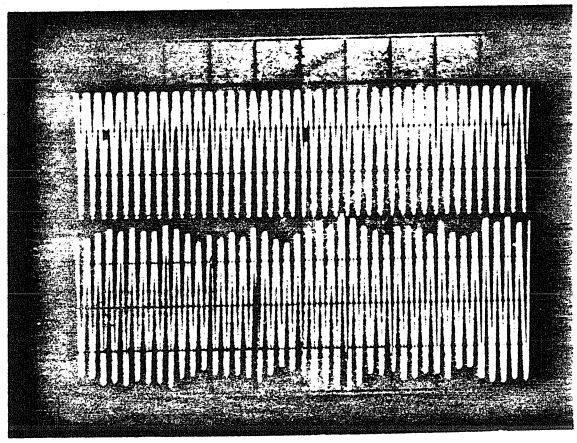

(c) Feedback ON

In-Phase Reinforcement

(ALL TRACES: 100 ms/div)

($Re^* = 850$)

Figure 35. Wall Shear Results of Active Control of Naturally Occurring T-S Waves

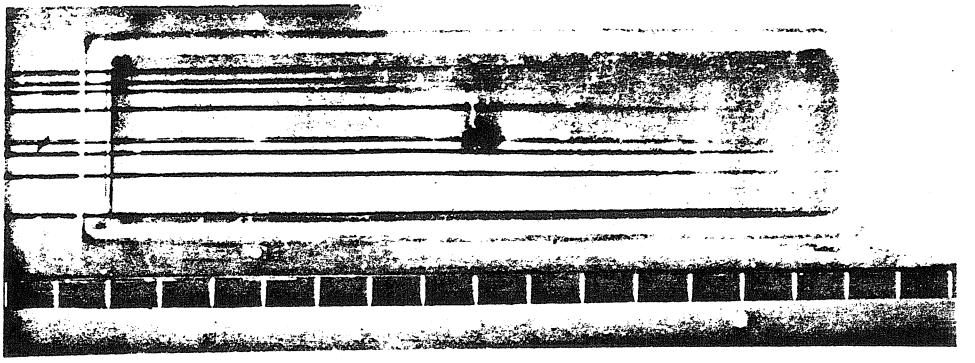

(a) NATURAL TRANSITION

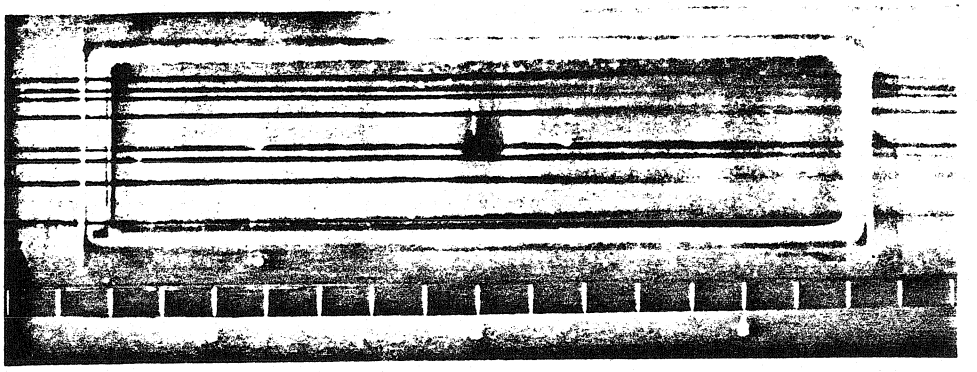

(b) NATURAL WAVE "CANCELLATION"

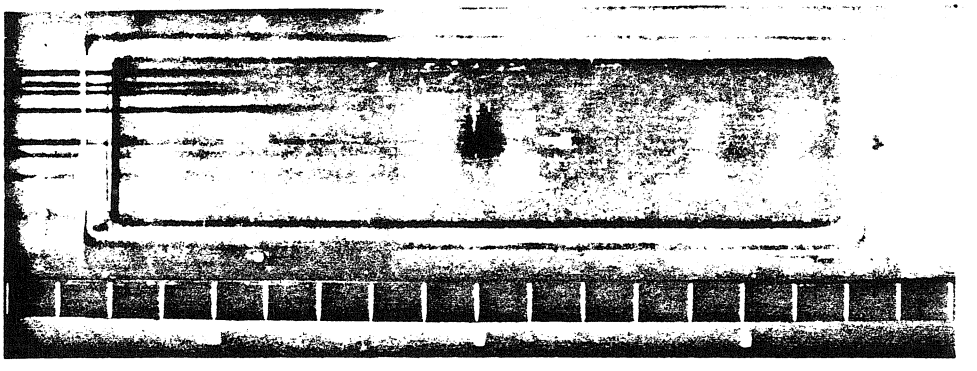

(c) NATURAL WAVE REINFORCEMENT
(FLOW IS LEFT TO RIGHT)

Figure 36. Boundary Layer Dye Streak Flow Visualization to Illustrate the Effect on Transition of Active Control of Naturally Occurring T-S Waves, U_∞ = 4 ft/sec

APPENDICES

APPENDIX A

AN APPLICATION OF THE SIMILARITY RELATIONS FOR ACTIVE HEATING

The use of strip heating to create effective normal wall velocity perturbations in the boundary layer was discussed in the Introduction. The relation between the effective normal wall velocity and the total heat supplied, heater geometry, Reynolds number, and fluid properties is

$$\left(\frac{v_w}{U_\infty}\right)_{eff} \approx Re_x^{-1} \frac{d\log\mu}{d\log T} \left(\frac{Q}{kTb}\right)\left(\frac{x_s}{\Delta}\right) , \qquad (A.1)$$

and the nondimensional forcing frequency is

$$F = \frac{2\pi f\nu}{U_\infty^2} . \qquad (A.2)$$

In general, instability waves may easily be excited when the strip heater is near the critical Reynolds number. For experimentally similar results, the Reynolds number, based on the strip heater position, and the nondimensional forcing frequency, F, should remain constant (i.e. the point on the neutral stability curve at which the strip heater operates remains fixed).

To illustrate how the scaling relations apply, assume that an experiment was run at given conditions (denoted by the subscript "1"), and that similar results are desired under new experimental conditions (denoted by the subscript "2"). Assume further that flat plate flows are studied in both cases, and the working fluid and ambient temperatures are the same. The independent variables are the freestream velocity, U_∞, and the strip heater spanwise length, b. It is required that

$$Re^*_2/Re^*_1 = 1, \tag{A.3}$$

so

$$\delta^*_2/\ \delta^*_1 = U_1/U_2, \tag{A.4}$$

$$\Delta_2/\ \Delta_1 = U_1/U_2, \tag{A.5}$$

$$x_{s;2}/x_{s;1} = U_1/U_2, \tag{A.6}$$

$$f_2/f_1 = (U_2/U_1)^2, \tag{A.7}$$

and

$$\frac{(Q/b)_2}{(Q/b)_1} = \frac{(\Delta/x_s)_2}{(\Delta/x_s)_1} = 1 , \qquad (A.8)$$

so

$$Q_2 = Q_1(b_2/b_1) . \qquad (A.9)$$

Typical results of forcing T-S waves with a single strip heater are shown in Figure 22. The values of the parameters for this case are

U_∞ = 1.2 m/sec (4 ft/sec)

x_s = 5.1 cm (2.0 in)

Δ = 0. 25 cm (0.1 in)

b = 35.6 cm (14 in)

f = 40 Hz (F = 1.55)

Q = 25 watts (St = 1.7×10^{-5})

The effective normalized wall velocity, based on the parameters listed above is

$$(v_w/U_\infty)_{eff} = 5 \times 10^{-4}.$$

The working fluid is water and the ambient temperature is 297°K. The pressure gradient was slightly adverse, with a Falkner-Skan $\beta = -0.05$.

The effects of various working fluids are accounted for in Equation A.1 by changes in the kinematic viscosity, viscosity-temperature relation, and the thermal coefficient of conduction.

Finally, it is noted that the heating element must be made thin enough to transfer heat to the fluid near the surface at the required frequencies. A lumped heat capacity analysis was used in the design of the strip heaters used in the present experiments. The heaters were 0.005 cm (0.002 inch) thick. Under typical experimental conditions (i.e. those outlined above), the frequency response was 500 Hz based on calculations (for a Blasius boundary layer) and confirmed by crude thermocouple measurements. The frequency response proved adequate to excite waves an order of magnitude lower in frequency, as was the case in the present experiments.

APPENDIX B

DESCRIPTION OF SELECTED PORTIONS OF THE MICROCOMPUTER SYSTEM

B.1 General Microcomputer System

The microcomputer system, designed in-house as a data acquisition and controller system for the present experiments, consists primarily of a CPU, Keyboard and Display Interface unit, memory, A/D and D/A converters, waveform synthesizer and interrupt controller, Direct Memory Access (DMA) controller, and floppy disk interface. In this Appendix, only the devices essential in the feedback control of T-S waves are discussed. These devices are the CPU, keyboard and display interface, memory, waveform synthesizer and interrupt controller, and A/D and D/A converters. These selected circuits are shown in gray in Figure B.1. The circuitry listed above was constructed on separate circuit boards, and connected over a 72-line system bus designed for optimal performance with the CPU and peripheral devices.

B.2 CPU

The Central Processing Unit (CPU) is the primary bus master in the present system, performing memory and Input/Output (I/O) data transfers, interrupt handling, along

with instruction and data processing. The CPU consists of an Intel 8085A microprocessor, Intel 8155 RAM;I/O;Timer, 4 kbytes of 2716 Eraseable Programmable Read Only Memory (EPROM), and various gates, latches, bus drivers and bus transceivers. The block diagram of the CPU is shown in Figure B.2.

The 8085A is an 8-bit data, 16-bit address, general purpose microprocessor, and operates at 2 MHz in the present system. The 8085A transfers data over an 8-bit bi-directional 3-state bus which is time-multiplexed with the 8 low-order address bits. Eight additional high-order, dedicated, address bits complete the 16-bit address bus, giving the 8085A direct access to 64 kbytes of memory. The 8085A has an 8-bit accumulator and flag register, and six 8-bit general-purpose registers (BC, DE, and HL). These general-purpose registers may also be used as three 16-bit registers, depending on the instruction being executed. The 8085A also has a 16-bit program counter and a 16-bit stack pointer.

The 8085A has five hardware interrupts. The lowest priority interrupt is INTR which, when asserted, causes the 8085A to fetch an instruction that is externally placed on the data bus. Generally, a CALL instruction along with two bytes of address data is externally placed on the bus (see Section B.5) to vector the CPU to an interrupt service sub-

routine stored in system memory. Three higher priority hardware interrupts (RST 5.5, 6.5, and 7.5) are provided for hard Restart (RST) vectors to low memory addresses (typically in the monitor program). The INTR and RST interrupts are software maskable, however the fifth, and highest priority, interrupt is nonmaskable. This is called the TRAP interrupt, used in the present system for single step program execution.

The 8085A is connected to an 8155 RAM;I/O;Timer that is used in the present system to supply scratch-pad RAM (address locations 2000H to 20FFH, where H denotes Hexadecimal) for the 8085A (in addition to the main system memory). The 8155 has a programmable timer/counter which is utilized during single step execution of a program. Three I/O ports are also provided by the 8155, which remain unused in the present system.

A 1-kbyte monitor program, used for performing simple operations (i.e. front panel keyboard/display scanning, memory and 8085A register loading, single step and program execution), is stored in EPROM at memory locations 0000H to 03FFH. An additional three kbytes of CPU EPROM is used for general-purpose semi-permanent program and data storage (memory locations 0400H to 0FFFH).

The final section of the CPU board consists of the system bus-interface circuitry. All of the peripheral

devices on the system bus require a demultiplexed address bus. An Intel 8212 I/O port is used to latch the lower eight bits of the Address/Data bus from the 8085A when Address Latch Enable (ALE) is asserted by the 8085A. The low-order and high-order address bytes are buffered by 8212s and sent to the system bus. Since data is transferred on the Address/Data bus only during the assertion of RD or WR (i.e. during read and write operations), the data lines need not be demultiplexed; they are, however, buffered by bi-directional bus transceivers (Intel 8216s), and then sent to the system bus. The 8085A control signals are also buffered and sent to the system bus in a similar fashion.

The only other bus master (i.e. device capable of initiating bus cycles) in the present system is the Direct Memory Access (DMA) controller. The DMA controller is external to the CPU circuitry and is used for high speed I/O-to-memory, memory-to-I/O, and memory-to-memory data transfer, without intervention from the CPU. The DMA controller requests bus master status by asserting HOLD. After the CPU has completed execution of the current instruction, a HLDA (hold acknowledge) is issued to the DMA by the 8085A. To ensure that the bus transceivers and bus drivers have ample time to float its output buses, a flip-flop is used to delay the HLDA signal by one clock period.

The CPU board is constructed to interface directly with the keyboard and display unit, bypassing the system bus. The CPU and keyboard/display circuit can function independently of the system bus.

B.3 Memory

Sixteen kbytes of 2114 static RAM are installed in the present system in addition to the scratch-pad RAM on the CPU board. Also, eight kbytes of 2716 EPROM, external to the CPU board, are installed in the present microcomputer system. All of the memory in the system is fully static, and thus easily interfaced to the DMA controller. The memory locations are:

EPROM: 7000H to 8FFFH

RAM: B000H to EFFFH

B.4 Keyboard and Display

The Keyboard/Display Unit (KDU) is a single board fabricated for front panel use. The KDU consists of a 24-key keyboard, a six digit general-purpose hexadecimal display, and a five digit Binary Coded Decimal (BCD) display. The block diagram of the KDU is shown in Figure B.3.

The keyboard is used for front-panel entry of data and commands into the CPU. It is comprised of 16 hexa-

decimal data entry keys and 8 command keys. Two of the command keys, RESET and VECT INTR, are connected (after passive debouncing) directly to the CPU. The other keys are scanned for key closure by an Intel 8279 Programmable Keyboard/Display Interface (KDI) chip.

The keyboard is arranged in three logical rows, with eight columns (the last row has six columns due to the hard connection of two keys directly to the CPU). The 8279 (KDI) generates row scan signals with a 3-to-8 line decoder (74LS156). When a key closure (debounced by the KDI) is detected by one of the eight column-return lines, the KDI interrupts the 8085A via RST 5.5. The code of the detected key is passed to the 8085A during the keyboard interrupt service routine stored in the monitor. The monitor program then decides what action to take, based on which key was struck.

The 8279 KDI is also used to output hexadecimal data to a six-digit seven-segment Light Emitting Diode (LED) display. Data are multiplexed to the LED display digits via two 4-bit KDI output ports. The output ports are synchronized to the decoded line-scan signals (shared by the keyboard) which are used to multiplex the seven-segment display data to the individual LED displays. The six-digit hexadecimal display is very flexible, and is used in the present system as a direct complement to the keyboard functions

(i.e. data and 8085A register entry and examination, display of program status and various messages, etc.).

A second five-digit LED decimal display is also available. This display uses packed BCD data, latched by an Intel 8255 Programmable Peripheral Interface (PPI). The PPI is software configured as three independent output ports, which latch the packed BCD data. The BCD data is decoded by five 7448 Seven-Segment Decoder/Driver chips. The 7448s directly interface to the individual LED displays (via current limiting resisters). This five digit display is used for display of decimal data only.

B.5 Waveform Synthesizer

The microcomputer synthesizes a waveform by continuously outputting a single period of the desired waveform, prestored in a look-up table in memory, via a D/A converter. In the present experiments, a sine wave was the main waveform synthesized for use in forcing T-S waves. A single sine wave period was broken up into 128 uniform samples, and stored sequentially in memory. The portion of memory where the digitized waveform was stored is referred to as a "look-up table", because the CPU merely uses prestored waveform amplitudes, without resorting to potentially lengthy calculations. The primary function of the waveform synthesizer unit is to produce a series of interrupts (to the CPU) at a

stable frequency. Each time the CPU receives an interrupt from the waveform synthesizer (via an Interrupt Controller) program, execution is immediately vectored to an interrupt service subroutine. This subroutine outputs the next element of the waveform, found in the look-up table, via a D/A converter. Since interrupts are used as the time base for the waveform (and the interrupts are derived from a stable clock), output frequency is stable (which would not be the case if software timing loops were employed).

The waveform synthesizer is comprised of a 4046 Phase Locked Loop (PLL), an Intel 8253 Programmable Interval Timer (PIT), and an Intel 8259A Programmable Interrupt Controller (PIC). The block diagram of the waveform synthesizer is shown in Figure B.4. This circuit corresponds to the Phase Locked Loop, and Programmable Interrupt Controller boxes shown in grey in Figure B.1.

The waveform synthesizer uses a 4046 PLL to multiply a stable reference frequency by an amount corresponding to the desired waveform frequency, to indirectly produce interrupts to the CPU. The system clock is used as the time base, which is divided in frequency to 128 Hz and is the reference signal input to the 4046 PLL. The PLL has a "divide by N" counter in its feedback loop to achieve frequency multiplication, where N is the number corresponding to the desired output frequency. Thus, the output of the

PLL is a square wave at 128N Hz which is used to send interrupts to the CPU. Since the sine wave look-up table has 128 entries, the final analog output frequency is N Hz.

Two 8253 PITs (PIT-I and PIT-II) are used in the waveform synthesizer circuitry. Each PIT is organized as three independent general-purpose 16-bit presettable down-counters; thus there are a total of six individual counters in the waveform synthesizer circuit. All modes of counter operation are software programmable. The 8253 PITs in the present microcomputer system are treated as an array of memory-mapped I/O ports by the system software. Software is used to configure the 8253 PIT counters to the required mode, and to initialize the counters with the desired quantities. In the present system, the PIT counters are used to divide the system clock for use by the 4046 PLL, act as "divide by N" square wave rate generators in the feedback loop of the PLL, and function as general-purpose down-counters (ex. for counting T-S wave zero crossings and for generating sampling gate delays).

The waveform synthesizer circuit is a completely general unit; however, to illustrate the primary use of the 8253 PITs in the present system, the portion of the feedback control algorithm which measures the mean frequency of the T-S waves, and produces interrupts at 128 times that frequency, is discussed below.

The feedback-control software programs PIT-I counter 0 for use as a "divide by N" counter to divide the system clock (predivided on the waveform synthesizer board by a flip/flop to 1.00 MHz) by 7813, to form a 128 Hz square wave. This signal is input as the reference signal to the 4046 PLL, and is also input to PIT-I counter 1 (refer to Fig. B.4). PIT-1 counter 1 is programmed to count down, from 1280, using the output of PIT-1 counter 0 as the count frequency (128 Hz). An interrupt is issued by PIT-I counter 1 after 10 seconds have elapsed. This forms a 10-second gate during which time T-S wave zero-crossings are counted by PIT-II counter 1. The counter is preloaded with 9999 and down-counts T-S wave zero-crossings detected by an analog zero-crossing voltage comparator, which is external to the microcomputer system. The count is latched by software in response to the interrupt issued at the end of the 10-second sampling gate. PIT-I counter 2 is loaded with the frequency count (subtracted from 9999) from PIT-II counter 1. PIT-I counter 2 is the the "divide by N" counter in the feedback loop of the 4046 PLL used to multiply the 128 Hz PLL input frequency. The output of the PLL is sent to this "divide by N" counter, and also to the input of PIT-II counter 0, which is used to remove the effect of the 10 second gate, by dividing the input by 10 (i.e. PIT-I counter 2 is used to multiply the input of the PLL by the

number of zero-crossings recorded in the 10-second gate, N = 10f, where f is the mean T-S wave frequency; therefore, the input to PIT-II counter 0 is 128(10f). The output of PIT-II counter 0 is a square wave at 128f Hz, which is used to interrupt the system). PIT-II counter 2 is a general-purpose counter that is not used by the feedback control software.

An 8259A Programmable Interrupt Controller (PIC) is used to handle up to eight vectored, priority interrupts for the CPU. In the present system the 8259A PIC accepts interrupt requests from the 8253 PITs, from a general front panel interrupt (INTR IN) input, and interrupts from the system bus sent by other peripheral devices in the microcomputer system (Fig. B.4).

The 8259A PIC responds to interrupt requests on the Interrupt Request (IR) lines. The 8259A is configured, under software control, to vector operation of the CPU to a preprogrammed location in memory in response to each interrupt. The PIC does this by issuing an INTR to the 8085A on the CPU board. When the 8085A acknowledges the interrupt, via INTA, the PIC places a CALL instruction on the data bus, followed by a two byte address vector. Since the dynamic addressing range of the 8259A PIC is limited, and addresses are separated by fixed intervals of several bytes (4 or 8 byte intervals), the first instruction after the vector is a

JMP (jump) instruction. The contiguous portion of memory that holds the JMP instructions is named the "jump table". In the present system, the software configures the 8259A PIC to use a 32-byte jump table (4-byte vector increments).

The interrupts are software maskable and may be prioritized in an arbitrary manner. The interrupts used by the waveform synthesizer are:

IR0: 128f Hz interrupt used in timing the output of data from the waveform look-up table to the D/A converters

IR1: Sampling gate interrupt (typically 10 sec)

IR2: Interrupt based on divided FREQ IN input (not used by feedback control algorithm)

IR3: General front panel interrupt (INTR IN)

IR4: to IR7: Used by microcomputer system peripheral devices

B.6 A/D and D/A Converters

The A/D and D/A converter circuit is used to simultaneously digitize up to four channels of analog input, and also to simultaneously output four channels of analog data. The block diagram of the A/D and D/A circuits is given in Figure B.5.

The A/D section uses four 8-bit, 50 KHz, Analog Devices AD570 A/D converters. The output of these con-

verters go to I/O ports on 8255 Programmable Peripheral Interfaces (PPIs), which are treated by the system software as an array of memory-mapped I/O ports. The PPIs are software configured as input ports that latch data from the A/D converters on software command. Each PPI has three I/O ports: Port A, Port B and Port C. Ports A and B are used as the A/D input latches (one port per A/D), and Port C is configured as an output port, and is used to send the convert pulse to the A/D converters under software command. Two 8255 PPIs (PPI-III and PPI-IV) are used to input data from the four A/D converters.

The D/A section uses four 4 MHz 10-bit MC3410 D/A converters. The data for these D/A converters are supplied by 8255 PPIs, configured as output ports. The eight most significant bits of each D/A are supplied by Ports A and B. Port C is logically split in half (as two independent 4-bit output ports) and is used to supply the two least significant bits to the D/A converters. Two 8255 PPIs (PPI-I and PPI-II) are used to output data to the four D/A converters. The feedback control software makes use of only the eight most significant bits of the D/A converters in synthesizing the output waveform.

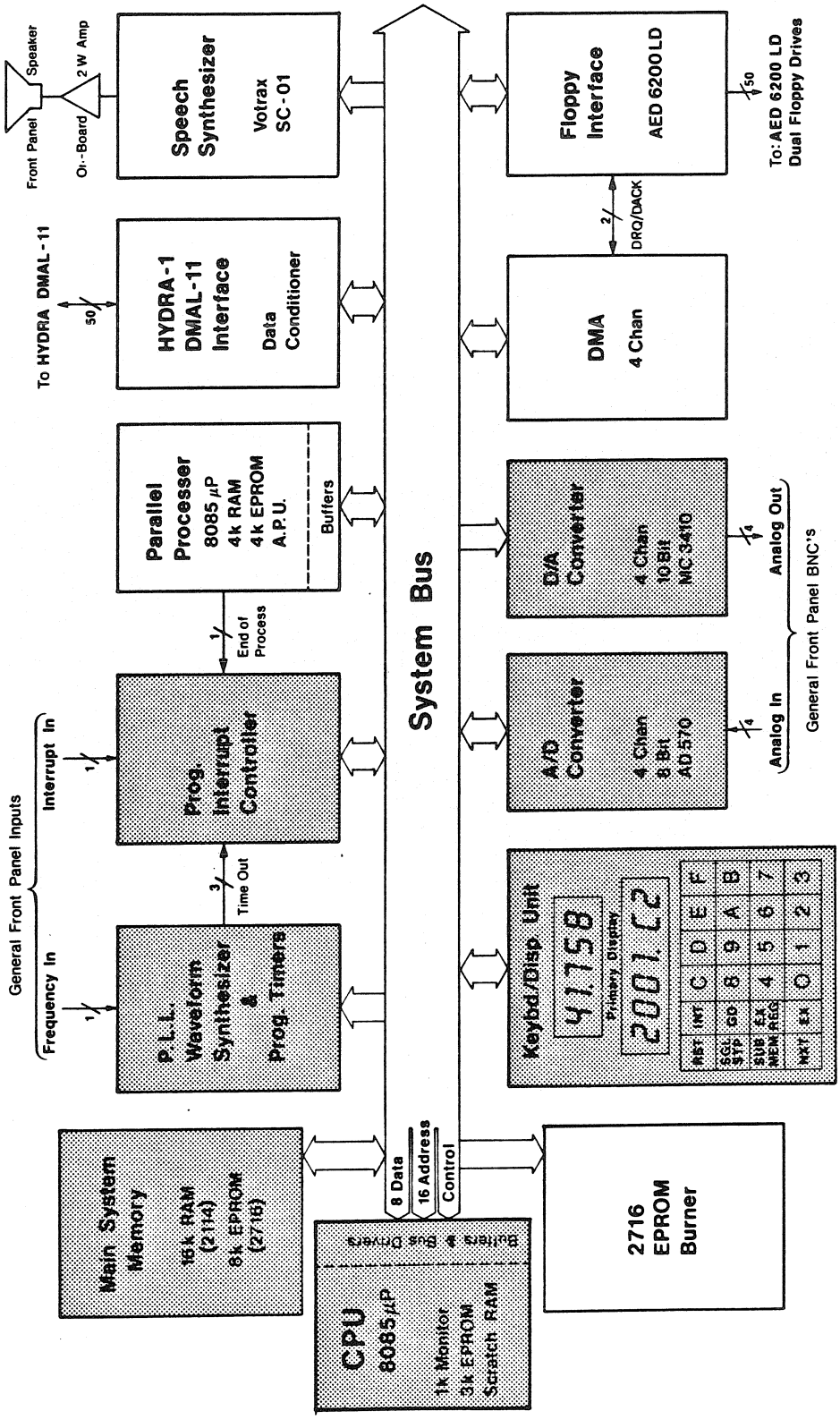

Figure B.1 Block Diagram of Feedback Control Portion (in Gray) of Microcomputer System

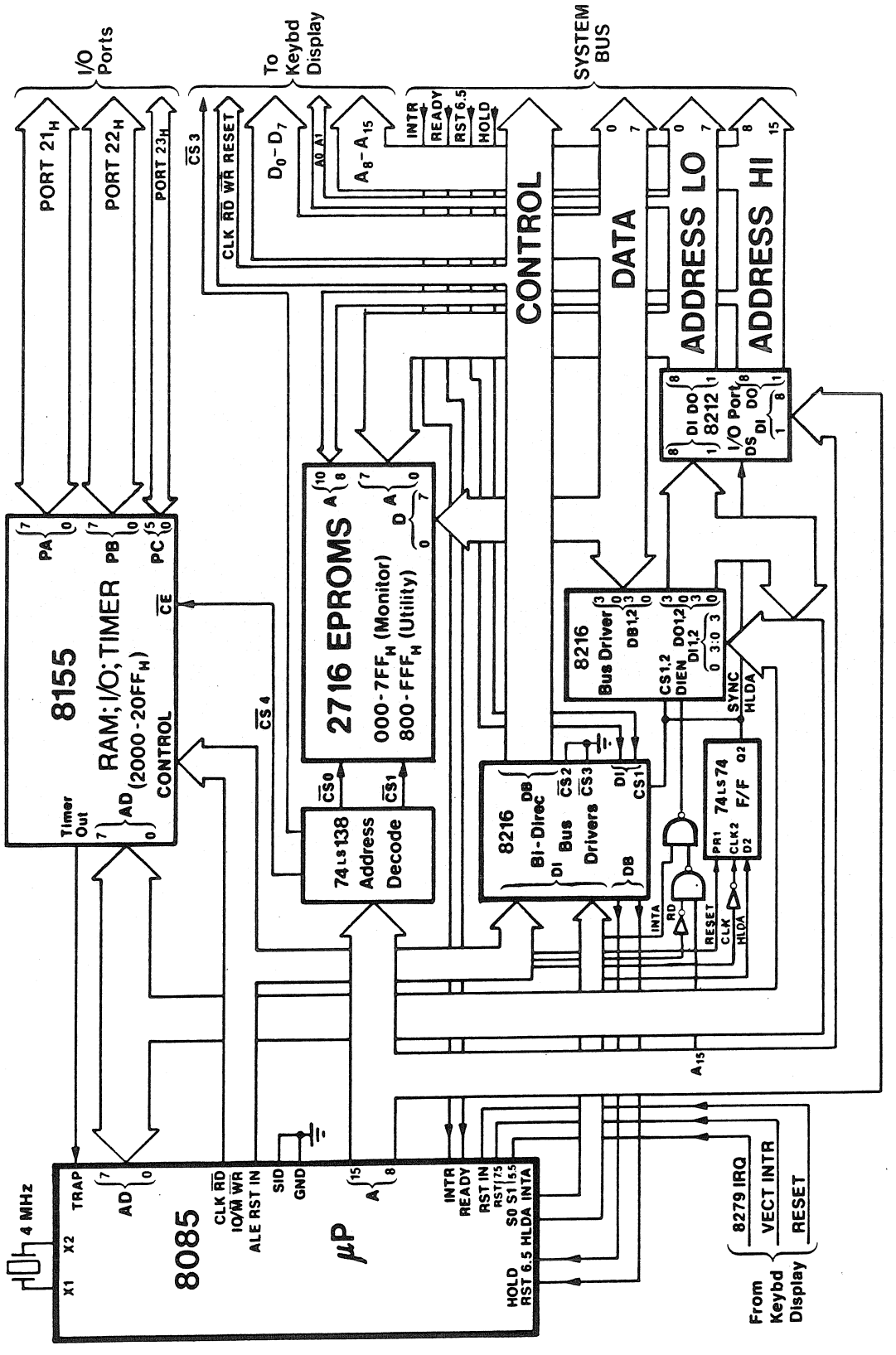

Figure B.2 CPU Block Diagram

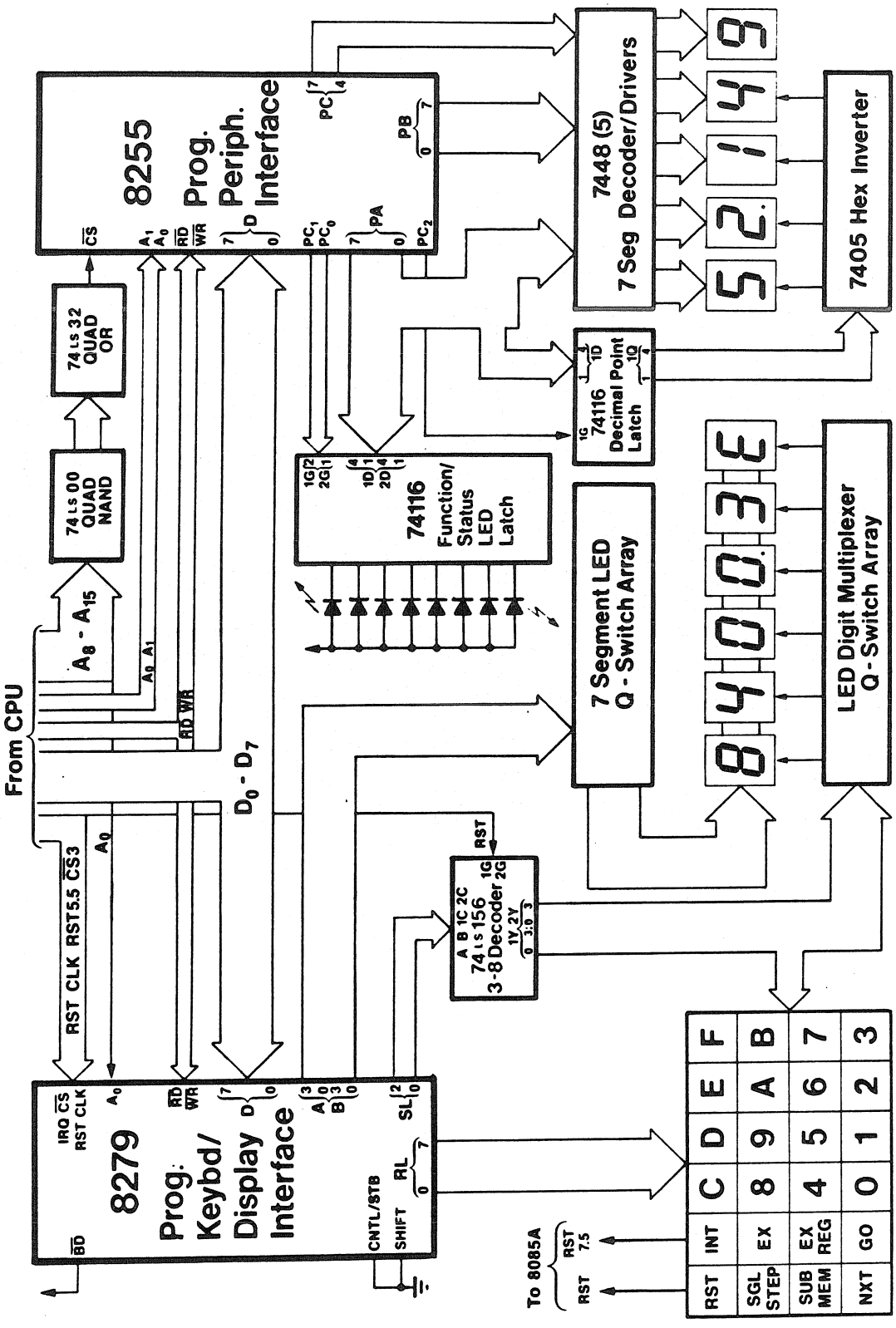

Figure B.3 Keyboard/Display Block Diagram

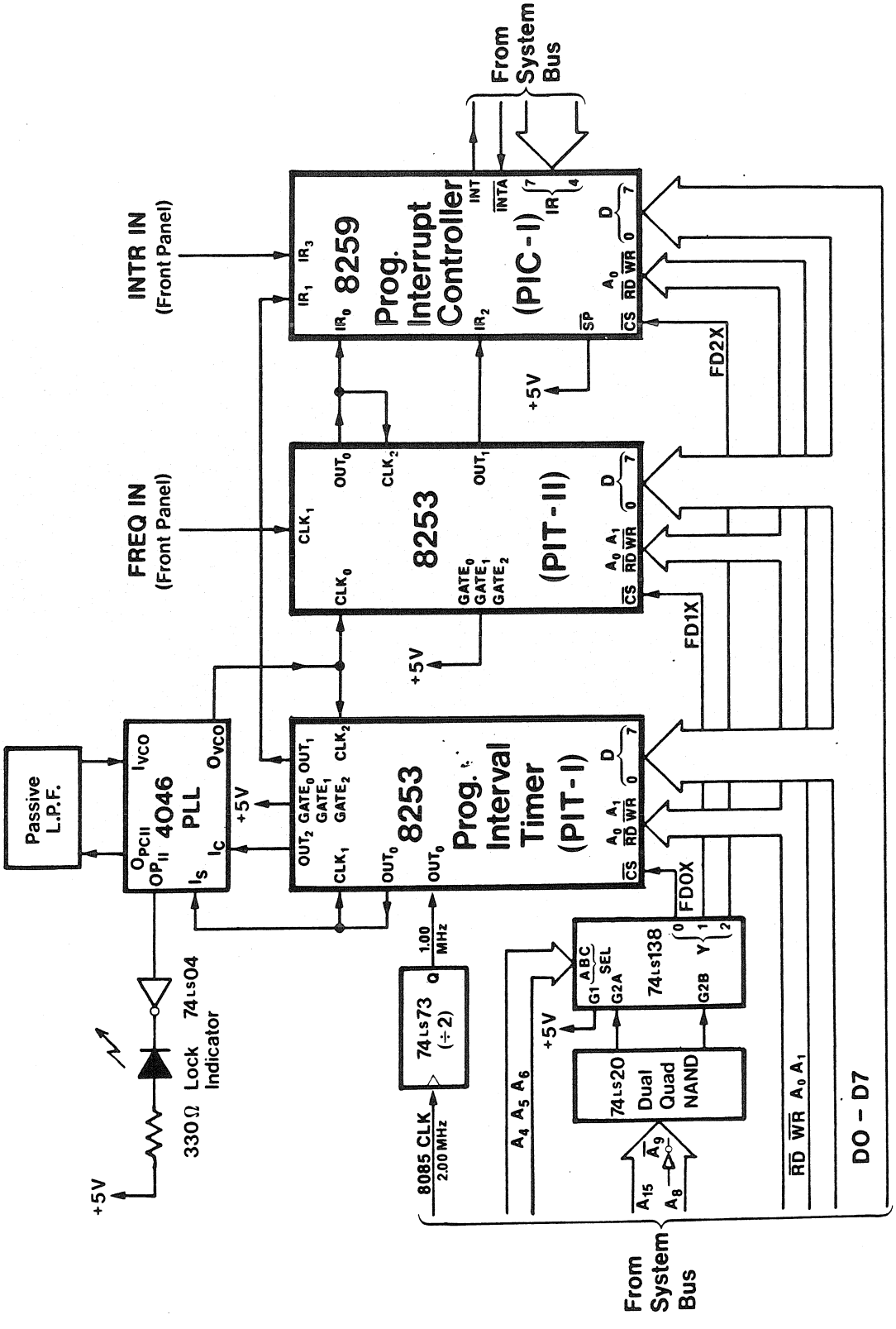

Figure B.4 Waveform Synthesizer Block Diagram

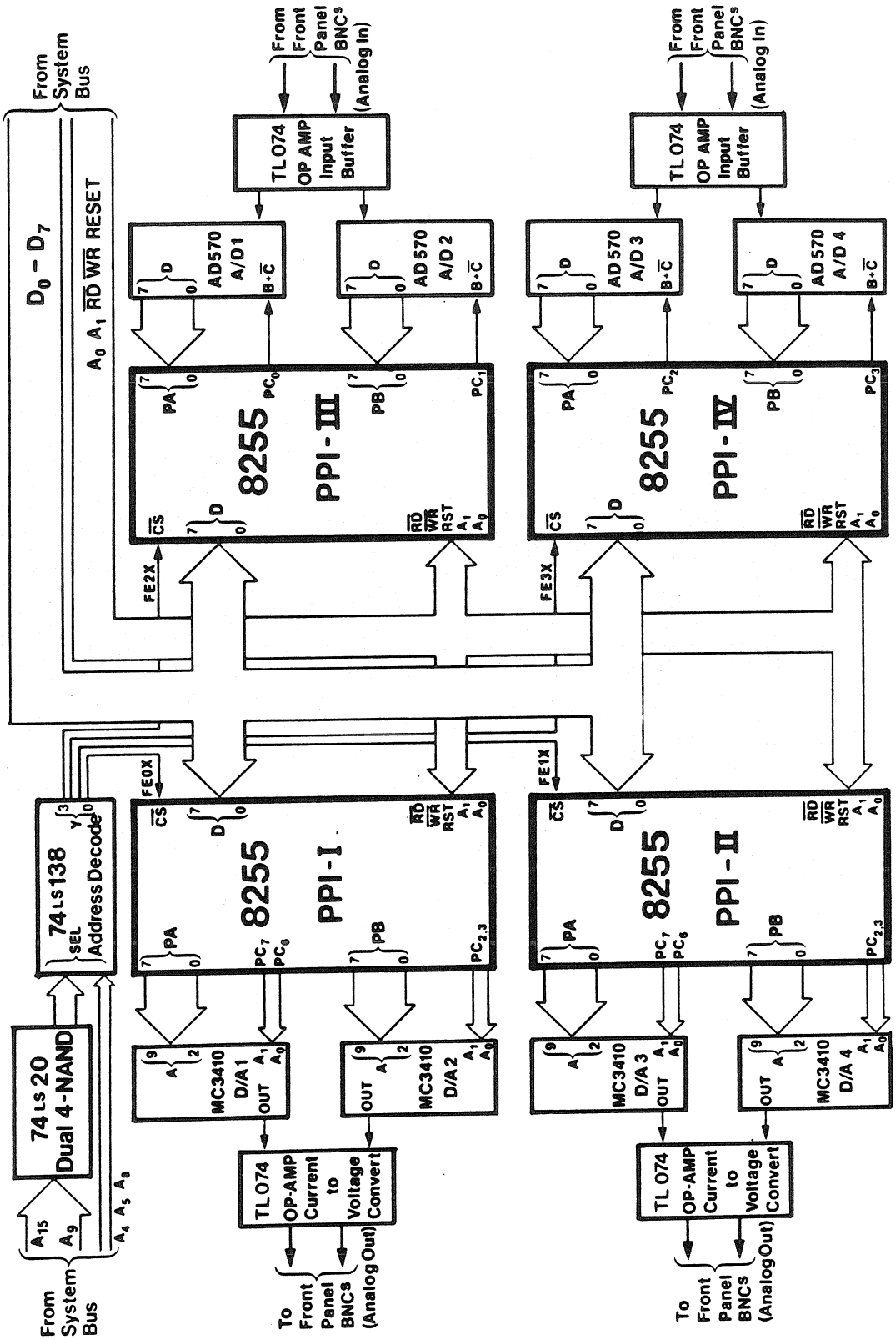

Figure B.5 A/D and D/A Block Diagram

APPENDIX C

IMPLEMENTATION OF THE FEEDBACK CONTROL ALGORITHM

The microprocessor system was used to determine the mean frequency of the natural T-S waves, and then synthesize waves at the T-S wave mean frequency, at an experimentally predetermined amplitude. The microprocessor maintained the waves at a predetermined phase relative to the natural T-S waves. As a first attempt at feedback control, an external analog processor was designed to reconstruct the natural waves by subtracting the forced waves (with appropriate gain) from the total wall shear signal (which represented the linear summation of the forced and the natural waves). The analog processor detected zero-crossings of the reconstructed waves, and sent a corresponding TTL pulse train to the INTR IN input of the microcomputer system. The feedback control program interrupt service subroutine counted each zero-crossing as it occurred. When a predetermined number of zero-crossings were counted (ex. six T-S wave periods), the subroutine reset the phase of the synthesized output sine wave to a predetermined phase. This predetermined phase was experimentally determined to yield the desired superposition of the forced and natural waves.

The following algorithm is implemented by the microprocessor:

Step 1 Initialize the counters on PIT-I and PIT-II to: generate a 128 Hz reference signal for the Phase Locked Loop, act as a "divide by N" counter in the feedback portion of the Phase Locked Loop, generate a 10-second gate, divide the output of the Phase Locked Loop by 10, and load PIT-II counter 1 with 9999 for down-counting zero-crossings. (see Appendix B, section B.5, for a detailed description of the counter operation).

Step 2 Mask all interrupts except IR1 (for interrupt at end of 10-second sampling gate)

Step 3 Determine the frequency of the natural T-S waves by counting the zero-crossings with PIT-II counter 1.

Step 4 Wait for IR1

Step 5 Service IR1 by latching PIT-II counter 1 count and subtract this count from 9999; load PIT-I counter 2 (PLL "divide by N" counter) with this count. Mask off IR1 and unmask IR0 and IR3.

Step 6 Wait for interrupts IR0 and IR3.

Step 7 Service IR0 by outputting next element of waveform look-up table.

Step 8 Service IR3 by counting the number of zero-crossings since the previous phase update. When the number of zero-crossings is equal to a preset number (ex. six zero-crossing interrupts) reset the look-up table pointer to a preset offset (this has the effect of impulsively updating the phase of the synthesized waves).

Step 9 Go to Step 6.

LISTING OF 8085 ASSEMBLY LANGUAGE FEEDBACK CONTROL PROGRAM

Loc.	Obj.	;Symbolic	Comments
2000	31 C2 20	;LXI SP, 20C2	initialize Stack
		;	pointer to loc 20C2
3	21 03 FD	;LXI H, FD03	Control word reg
		;	for PIT-I
6	36 37	;MVI M, 37	Set PIT-I counter 0
		;	Mode 3 (BCD)
8	36 71	;MVI M, 71	Set PIT-I counter 1
		;	Mode 0 (BCD)
A	36 B7	;MVI M, B7	Set PIT-I counter 2
		;	Mode 3 (BCD)
C	2B	;DCX H	Set (HL) = FD01
D	2B	;DCX H	(PIT-I cntr 1 addr)
		;	
E	36 80	;MVI M, 80	PIT-I cntr 1 loaded
2010	36 12	;MVI M, 12	w/ div by 1280_{10}
		;	to produce a 10^{0} sec
		;	gate to PIC-I IR1
12	2B	;DCX H	Set (HL) = FD00
		;	(PIT-I cntr 0 addr)
		;	
13	36 13	;MVI M, 13	PIT-I cntr 0 loaded
15	36 78	;MVI M, 78	w/ div by 7813_{10}
		;	to produce a
		;	128_{10} Hz square
		;	wave into PLL
17	21 13 FD	;LXI H, FD13	Control word reg
		;	for PIT-II
1A	36 71	;MVI M, 71	Set PIT-II counter 1
		;	Mode 0 (BCD)
1C	36 37	;MVI M, 31	Set PIT-II counter 0
		;	Mode 3 (BCD)
1E	2B	;DCX H	
1F	2B	;DCX H	Set (HL) = FD11
		;	
2020	36 99	;MVI M, 99	load PIT-II cntr 1
22	36 99	;MVI M, 99	w/9999_{10}, which
		;	is counted down by
		;	FREQ IN
24	2B	;DCX H	Set (HL) = FD10

```
  25 | 36 10          ;MVI M, 10       load PIT-II cntr 0
  27 | 36 00          ;MVI M, 00       w/div by 10(10) for a
     |                ;                128(10) x fTS Hz
     |                ;                (div by n cntr in PLL)
  29 | 21 13 FD       ;LXI H, FD13     Reload HL with PIT-II
     |                ;                control wd reg address
  2C | 01 11 FD       ;LXI B, FD11     Load BC with PIT-II
     |                ;                cntr 1 addr, (T-S wave
     |                ;                FREQ IN counter)
     |                ;
  2F | 3E 96          ;MVI A, 96       PIC-I initialization
2031 | 32 20 FD       ;STA FD20        control word 1 (ICW 1):
     |                ;                edge triggered, address
     |                ;                interval = 4, jump
     |                ;                table LSB 80
     |                ;
  34 | 3E 20          ;MVI A, 20       PIC-I ICW 2: jump table
  36 | 32 21 FD       ;STA FD21        MSB = 20, jump table
     |                ;                starts at 2080
     |                ;
  39 | 3E FD          ;MVI A, FD       PIC-I operation control
  3B | 32 21 FD       ;STA FD21        word 1 (OCW 1): mask
     |                ;                all interrupts except
     |                ;                IR1 (10(10) sec gate)
  3E | FB             ;EI              Enable interrupts

*************** INITIALIZATION COMPLETE ***************

 203F | 76             ;HLT             Wait 10 sec for PIT-II
      |                ;                cntr 1 to count down
      |                ;                (from 9999(10) the no.
      |                ;                of T-S wave zero x-ings
      |                ;                input by FREQ IN
      |                ;
 2040 | 3E 80          ;MVI A, 80       Control word to set
   42 | 32 21 FD       ;STA FD21        PPI-I for output all
      |                ;                ports (D/A's 1 & 2)
   45 | 3E F6          ;MVI A, F6       OCW 1: Mask all
   47 | 32 21 FD       ;STA FD21        interrupts but IR0
      |                ;                and IR3
   4A | 01 00 08       ;LXI B, 0800     Load (BC) w/starting
      |                ;                address of sine-wave
      |                ;                look-up table
   4D | FB             ;EI              Enable interrupts
   4E | 76             ;HLT             Wait in loop for sine
   4F | C3 4E 20       ;JMP 204E        wave output and phase
      |                ;                update interrupts
```

```
************ IR1 INTERRUPT SERVICE ROUTINE ************

2052| 36 40        ;MVI M, 40      Latch PIT-II counter 1
    |              ;
  54| 0A           ;LDAX B         Get LSB of TS freq
  55| 5F           ;MOV E, A       count, store in reg E
  56| 3E 99        ;MVI A, 99      and subtract
  58| 93           ;SUB E          from 99(10), and
  59| 5F           ;MOV E, A       store result in reg E
    |              ;
  5A| 0A           ;LDAX B         Get MSB of TS freq
  5B| 57           ;MOV D, A       count, store in reg D
  5C| 3E 99        ;MVI A, 99      and subtract
  5E| 92           ;SUB D          from 99(10), and
  5F| 57           ;MOV D, A       store result in reg D
    |              ;
2060| 21 02 FD     ;LXI H, FD02    Load (HL) w/PIT-II
    |              ;               counter 2 address
  63| 73           ;MOV M, E       Store MSB & LSB of
  64| 72           ;MOV M, D       frequency count in
  65| 00           ;NOP            PIT-I counter 2
  66| 00           ;NOP            (PLL div by n cntr)
    |              ;
  67| CD 63 03     ;CALL           Display frequency in
    |              ;               addr field of display
    |              ;
  6A| 3E 20        ;MVI A, 20      OCW 2: Non-specific
  6C| 32 20 FD     ;STA FD20       End of Interrupt (EOI)
    |              ;               sent to PIC-I control
    |              ;               word register
    |              ;
  6F| C9           ;RET            Return (to 2040) to
    |              ;               start outputting
    |              ;               sine-wave

************ IR0 INTERRUPT SERVICE ROUTINE ************

2070| 0C           ;INR C          Increment sine-wave
    |              ;               look-up table counter
  71| 3E 7F        ;MVI A, 7F      Load accumulator with
    |              ;               mask for 7F (128(10))
    |              ;               byte sine wave
  73| A1           ;ANA C          Make count in reg C
  74| 4F           ;MOV C, A       modulo 7F
  75| 0A           ;LDAX B         Get current sine-wave
  76| 32 00 FE     ;STA FE00       amplitude and output
    |              ;               to D/A 1
```

```
   79| 3E 20        ;MVI A, 20      OCW 2: send non-
   7B| 32 20 FD     ;STA FD20       specific EOI to PIC-I
                    ;               control word register
   7E| FB           ;EI             Enable interrupts
   7F| C9           ;RET            Return to wait loop
     |               ;               at 204E
```

********** IR3 INTERRUPT SERVICE ROUTINE **********

```
 C000| 21 18 C0     ;LXI H, C018    Get number of zero
    3| 35           ;DCR M          crossings to delay
    4| 7E           ;MOV A, M       before updating phase,
    5| C2 11 C0     ;JNZ C011       decrement count and
                    ;               exit int serv routine
                    ;               if count non zero
                    ;               (number of T-S wave
                    ;               zero x-ings to go is
                    ;               stored in C018)
                    ;
    8| 23           ;INX H          Reinitialize number
    9| 7E           ;MOV A, M       of zero crossings to
    A| 2B           ;DCX H          wait (total delay is
    B| 77           ;MOV M, A       prestored in C018)
                    ;
    C| 23           ;INX H          Set (HL) to C01A (pre-
    D| 23           ;INX H          stored phase shift)
    E| 4E           ;MOV C, M       Reset sine-wave look-up
    F| 06 08        ;MVI B, 08      table pointer to
                    ;               correct phase
                    ;
 C011| 3E 20        ;MVI A, 20      Issue non-specific
   13| 32 20 FD     ;STA 20FD       EOI to PIC-I
   16| FB           ;EI             Enable interrupts
   17| C9           ;RET            Return to wait loop
                    ;               at 204E
                    ;
   18| --           ;(data)         Number of additional
                    ;               interrupts to wait
                    ;               until phase update
   19| --           ;(data)         Preload w/number of
                    ;               zero crossings to delay
                    ;               (in HEX)
                    ;               between phase updates
   1A| --           ;(data)         Preload w/predetermined
     |              ;               phase shift (in HEX)
```

```
************** PIC-I JUMP TABLE VECTORS ***************

2080| C3 70 20      ;JMP 2070        IR0 Vector
  84| C3 52 20      ;JMP 2052        IR1 Vector
  8C| C3 00 C0      ;JMP C000        IR3 Vector
```

NOTES

1) All numerical values are HEXadecimal unless otherwise indicated.

2) Memory map address assignments of peripheral devices:

INTEL 8255 Programmable Peripheral Interface (PPI-I)

- FE00 Port A output latch (8 MSB to D/A 1)
- FE01 Port B output latch (8 MSB to D/A 2)
- FE02 Port C split output latch (2 LSB to D/A 1 and 2 LSB to D/A 2)
- FE03 Control Word Register

INTEL 8253 Programmable Interval Timer (PIT-I)

- FD00 Load/Read Counter 0; (divides system clock for use as input to PLL
- FD01 Load/Read Counter 1; (10_{10} second gate for FREQ IN sampling)
- FD02 Load/Read Counter 2; (PLL divide by N counter)
- FD03 Control Word Register

INTEL 8253 Programmable Interval Timer (PIT-II)

- FD10 Load/Read Counter 0; (divides by length of FREQ IN sampling gate to restore interrupt frequency to 128_{10} x f_{TS} Hz)
- FD11 Load/Read Counter 1; (FREQ IN down counter)
- FD12 Load/Read Counter 2; (general purpose down counter, not used in feedback program)
- FD13 Control Word Register

INTEL 8259 Programmable Interrupt Controller (PIC-I)

- FD20) These two locations are used for setting the
- FD21) Initialization and Operation Control Words